Reducing Artificial Lung Fouling: Nitric Oxide Release and Microscale Clot Evaluation

Submitted in partial fulfillment of the requirements for the

degree of

Doctor of Philosophy

in

Biomedical Engineering

Angela Lai
B.S., Biomedical Engineering, Boston University

Carnegie Mellon University
Pittsburgh, PA

December 2019

Acknowledgements

I am deeply grateful to the many people who have helped me in my time here at Carnegie Mellon Biomedical Engineering Department and I would like to acknowledge them here. First and foremost, I would like to thank my advisor, Keith E. Cook, for his endless patience and truly kind mentorship. It has been a privilege learning from Keith as he imparted wisdom and guidance both academically and personally. My time spent under Keith's mentorship has been instrumental to making me a more capable scientist, and also a better leader and person.

I would like to thank my committee members for providing guidance and discussion to direct my research in the right direction. To Dr. Conrad Zapanta, thank you for teaching me how to teach and introducing me to the world of engineering education. Your guidance in the past years when I TA'd with you have been invaluable. To Dr. Luisa Hiller, thank you for being so gracious and allowing me to use your space and letting me be a pseudo-member of your wonderful lab. To Dr. Charlie Ren, thank you for encouraging discussions and your enthusiasm and interest in my projects.

My work wouldn't be possible without the generous funding from the National Institutes of Health under award number R01HL089456. I'd like to thank Dr. Jim Antaki who has also been instrumental in my growth as a researcher. I'd also like to thank the BME Department for providing support through the past 5 years, and Misti West, Maryia Rakach, Keri Baker and Mike Scampone for tolerating me.

I'd like to thank my lab mates, both past and present, who have put in countless hours to start our large animal studies at Allegheny General Hospital. In particular, I would like to thank David Skoog, Chi Chi Do-Nguyen, Caitlin Demarest, Neil Carleton, and Rei Ukita for their sleepless nights and early mornings at the North Side. Those were some of the best and worst times of my PhD. To my current lab mates, Kalliope Roberts, Erica Comber, Suji Shin, Nao Ume, and Maiquyen Nguyen, thank you for your constant support, collaboration, and teaching me new things. I am looking forward to hearing about your research endeavors. In the past 5 years I've also had many undergraduate students work directly with me, and I am particularly grateful to them for their time and contributions to each part of my thesis.

Finally, I would like to thank my friends and family. Thank you to Stefanie, Rei, Andrew, and Sarah for our annual Secret Santas and sharing PhD milestones since 2014. To Elaine and Jooli, thank you for being the best neighbors. To Timmy, thanks for always having my back and keeping me sane. My family has always been supportive of every decision I've made, and I am grateful they believed in me through the years. Thank you for your endless support, Clare, 老妈和老爸.

Abstract

The prevalence of obstructive chronic lung disease in the United States is close to 15% and affects 35 million Americans today. Artificial lungs are employed to support patients that are affected most severely, but need to be replaced every one to four weeks primarily due to clot formation on circuit and oxygenator surfaces. A secondary issue that leads to device replacement is biofouling of the oxygenator surface from adhesion of bacteria from infection. Device surface fouling from clot and bacteria can be reduced through use of anticoagulant drugs, antibiotic drugs, and surface coatings. However, none of these current treatments have produced long-term effectiveness without significant side effects and risks. To address this clinical need, two approaches were used. First, surface generated nitric oxide (NO) from a novel material, Cu-PDMS, was tested for its antithrombotic and antimicrobial properties in the context of hollow fiber membrane artificial lungs. Second, the formation of clot inside hollow fiber membrane lungs was studied at the macro- and micro-scale to determine design recommendations to reduce coagulation.

In this thesis work, miniature artificial lungs were tested in parallel, one with 10% wt Cu-PDMS hollow fibers and one with polymethylpentene hollow fibers, the clinical standard. To study the longer-term effects of surface generated NO from Cu-PDMS hollow fibers, this study was conducted in a 72-hour veno-venous extracorporeal membrane oxygenation attachment in a sheep model. The Cu-PDMS fibers markedly reduced blood flow resistance, an indicator of clot formation, when compared to PMP fibers and produced the most effect in the 12-36-hour range. This material was then studied for its antimicrobial effect in an environment that simulated artificial lung

conditions *in vitro*. This study leveraged known antimicrobial agents, NO and copper, to prevent bacterial adhesion in a bioreactor system that simulated a blood stream infection in an ECMO circuit. Short-term and long-term effects of these agents were observed on the growth of Gram-negative bacteria, *P. aeruginosa*, and Gram-positive bacteria, *S. aureus*. Reduced adhesion of both strains of bacteria was observed after independent 4-hour exposure of surface generated NO, gaseous NO, and copper. However, the antimicrobial effects were short-term, and the combination of NO delivery with copper did not provide an enhanced antimicrobial effect. Lastly, the effect of different fiber bundle parameters on the initiation and progression of clot formation was studied. Current commercial oxygenators vary widely and are difficult to compare. There is no consensus on how artificial lung parameters such as packing density, path length, and frontal area affect clot formation. This study used a standardized platform in which human blood was pumped through a one-directional flow circuit that included 3D printed urethane acrylate flow chambers of various parameters that simulated the flows and conditions in an adult Quadrox oxygenator with 2 L/min flow. Micro computed tomography captured clot formation at the macro-scale, and fluorescence imaging captured clot formation at the micro-scale. These high throughput, easily repeatable studies concluded that a longer path length and small frontal area with a loosely packed fiber bundle can reduce coagulation. Furthermore, these results enable validation of computational clot models for predicting clot in an artificial lung and inform future artificial lung design.

Table of Contents

Acknowledgements iii
Abstract v
1 Motivation: Chronic Lung Disease 1
1.1 Current Treatments 2
1.1.1 Mechanical Ventilation 2
1.1.2 Lung Transplantation 3
1.1.3 Extracorporeal Life Support 4
1.1.3.1 Extracorporeal Membrane Oxygenation (ECMO) 6
1.1.3.2 Extracorporeal Carbon Dioxide Removal ($ECCO_2R$) 8
1.1.4 Artificial Lungs 8
1.2 Blood Compatibility in Medical Devices 9
1.2.1 Coagulation Cascade 10
1.2.1.1 Intrinsic Pathway: Surface activation 12
1.2.2 Platelet Activation 12
1.3 Preventing Clot Formation in Artificial Lungs 14
1.3.1 Anticoagulant Therapies 14
1.3.2 Heparin 14
1.3.3 Direct Thrombin Inhibitors 16
1.3.4 Nitric Oxide 17
1.3.4.1 Biomaterials Loaded with Nitric Oxide Donors 18
1.3.4.2 Surface Generated Nitric Oxide 19
1.3.4.3 Gaseous Nitric Oxide Delivery 20
1.3.4.4 Risks of using NO 21
1.3.4.5 Surface Coatings in ECLS Circuit and Artificial Lung 22
1.4 Modeling Coagulation and Predicting Clot in an Artificial Lung 24
1.4.1 Current Computational Methods in Artificial Lungs 25
1.4.2 Computational Models for Predicting Clot 26
1.5 Infection During ECMO 28
1.5.1 Current treatment 30
1.5.2 Nitric oxide as an Antibacterial Agent 31

1.5.2.1 Mechanism of Bacterial Regulation by Nitric Oxide 32
1.5.2.2 Nitric Oxide Delivery Platforms for Antimicrobial Effect in Medical Devices 32
1.5.2.3 Bacterial Response to Nitric Oxide 33
1.5.3 Copper as an antibacterial agent 34
1.5.3.1 Mechanisms of Bacterial Regulation by Copper 34
1.5.3.2 Bacterial Response to Copper 35
1.5.4 Methods for Evaluating Antimicrobial Efficacy 36
1.6 Summary of Study 37
2 Surface Generated NO from Cu-PDMS as an Anticoagulant Agent in a Short-Term *in vivo* Sheep Experiment 39
2.1 Introduction 39
2.2 Cu-PDMS Surface Evaluation Methods 41
2.2.1 Nitric Oxide Generating Device and Circuit Components 41
2.3 *In Vivo* Experimental Methods 43
2.3.1 Data Acquisition and Blood Sampling 46
2.3.2 Statistical Analysis 49
2.4 Results 51
2.4.1 Coagulation and inflammation 52
2.4.2 Device Function 53
2.4.3 Sheep Necropsy and Copper Content 58
2.5 Discussion 59
2.5.1 Clot Formation 59
2.5.2 Improving the Anticoagulant Function of NO Generating Fibers 60
2.5.3 Side-Effects – Oxygen Transfer and Serum Copper 61
2.5.4 Effect of Study Design and Test Devices on Clot Formation and Study Conclusions 64
2.6 Conclusion 65
3 Two-Pronged Method for Preventing Bacterial Adhesion using Nitric Oxide and Copper 66
3.1 Introduction 66
3.2 Study Design and Methodology 68
3.2.1 Bioreactor and Cellulose Membrane Preparation 68

3.2.2 Surface Characterization 69
3.2.3 Strains and Media 70
3.2.4 Preliminary Flow and Conventional Shaking Experiments 71
3.2.5 Experimental Setup: Role of Copper and Nitric Oxide Flux on Bacterial Viability 73
3.2.6 Statistical Analysis 76
3.3 Results 77
3.3.1 Membrane Characterization 77
3.3.2 Growth Curves 78
3.3.3 Bacterial Adhesion Under Flow and Conventional Shaking Conditions 78
3.3.4 Inhibition of P. aeruginosa Bacteria Adhesion by Cu-PDMS Membranes 80
3.3.5 Inhibition of S. aureus Adhesion Under Oxygenator Conditions 82
3.4 Discussion 83
3.4.1 Effects of Flow Chamber on Gaseous Nitric Oxide and Surface Generated Nitric Oxide Delivery 83
3.4.2 Bacterial Mechanisms to Counter Antimicrobial Therapeutics 85
3.4.3 Bacterial Response to Copper on Cu-PDMS Membranes 87
3.4.4 Minimal Effect on Planktonic Bacteria 88
3.5 Conclusion 90
4 Macro- and Micro-scale Evaluation of Clot Formation in an Oxygenator Hollow Fiber Bundle 91
4.1 Introduction 91
4.1.1 Hollow Fiber Parameters That May Affect Coagulation 92
4.2 Methodology 93
4.2.1 Experimental Design of the Flow Chamber 93
4.2.2 Experimental Setup of Benchtop Experiment 95
4.2.3 Micro-Computed Tomography Scans 97
4.2.4 Equivalent Surface Area to Volume Distance 98
4.2.5 Immunofluorescent Staining and Imaging of Clot Inside Flow Chamber 99
4.2.6 Effect of Temperature on Clot Formation 101
4.2.7 Statistical Analysis 101
4.3 Results 102

4.3.1 Baseline and Inlet Conditions 102
4.3.2 Effect of Temperature on Clot Formation in Flow Chambers 103
4.3.3 Macroscale Effects from Various Hollow Fiber Bundle Parameters 104
4.3.3.1 Effects of Packing Density 104
4.3.3.2 Effects of Blood Flow Velocity 107
4.3.3.3 Effects of Path Length 110
4.3.4 Microscale Effects from Various Hollow Fiber Bundle Parameters 113
4.4 Discussion and Conclusion 120
4.4.1 An Ideal Artificial Lung Fiber Bundle 121
4.4.2 Informing a Computational Model of Clot Formation 122
4.4.3 Experimental Limitations 124
5 Conclusion 127
5.1 Surface Generated NO from Cu-PDMS Hollow Fibers as an Anticoagulant in Short-term in vivo Sheep Experiment 127
5.2 Two-Pronged Method for Preventing Bacterial Adhesion using Nitric Oxide and Copper 128
5.3 Macro- and Micro-scale Evaluation of Clot Formation in an Oxygenator Hollow Fiber Bundle 129
5.4 Limitations and Future Work 130
5.4.1 Antimicrobial and Anti-platelet Effect of Surface Generated NO form Cu-PDMS 130
5.4.2 Computational Model of Clot in Hollow Fiber Bundle 131
6 References 132
7 Appendix 149
7.1 Shear Stress and Reynolds Numbers for each Flow Chamber 149
7.2 FIJI Macro for Clot Analysis 149
7.3 Thrombin and FXa Activity from Select Flow Chamber Experiments 150

List of Tables

Table 1. Failure times (hours) for all devices attached to each sheep. 55

Table 2. Oxygen exchange in mL/min/m2 over three days, with number of devices in each group per day. 57

Table 3. Testing Matrix reflecting PDMS surface conditions. 75

Table 4-1. The tested parameters in the benchtop flow experiments. 95

Table 4-2. Hematology of each donor group. All results are within normal clinical ranges. N = 6 for each group 102

Table 4-3. Baseline resistance values for each packing density and path length condition. 103

List of Figures

Figure 1-1. An example of gas exchange through a mat of hollow fibers. Gas flows through the lumen of the fibers and blood flows external to the fibers. 5

Figure 1-2. Two approaches for venovenous ECMO. The first depicts cannula inserted into the internal jugular vein and the femoral vein (A). When flow is started, blood is drawn from the femoral drainage cannula into the pump, passing through the oxygenator before it is reinfused into the internal jugular cannula. The second depicts a single cannulation site, using a double lumen cannula for both drainage and reinfusion (B). Reproduced with permission from Brodie D, Bacchetta M, *N Engl J Med* 2011, Copyright Massachusetts Medical Society. 7

Figure 1-3. The coagulation cascade is initiated by an artificial surface (intrinsic pathway) or a tissue based injury (extrinsic pathway). Factor Xa is the gateway for both pathways to join at the common pathway, which ultimately leads to a cross linked fibrin clot. 11

Figure 1-4. Blood contacting medical device associated thrombosis. Protein adsorption on the artificial surface results in platelet activation, adhesion, and aggregation. Contact pathway activation also results in platelet activation from thrombin and fibrin strands binding to platelet surfaces. Used with permission from *J Thromb Haemost,* 101, V.2, Jaffer, I.H. and Weitz J.I., Medical device-induced thrombosis: what causes it and how can we prevent it?, pp 682-689, Copyright (2015), with permission from Elsevier. 13

Figure 1-5. Kaplan-Meier survival curve for the Mazzeffi study. The patients who experienced a bleeding event had lower survival than patients that did not experience a bleeding event. Reproduced from The Annals of Thoracic Surgery, Vol 101 Issue 2, Mazzeffi M., Greenwood J., Tanaka K., et al., “Bleeding, Transfusion, and Mortality on Extracorporeal Life Support: ECLS Working Group on Thrombosis and Hemostasis”, pg. 682-689, Copyright (2016), with permission from Elsevier. 16

Figure 1-6. Fluid flow path lines in an oxygenator fiber bundle, flow is from the center towards the outer edge. Reproduced with permission from Ahmadi G. and Mazaheri A.R., Artificial Organs 2005, Copyright John Wiley and Sons. 25

Figure 1-7. (a) Simulated thrombus in a Thoratec HeartMate II inlet straightener and clinical observations of clot in (b) and (c). Reproduced with permission under the Creative Commons License from Wu W., Yang F., “High fidelity computational simulation of thrombus formation in a Thoratec HeartMate II continuous flow ventricular assist device”, *Nature Scientific Reports* (2016)..... 27

Figure 2-1. The reduction - oxidation reaction that occurs at the surface of a Cu-PDMS membrane when it is supplied with a NO donor, such as GSNO. 40

Figure 2-2. A Cu-PDMS (A) and a PMP (B) miniature artificial lung. (C) A schematic shows the flow of blood through a miniature artificial lung and the materials it will encounter. 42

Figure 2-3. Timeline of surgical and experimental events. Two sets of Cu-PDMS and PMP devices were attached in parallel. 43

Figure 2-4. VV-ECMO circuit connecting a Cu-PDMS and a PMP device in parallel in a sheep model. The experimental timeline is as follows: T=0 Baseline samples; T=2 Circuit attachment; T=6 Device attachment set 1; Device attachment set 2 for each experiment. 45

Figure 2-5. Energy dispersive microscopy is used to characterize the surface of Cu-PDMS fibers for copper exposed on the surface (A). Then, the image is converted to binary (B) and then all of the pixels representing copper are counted using ImageJ. Scale Bar 20 μm. 51

Figure 2-6. White blood cell count and platelet counts averaged over all subjects. Data are averaged over one day and presented with a standard deviation. 53

Figure 2-7. Normalized resistances to an averaged baseline show significant difference between Cu-PDMS and control devices. Data are averaged over 6-hour periods and presented with the standard deviation. 54

Figure 2-8. Failure of Cu-PDMS and control PMP devices over 72 hours (N = 8). The ● represents a device that was removed before it was failed, data from this was used as a censored event in Kaplan-Meier survival analysis. 55

Figure 2-9. Clot formation in lungs. As expected, devices that did not reach failure (a,c) have less clot than those that fail (b,d). (a) 50% of Cu-PDMS devices had black gas exchanging fibers visible and some white clot formation on the housing and edges. The other 50% of Cu-PDMS devices (b) failed. Only one PMP device (c) survived to 72 hours, and the rest (d) 87.5% failed and had clot originating from the fiber bundle, and no gas exchanging fibers can be seen. 56

Figure 2-10. Oxygen transfer on D1 at 300 and 600 mL/min blood flow rate, and 600 and 1200 mL/min oxygen flow rate respectively (A). Data that had variable inlet conditions and high initial resistance were excluded. 57

Figure 2-11. Representative SEM images of gas exchanging fibers and weaving fibers. (a) outlines a weaving fiber with pronounced protein deposition and (b) outlines a gas exchanging fiber. These are figures representing typical surfaces of failed devices looking at the middle of the fiber bundle. (87.5% of the PMP devices and 50% of the Cu-PDMS devices). 58

Figure 3-1. A schematic of the bioreactor setup that simulates the conditions of a gas exchanging membrane of a hollow fiber of an oxygenator. There is a gas side and a fluid side and a membrane that is sandwiched between the two bioreactor pieces. 69

Figure 3-2. Experimental setup with a single direction of flow (A). The bioreactor chamber has a blood side and a gas side, divided by a permeable membrane which represents the hollow fiber membrane (B). Gas is provided at the same rate as in a hollow fiber membrane oxygenator (C). 74

Figure 3-3. The EDS image shows 15 ± 1% Cu-PDMS copper expression at the surface representing the active area available to catalyze the NO release from GSNO. The copper is seen in white. SB = 900 µm 77

Figure 3-4. A reduction of S. aureus bacteria can be seen in the experimental bioreactor circuit case under flow when compared to the conventional coupon method in both the number of bacteria adhered to the membrane and in the media surrounding the membrane. 79

Figure 3-5. P. aeruginosa bacterial adhesion on membrane after exposure to copper, surface generated nitric oxide (NO), or gaseous NO. (A) The short-term viability of adhered bacteria, measured in optical density after incubation in TSB for 6-hr. (B) The effects of these antibacterial agents after 18-hr growth of bacteria on an agar plate in log(CFU/mL)..... 81

Figure 3-6. S. aureus adhesion on the membrane after a 4-hr flow experiment. (A) The short-term viability of adhered bacteria that is measured after incubation and 6-hr growth with turbidity at OD_{600nm}. (B) The long-term viability of bacteria adhered to the membrane grown on agar plates..... 83

Figure 3-7. The planktonic *S. aureus* bacteria was affected negatively by both NO delivery mechanisms in the short-term when compared to the negative control (A). The viable bacteria on membranes showed that those effects from NO did not persist after growth on agar plates, and in fact had a slightly positive effect (B). 88

Figure 3-8. Effect of surface generated NO, gaseous NO, and a Cu-PDMS membrane on planktonic P. aeruginosa bacteria. (A) The short-term effects of NO are antibacterial but mild. (B) The effects of NO and copper from the Cu-PDMS membrane are not seen in the planktonic *S. aureus* bacteria. 89

Figure 4-1. A CAD of the flow chamber for 2 cm long (A) and 4 cm long (B) path lengths. 93

Figure 4-2. The various tested packing densities of hollow fibers in the flow chamber. 93

Figure 4-3. The experimental flow circuit invovles one-way flow from a syringe pump, connected to the flow chamber and then to a waste container. A manometer measures the pressure drop across each experimental device. 96

Figure 4-4. An image of the 3D reconstruction of a µCT scan in Slicer 4 software (A). These are then averaged with other scans, and the rods in the chamber are subtracted to create the 3D probability map of where clot is most likely to form, red being more likely and blue less likely (B). 98

Figure 4-5. Three regions of interests are indicated here in black outlined in red, representing the back side of the fiber (left), the middle flow region (middle), and the front side of the fiber (right). Fluorescent intensities were quantified in these three regions. 100

Figure 4-6. Clot volume through a 2 cm device at 37°C and one at 22°C. There is not a significant difference between the two sets. 103

Figure 4-7. Probability map of clot formation in devices with various packing densities. Blood flow is from top to bottom. 104

Figure 4-8. The change in resistance in natural log over the 15-minute experiment. A higher packing density correlates with a higher resistance. 105

Figure 4-9. Clot volume in flow chambers with various packing densities. The 60% packing density device had more clot than the 40% or 50% packing density devices in the entire length of the flow chamber. 105

Figure 4-10. The clot volume in a 1 mm slice at equivalent distances from the inlet in flow chambers with various packing densities after a 15-minute experiment. 106

Figure 4-11. Probability maps for clot formation in low (3.68 mL/min), medium (4.38 mL/min), and high (5.46 mL/min) velocities. Pink is higher probability of clot, and blue is least probability of clot. 107

Figure 4-12. Resistance of flow chambers experiencing various flows for a 15 minute experiment. 108

Figure 4-13. Clot volume from CT scans show a trend of more clot at the outlet side of the flow chamber, as well as slightly more clot in the devices experiencing lowest flow. 108

Figure 4-14. Clot in a 1 mm segment of experimental devices at the same equivalent distance based on surface area for different flow rates after a 15-minute experiment. 109

Figure 4-15. Probability map of clot formation in 4 cm (left) and a 2 cm (right) device. Flow is from top to bottom and higher probability is represented with pink and least probability is represented in dark blue. 110

Figure 4-16. Resistance change through the flow chamber over a 15-minute experiment. 111

Figure 4-17. The clot volume quantified from CT scans show more clot overall in the shorter 2 cm devices than in the 4 cm devices. 111

Figure 4-18. Clot volume in a 1 mm slice at an equivalent distance from the inlet after a 15-minute experiment in a 2 and 4 cm path length flow chamber. 112

Figure 4-19. Fluorescent staining of fibrin and platelets showed clot depositing in the direction of flow (left to right) and colocalization of platelets close to the rods. 113

Figure 4-20. Maximum intensity projection of one representative field at the outlet. Fibrin is in magenta, platelets in green, and the plastic rods are in blue. 114

Figure 4-21. Averaged fluorescent images of low flow (3.65 mL/min) and high flow (5.46 mL/min) conditions at the inlet and outlet of a 2 cm long flow chamber. Fibrin (magenta), platelets (green) and the plastic rods (blue) are seen in each field. SB = 200 µm 115

Figure 4-22. The platelet and fibrin probability of depositing in certain areas between hollow fibers under low flow(16 cm/min blood velocity). The outlet reflects the higher clot volume that was also seen in the µCT scans. Scale bar is 200 µm. 116

Figure 4-23. The platelet and fibrin deposition map on an area between hollow fibers at high flow (25 cm/min blood velocity) through a fiber bundle. Scale bar is 200 µm. 116

Figure 4-24. Change in total pixel count of fibrin and platelets from the inlet to outlet. In all cases, there was more signal detected at the outlet of the flow chamber. These cases show that there was more fibrin and platelet deposition in the low flow experiments when compared to the faster flow. 117

Figure 4-25. The averaged fluorescent images for a 40% packing density and 60% packing density conditions at the inlet and outlet of a 2 cm long flow chamber. Fibrin (magenta), platelets (green) and plastic 3D printed rods (blue) are in each field. SB = 200 µm. 118

Figure 4-26. Platelet and fibrin average deposition in a 60% packing density flow chamber after 15 minutes of blood flow. 119

Figure 4-27. Average platelet and fibrin deposition in a 40% packing density flow chamber after 15 minutes of flow. There is more deposition at the outlet than at the inlet. Additionally, the wide spacing between fibers do not have much fibrin tendrils bridging between adjacent rods. However, they can still be seen growing in the direction of flow. SB is 200 µm. 119

Figure 4-28. Total pixel count of the 15 imaged regions of interest increased from the inlet to outlet in all packing density devices. This means more platelets and fibrin were adhered to the outlet end of each device. Also, there were more fibrin and platelets adhered to the back end of the hollow fiber rods. In particular, the 60% packing density devices had more clot than the 40% ones. 120

Figure 4-29. Potential future flow chamber with a centered array of fibers to avoid flow effects from the inlet and outlet. The flow through this chamber would be fully developed. 121

1 Motivation: Chronic Lung Disease

Our lungs are internal organs, but with every breath we take they directly interface with the outside environment. The inhalation of small particulates, such as those from smoking or air pollution are the cause of lung disease. Other factors include occupational exposures, indoor sources of combustion, and most recently, the CDC reported on the risks of vaping.[63] The prevalence of obstructive chronic lung diseases in the United States is close to 15% and affects 35 million Americans today.[31,68] The most common forms of lung disease in the U.S. are chronic obstructive pulmonary disease (COPD), cystic fibrosis (CF), asthma, and interstitial lung disease (ILD).

COPD is now the fourth leading cause of death of adults in America, and affects 16 million people.[31] It is characterized by the obstruction of airflow by inflammation and/or destruction of alveoli. This interferes with normal breathing and oxygen and carbon dioxide exchange.[14,67,107] While there is no cure for COPD, patients can manage their symptoms with medication, long-term administration of oxygen, or use of bronchodilators to open the airways, reduce inflammation, and reduce the frequency and severity of exacerbations.

CF is a hereditary disease that is diagnosed mainly in newborns and affects approximately 30,000 Americans today, with more than 10 million Americans unknowingly carrying the defective CF gene. CF causes patients to secrete a thick mucus in the lungs, pancreas, and other organs. This mucus blocks airways in the lungs and causes a combination of airway obstruction, infection, and inflammation. This leads to an obstruction to breathing and an inability to clear pathogens. This mucus also blocks digestive pathways and interferes with proper digestion.

Asthma is an inflammatory disease characterized by excessive sensitivity of the lungs to stimuli, such as allergies, particles in the air, or even odors. When provoked, the inflammation in the lungs is exacerbated and the airways end up producing mucus that worsens the obstruction and can lead to an asthma attack. An estimated 22.9 million Americans have asthma today and it is the leading chronic illness of children in the United States. Untreated asthma can progress to become COPD.[31]

Interstitial lung disease (ILD) is used to define a variety of chronic lung disorders that are characterized by three stages: (1) lung tissue is damaged, (2) air sac walls become inflamed, and (3) fibrosis occurs in the interstitial tissue, causing the lungs to become stiff. The most well-known type of ILD is idiopathic pulmonary fibrosis (IPF), due to its unknown etiology, poor prognosis, and modest response to therapeutics. In the United States, 80.9 per 100,000 men and 67.2 per 100,000 women suffer from ILD, although more may live with it undiagnosed.[101,167]

1.1 Current Treatments

Current treatments for lung disease patients focus on providing oxygen and carbon dioxide transfer at physiological rates and, in some cases, reducing right ventricle work loads. Below are the most commonly used solutions to treat patients with respiratory failure.

1.1.1 Mechanical Ventilation

Mechanical ventilation is the most common non-invasive support system for patients experiencing respiratory failure. It is a mechanical system that is used to assist or replace breathing in patients with limited respiratory capacities. In a non-invasive mechanical ventilation setting, patients are conscious and are ventilated with positive

pressure through a face or nasal mask and are supplied with high oxygen content gas to facilitate oxygen exchange. If this does not provide enough respiratory support, invasive mechanical ventilation is used. In this setting, an endotracheal tube is inserted inside the patient's trachea, either from the mouth or through a tracheostomy in the throat and positive pressure is used to inflate and deflate the lungs. Mechanical ventilation is used as a short-term means of support as the repeated high pressures cause lung injury from overdistention and also lung infection.[148,176,189] An international multi-center study with 5131 patients on this therapy for longer than 12 hours experience the following: barotrauma, (3.0%); ARDS, (4.4%); pneumonia, (9.8%); sepsis, 457 (9.7%); shock (22.1%); acute renal failure (18.7%).[57]

1.1.2 Lung Transplantation

Currently, lung transplantation is the only long-term solution for patients suffering from chronic lung disease. During lung transplantation, diseased lung is partially or totally replaced by lungs that come from a donor. Bilateral or single lung transplants are possible. However, bilateral lung transplantation has better outcomes compared to single lung transplantation, (median 7.0 years to 4.5 years) most likely due to a better match in donor and recipient grafts for function and anatomical size.[204] Very sick patients who cannot survive the waiting list for a cadaveric lung transplantation, may also be able to receive lungs from two living donors in a procedure called bilateral living-donor lobar lung transplantation. This procedure has been developed to supplement the brain-dead donor shortage, but places 3 people at risk and so is not performed often. Even under these circumstances, the number of lung transplants that are performed in the U.S. is less than 4,000 a year due to the shortage of available donor lungs and the

high requirements for the recipient. There are around 3,000 bilateral lung and around 1,000 single lung transplants done per year.[146,203,204] Lung transplant recipients face immense challenges from the surgery, including immunosuppression, rejection, and the underlying disease. Based on an international, multi-center study, the 5-year survival rate post transplantation is 53%, the worst of any organ transplant.[203]

1.1.3 Extracorporeal Life Support

Extracorporeal life support (ECLS) is a prolonged but temporary support of heart or lung function using extracorporeal blood circuits that lasts between 2-10 days.[37] ECLS has grown out of cardiopulmonary bypass, during which heart-lung machines take over all heart and lung function for a few hours. During ECLS, blood is pumped from a patient, through an artificial lung (i.e. oxygenator) and then back into the patient. ECLS circuits include vascular access catheters, connective tubing, a blood pump, an artificial lung, sometimes a heat exchanger, and a slew of monitoring and measuring devices for regulation.

The artificial lung, also known as an oxygenator, provides the gas exchange within the ECLS circuit and also contains the most surface area (1.8-2.4 m^2). It is composed of a densely packed bundle of hollow fibers, which are shaped like small straws, with diameters ranging from 200-400 µm. Gas flows through the lumen of these hollow fibers and blood flows external to these fibers. Gas exchange occurs through the porous membrane of the fiber walls due to diffusion. These fibers make up around 90% of the total surface area of the ELS circuit, and thus are especially prone to clot formation, which leads to decreased functionality and risk of embolization

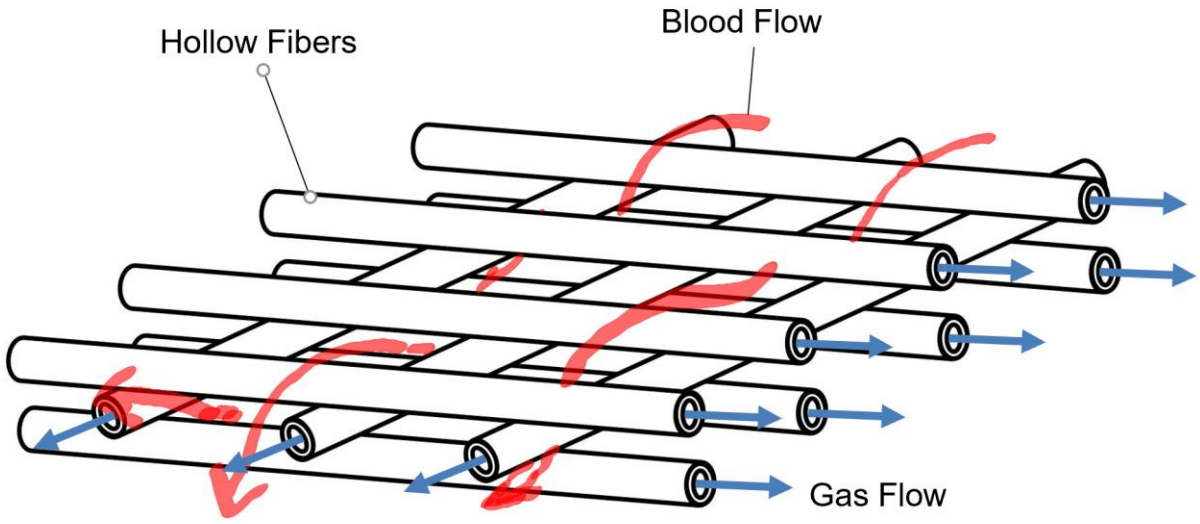

Figure 1-1. An example of gas exchange through a mat of hollow fibers. Gas flows through the lumen of the fibers and blood flows external to the fibers.

The configuration of the fibers varies widely between commercially available artificial lungs, from fiber spacing, cross-angles, and overall dimensions of the fiber bundle. The parameters that are varied in different oxygenator fiber bundle designs are: (1) bundle shape which depends on path length (L), the distance from the inlet face of the fiber bundle to the outlet in the direction of blood flow and frontal area (A_f), the area of the fiber bundle perpendicular to direction of blood flow; and (2) packing density, the percentage of the volume of the fiber bundle that is taken up by the hollow fibers and is a factor of fiber diameter and spacing. These hollow fibers were originally made from microporous polypropylene (PP) for short-term (hours-long) applications, but are not viable for long-term (days-long) uses due to the adsorption of plasma through the pores and the resulting plasma leakage.[46] This happens when blood plasma enters the gas portion of the oxygenator through the micropores. This problem led to the development of commercial artificial lungs made with polymethylpentene (PMP) hollow fibers. PMP

fibers have a thin, tight membrane that separates the blood and gas phases of the membrane oxygenator and eliminates nearly all plasma leakage.[46,116,187]

1.1.3.1 Extracorporeal Membrane Oxygenation (ECMO)

At the moment, extracorporeal membrane oxygenation (ECMO) is used as a means of support for patients that are suffering from respiratory disease. During ECMO, the patient's blood is drained from the vena cava or femoral vein, through a membrane oxygenator that provides gas exchange, and then reinfused to the patient's venous or arterial circulation. Common methods of cannulation include veno-venous (VV) femoral-femoral, veno-arterial (VA) femoral-atrial, and single dual-lumen catheter. VV-ECMO is often used to support patients with hypoxemic and hypercarbic respiratory failure as it provides both oxygenation and CO_2 removal. Veno-arterial (VA) ECMO returns blood to a large artery and provides respiratory and cardiac unloading and provide support for patients with cardiac circulatory failure.

ECMO as a bridge to transplant has increased in recent years, with excellent results as an outcome of revision of how lungs are more often allocated to patients on ECMO. Patients on ECMO are rated with a higher urgency and thus receive lungs in a much shorter time frame. Hakim et al. describes a study in which the use of ECMO as a bridge to transplant results in a 87% success rate, and a one-year and 3-year survival at 85% and 80%, respectively.[86] These outcomes are comparable to the national average of bilateral lung transplantation.[203]

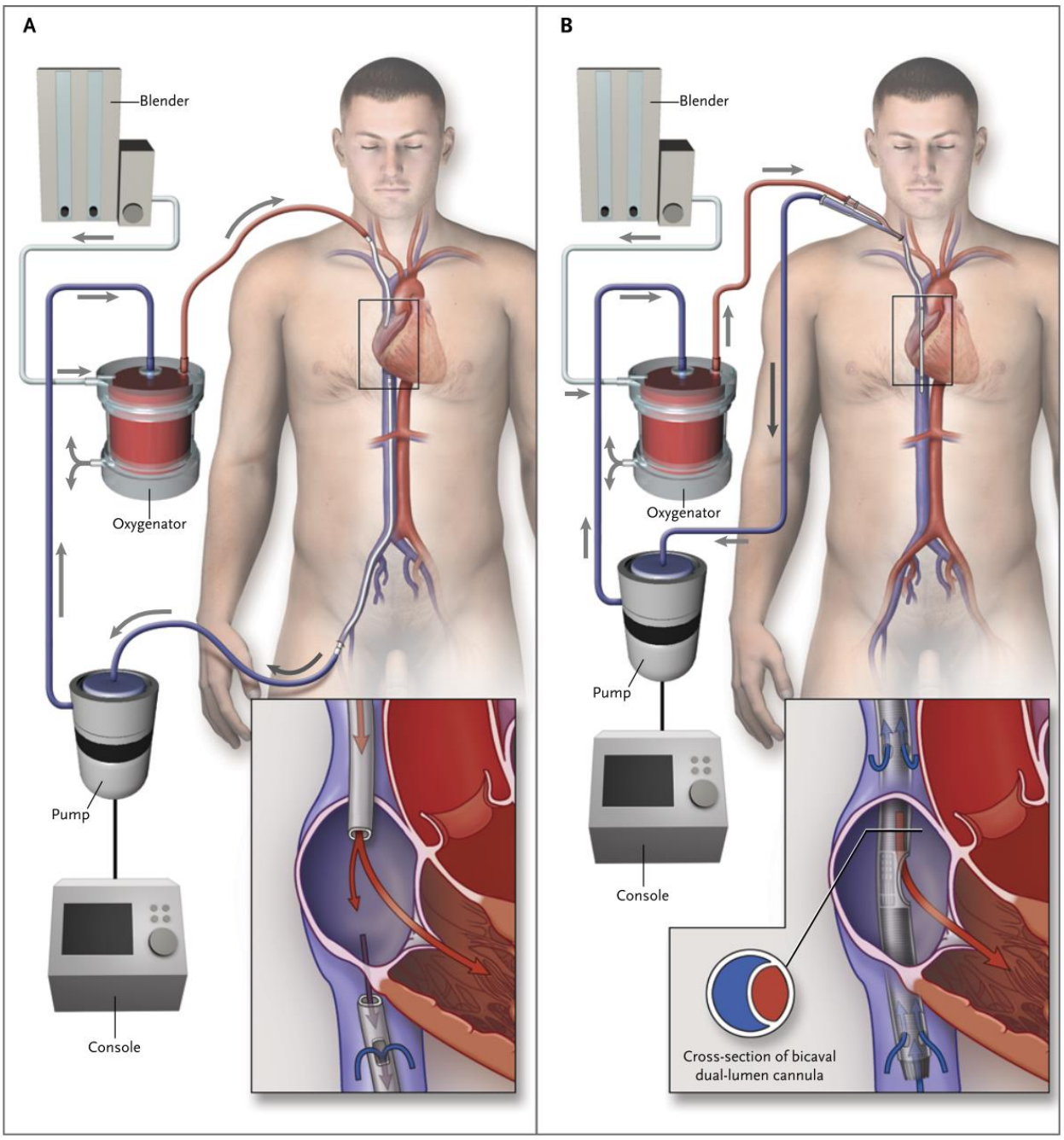

Figure 1-2. Two approaches for venovenous ECMO. The first depicts cannula inserted into the internal jugular vein and the femoral vein (A). When flow is started, blood is drawn from the femoral drainage cannula into the pump, passing through the oxygenator before it is reinfused into the internal jugular cannula. The second depicts a single cannulation site, using a double lumen cannula for both drainage and reinfusion (B). Reproduced with permission from Brodie D, Bacchetta M, *N Engl J Med* 2011, Copyright Massachusetts Medical Society.

There is significant variability in anticoagulant use across centers that use ECMO. In particular, the risks of bleeding from long-term use of anticoagulant drugs have limited ECMO from evolving from a bridge to transplant to a destination therapy.

1.1.3.2 Extracorporeal Carbon Dioxide Removal ($ECCO_2R$)

$ECCO_2R$ is a variant of VV-ECMO, in which only carbon dioxide is removed from the blood using ELS systems. Since carbon dioxide has higher solubility and diffusivity in blood than oxygen, lower flow rates (< 1L/min) and smaller catheters can be used. The most common cannulation options are veno-venous (VV) or arterial-venous (AV). In the VV setup, an appropriate low flow pump should be used. Alternatively in the AV setup, blood is sent to an oxygenator from an artery and flow is driven by arterial pressure. In this instance, an arterio-venous gradient of 60 mmHg and a sufficient cardiac output must be maintained to avoid hypotension.[111] A local Pittsburgh start-up company, A-Lung, capitalizes on the VV $ECCO_2R$ mechanism in their Hemolung RAS system.[4] $ECCO_2R$ is mainly used in patients with hypercarbic respiratory failure, as seen in COPD or patients requiring ultra-protective ventilation strategies for acute respiratory distress syndrome. However, $ECCO_2R$ cannot provide oxygen transfer, and thus is not a viable option for long-term support of chronic lung disease patients.

1.1.4 Artificial Lungs

Recently, researchers have developed a novel design for artificial lungs intended for long term use. Rather than a bridge to transplant, these low resistance devices are designed for destination therapy. In particular, a thoracic artificial lung (TAL) has a pumpless configuration that can allow for more mobility and the same respiratory support as a conventional oxygenator in an ECMO circuit. The low resistant gas

exchanger is connected to a pulmonary artery to left atrium (PA-LA) configuration, or a pulmonary artery to pulmonary artery configuration. Flow is driven by the right ventricle, which eliminates the large circuit and a pump that can mechanically damage and activate blood. The MC3 Biolung is a TAL with a 1.8 mmHg/(L/min) resistance that has been successfully used in a 7-day and 30-day study in sheep. Even without the employment of an antithrombogenic surface coating, the MC3 Biolung supported a sheep for 30 days.[161] However, during this experiment the Biolung was replaced every 9.5 days on average due to thrombus formation. A new version of the TAL, the cTAL, has a compliant housing and an angled inlet and outlet that dampens the effects of a pulsatility on flow as well as lowers the resistance.[163,169] Skoog *et al* have shown the cTAL to be successful in a 14-day sheep study without the use of antithrombogenic surface coatings, and also have no detrimental physiological effect on sheep hematology.[175] Ultimately, coagulation still occurs in artificial lungs and is the main reason why many blood contacting devices need to be removed and replaced.

1.2 Blood Compatibility in Medical Devices

While promising, the performance of these artificial lungs could be further enhanced by employing anticoagulant and antifouling therapies as well as by studying the origin of clot formation in the artificial lung hollow fiber bundle to inform future designs. More than 200 million blood contacting medical devices are being used worldwide, with most using the same clinical materials available since the 1950s.[151] To this day, the problem that still persists is early thrombotic formation on blood contacting surfaces leading to early device failure and patient complications. Clot formation in artificial lungs is especially difficult to prevent due to the large, relatively dense, gas

exchange membrane surface area. In these devices, clot formation leads to decreased gas exchange efficiency, high blood flow resistance and shear stresses, and risk of thromboembolism. During ECMO, the device needs to be replaced after 1-4 weeks of use, despite the use of systemic anticoagulants and surface coatings.[30,64,89,127,179] These anticoagulants also create a significant risk of bleeding complications to the patient, with 30% to 60% of patients having a significant bleeding event. [45,130,138,166] To better understand how to prevent clot formation in medical devices, the intricacies of coagulation at an artificial surface are described below.

1.2.1 Coagulation Cascade

The coagulation cascade describes the mechanisms behind blood clot formation, and is a series of enzymatic reactions that results in a stabilized fibrin network that is clot. There are two pathways, the intrinsic and extrinsic pathway, that combine to form the common pathway. The extrinsic cascade characterizes the formation of clot originating from vessel injury and from tissue factor (TF). It is what causes a clot to form one's tissues. The intrinsic cascade initiates clot formation from the artificial surfaces found in medical devices and the activation of factor XII. Both pathways lead to the common coagulation pathway, which starts with factor X and the conversion of prothrombin to thrombin, which activates platelets and cleaves fibrinogen into fibrin. Cross-linked fibrin then forms a solid clot.

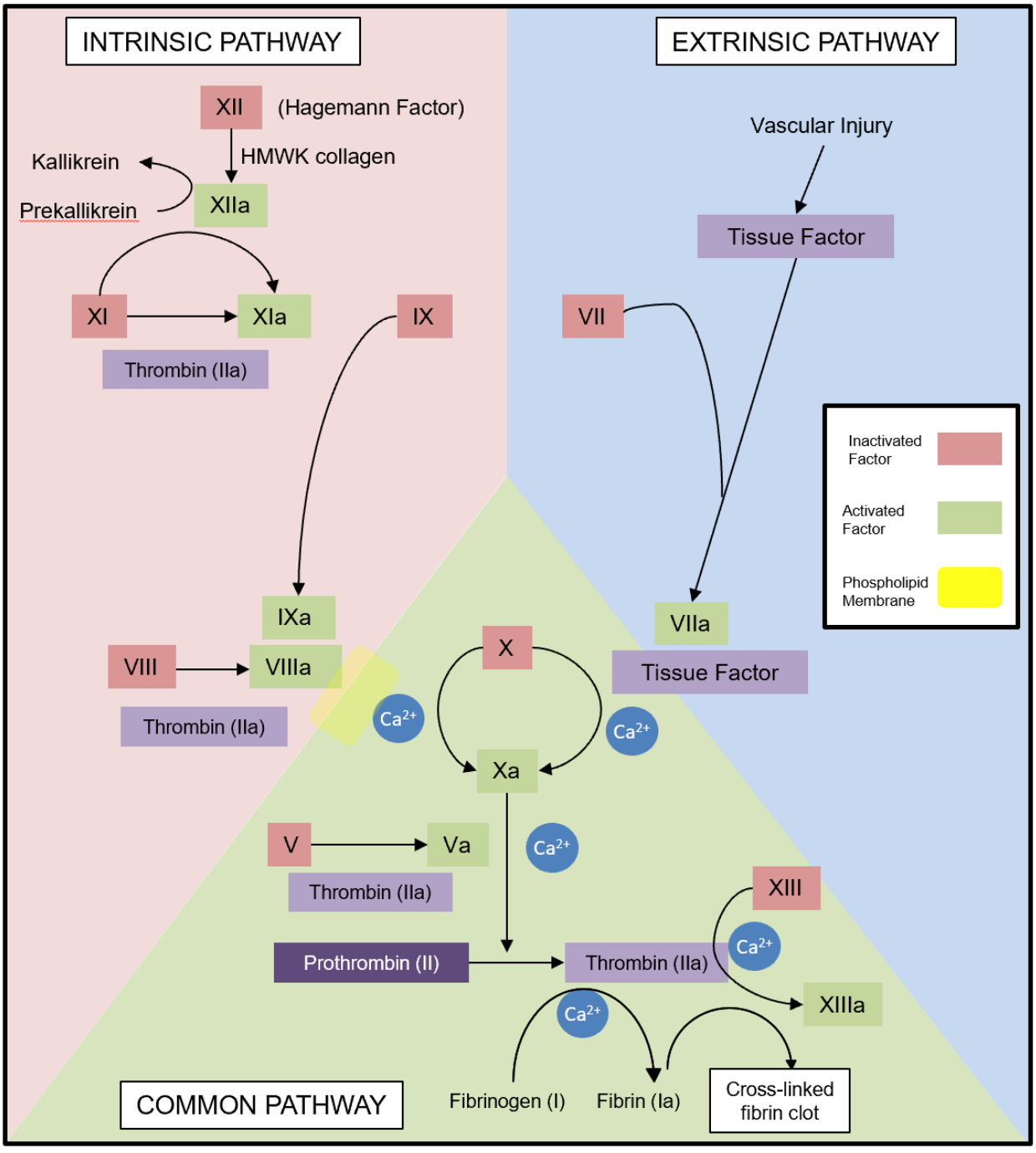

Figure 1-3. The coagulation cascade is initiated by an artificial surface (intrinsic pathway) or a tissue based injury (extrinsic pathway). Factor Xa is the gateway for both pathways to join at the common pathway, which ultimately leads to a cross linked fibrin clot.

1.2.1.1 Intrinsic Pathway: Surface activation

The intrinsic cascade is initiated by blood contact on artificial surfaces, and thus is also called the contact pathway. As soon as blood contacts the surface, plasma proteins are immediately adsorbed (< 1 sec) and form a monolayer of bound proteins. Additionally, factor XII (FXII) changes conformation after contact with an artificial surface, which results in the generation of an active form of FXII (FXIIa). This activated enzyme then activates plasma prekallikrein to kallikrein. This kallikrein then continues to activate FXII, and the FXIIa continues to activate prekallikrein, in a feedback loop. The generated FXIIa also binds to its substrate FXI and activates it to FXIa, Next FXIa protolysis on FIX to FIXa which then forms the intrinsic tenase complex with FVIIIa on the membrane surface, which ultimately activates FX to FXa. FXa then leads to the common pathway of the coagulation cascade, which ends in thrombin generation and clot formation.

1.2.2 Platelet Activation

In blood, platelets are also activated by the artificial surface. The platelet is a small, non-nucleated cell that becomes activated due to a variety of factors such as biological agonists like adenosine diphosphate (ADP) as well as physical agonists such as shear rates. Once activated, platelets express various surface integrins that facilitate binding to one another (i.e. aggregation) and to proteins that are adhered to an artificial surface, contributing to clot formation. Platelet-platelet aggregation and platelet-surface adhesion has been demonstrated via multiple ligands, such as von Willebrand factor (VWF), fibrinogen, and fibronectin. This interaction is mediated by the platelet surface integrin $\alpha II_b\beta_3$. At low shear rates, fibrinogen is the dominant ligand, and bridges between integrin $\alpha II_b\beta_3$ on the surface of adjacent platelets and stabilizes thrombus.[162]

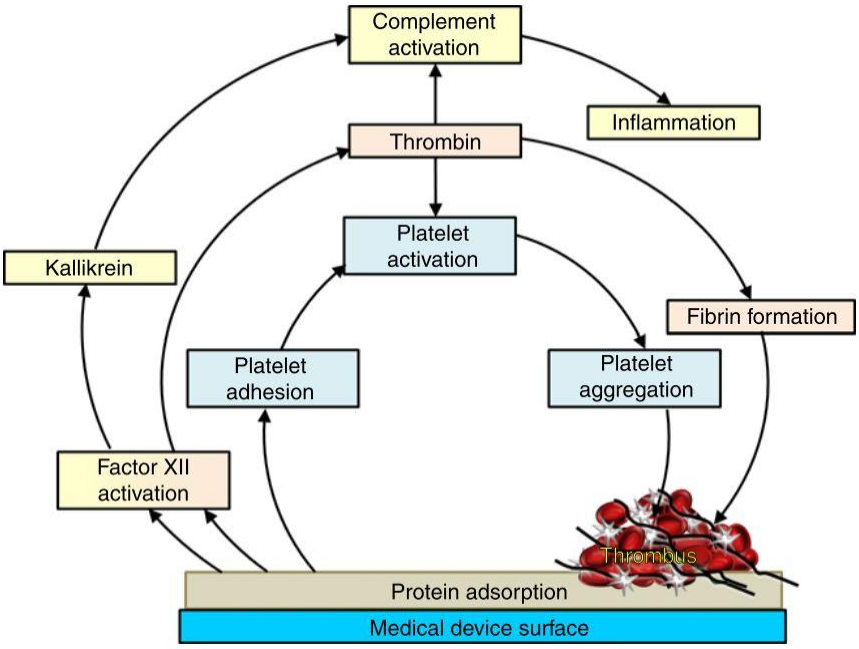

Figure 1-4. Blood contacting medical device associated thrombosis. Protein adsorption on the artificial surface results in platelet activation, adhesion, and aggregation. Contact pathway activation also results in platelet activation from thrombin and fibrin strands binding to platelet surfaces. Used with permission from *J Thromb Haemost,* 101, V.2, Jaffer, I.H. and Weitz J.I., Medical device-induced thrombosis: what causes it and how can we prevent it?, pp 682-689, Copyright (2015), with permission from Elsevier.

VWF plays a major role in initiating aggregation under high shear rates (> 1000 s^{-1}) by binding to platelet membrane integrin $\alpha IIb\beta_3$ and glycoprotein (GP)Ib. The platelet membrane also expresses several G-protein coupled receptors for agonists such as adenosine diphosphate (ADP), thrombin, thromboxane A2, and calcium (Ca^{2+}).

Once activated, platelets accelerate coagulation by releasing small vesicles filled with agonists, called granules, and by cytoplasmic Ca^{2+} release. The increase in intracellular Ca^{2+} results in the formation and reorganization of cytoskeletal filaments inside the platelet, causing the formation of spreading with lamellipodia and filopodia, and also promotes integrin $\alpha IIb\beta_3$ clustering and increased receptor avidity.[97,172] Platelet membranes also further express receptors for increased adhesion, such as p-selectin. There are two types of granules that are released by platelets. Alpha granules contain

soluble proteins and membrane-bound proteins that fuse with the platelet membrane, such as p-selectin, fibrinogen, and von Willebrand factor, increasing the expression of coagulation cascade cofactors and enzymes.[170] Dense granules contain large concentrations of ADP, adenosine triphosphate (ATP), serotonin, and calcium. As these granules are released, the intracellular space is inundated with agonists and activation factors, causing a positive feedback loop as platelets in the local environment are also activated and release their own granules, aggregate, and adsorb to a surface.

1.3 Preventing Clot Formation in Artificial Lungs

1.3.1 Anticoagulant Therapies

Contact with synthetic, non-endothelial surfaces, shear stresses, turbulence, and cavitation forces can all activate the coagulation cascade. Due to the several square meters of artificial surface that is exposed to blood, the use of an anticoagulant is absolutely required during ECMO and ELS. Anticoagulants can target the intrinsic, extrinsic, or common branches of the coagulation cascade, or target platelets and how they interact with proteins and one other. Anticoagulants all have various half-lives in the body and thus all induce different effects when in use for long-term. Anticoagulant drugs with a shorter half-life can be easily reversed and will have a lower chance of causing a hemorrhage, but also need to be constantly infused to maintain the same effect. These anticoagulant agents range from endogenously produced molecules to synthetically made drugs that mimic those effects.

1.3.2 Heparin

Unfractionated heparin is the default anticoagulant used for ELS, but is not an ideal drug. It works by binding to antithrombin III (ATIII) and forming a complex that

accelerates the inactivation of coagulation enzymes thrombin (factor IIa), factor Xa, and factor IXa by approximately 1000 fold.[16,92] Of these factors, thrombin is the most sensitive to heparin/ATIII inhibition. Unfractionated heparin has a relatively short half-life of 60-90 minutes, and the low molecular weight heparin (LMWH) has a half-life of 4-5 hours. As such, LMWH can be administered once or twice a day, and unfractionated heparin can be infused continuously. Heparin is used two ways in the context of ECMO. First, heparin is first bolused into the system for cannulation, and then supplied as a constant infusion at rates of 25-100 U/kg/hour.

The use of heparin is a challenging balancing act, teetering between too much systemic anticoagulation putting patients at risk for bleeding events, or too little which cannot prevent thrombosis. In some cases, patients experience both risks as well. Bleeding events have been estimated to occur in 30%-60% of ECLS patients, and transfusion requirements are also substantial. In the multi-center Mazzeffi study, inhospital mortality of patients on ECMO that had a bleeding event increased as well with a crude odds ratio of 2.22.[130] Because of this high risk of bleeding, narrow therapeutic window, and need for frequent monitoring, there is a need for safer anticoagulants.

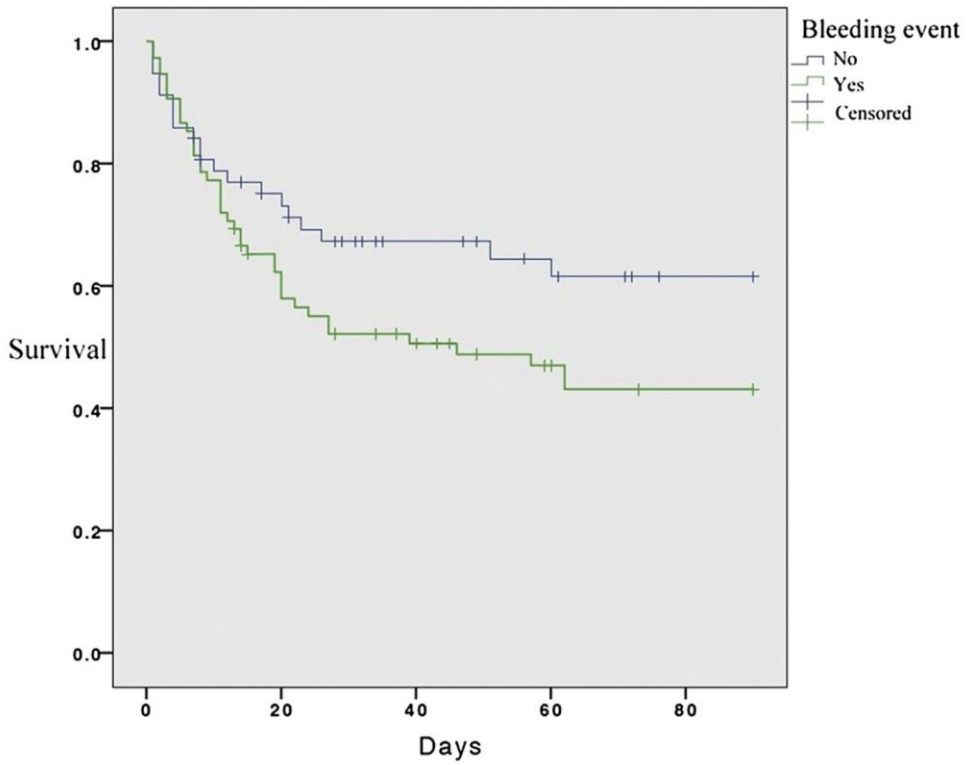

Figure 1-5. Kaplan-Meier survival curve for the Mazzeffi study. The patients who experienced a bleeding event had lower survival than patients that did not experience a bleeding event. Reproduced from The Annals of Thoracic Surgery, Vol 101 Issue 2, Mazzeffi M., Greenwood J., Tanaka K., et al., "Bleeding, Transfusion, and Mortality on Extracorporeal Life Support: ECLS Working Group on Thrombosis and Hemostasis", pg. 682-689, Copyright (2016), with permission from Elsevier.

1.3.3 Direct Thrombin Inhibitors

As the name implies, direct thrombin inhibitors (DTI) target the activity of thrombin (also known as Factor IIa). DTIs can act upon thrombin directly, without needing a cofactor like heparin. These have been utilized in ELS circuits when heparin is not recommended to be used, such as a heparin-induced thrombocytopenia. The mechanism of action is these DTI can bind to thrombin even when they are enmeshed in a clot, as well as in plasma. The first DTI available for patients was argatroban, first discovered in 1981. Argatroban has a small size (~500 Da), can be cleared solely through hepatic mechanisms, with a half-life of around ~50 minutes. Patients receiving argatroban during ECMO have experienced similar thrombotic complications compared

to others on heparin therapy.[32] Another DTI drug is bivalirudin, and is a slightly larger molecule (~2000 Da) that needs to be delivered intravenously. The half-life of bivalirudin is around 30 minutes due to its partial enzymatic cleavage, which is attractive for short term procedures.[127] In an ECMO setting, only small case reports and single-center retrospective reviews have been generated to describe bivalirudin use. These mainly demonstrate no difference in bleeding and thrombotic complications when compared to heparin use and is feasible to use given that the patients are also closely monitored. The primary disadvantages of using DTIs in the context of ELS are the lack of standardization and experience using these drugs as well as there still being a risk of bleeding and clotting.[3]

1.3.4 Nitric Oxide

Nitric oxide (NO) is an endogenously produced uncharged lipophilic messenger molecule in vertebrates, regulating many processes such as blood flow, neural communication, and, of most interest to this field, thrombosis. NO acts upon platelets by diffusing through the plasma membrane and binding to guanylate cyclase. Once activated, guanylate cyclase will promote the conversion of guanosine triphosphate (GTP) to cyclic guanosine 3'-5' monophosphate (cGMP). The increase of cGMP in the intracellular matrix decreases Ca^{2+}, which inhibits platelet aggregation and activation. Binding of NO to guanylate cyclase increases cGMP levels which inactivates platelet surface adhesion receptors like glycoprotein IIb/IIIa, and p-selectin. An increase of cGMP also causes a structural change that reduces platelet efficiency.[26,75,152]

However, these platelets regain functionality within seconds as the half-life of NO is only 0.05-2 ms in whole blood.[105,152] This specific trait allows for local anti-platelet

effects, only where NO is being delivered, which then provides anticoagulation activity sequestered only on the artificial surface and does not act systemically. This local inhibition is perfect to be leveraged in a blood contacting medical device such as the artificial lung. Delivery of NO through the ECMO circuit surface has demonstrated retention of platelet functionality, such as local platelet inhibition, reduction in platelet surface binding, and retention of platelet function away from the delivery surface. The short half-life of NO in whole blood is the is due to its almost immediate uptake by hemoglobin and also leads to the main downside of using NO, which is methemoglobin formation.[108,127,152] This form of hemoglobin transfers oxygen less efficiently and is elaborated upon in section 1.4.4.4.

While all properties of the endothelial vessel wall are not likely to be duplicated in a synthetic material, the production of NO at a synthetic material surface has been created using various different approaches for blood bearing medical devices.

1.3.4.1 Biomaterials Loaded with Nitric Oxide Donors

Nitric oxide donors (NO-donors) are functional moieties or small drugs that can generate NO after exogenous administration. There are four classes of widely used NO-donors, namely, diazeniumdiolates, S-nitrosothiols, metal-nitrosyl complexes, and nitrobenzene derivatives.[106] These donors have been incorporated into many materials to aid delivery. In the context of this thesis, we will restrict discussion to just S-nitrosothiols due to their wide use in medical applications.

Naturally occurring S-nitrosothiols (RSNOs) are found in plants and animals, such as S-nitroso-L-glutathione (GNSO) and S-nitroso-L-cysteine (CysNO), and consist of a molecular bond between a thiol and nitric oxide (S-NO).[78,194] NO is released from S-

nitrosothiols due to the degradation of that bond at room temperature, but can be catalyzed by heat, UV light, transition metals, and ascorbate.[123,147,174] These modulating factors have uniquely allowed for controlled release of NO from RSNOs in many different forms. In the context of medical devices, this has been applied in blood contacting surfaces of catheters for anti-platelet effects.[23] Numerous *in vitro* and *in vivo* studies have shown that NO released from doped surfaces reduce platelet adhesion, and that they instead remain in circulation instead of being recruited to a clot.[1,2,24,209] E.J. Brisbois *et al* applied various surface coatings doped with RSNO to a rabbit model for four hours of extracorporeal circulation. This surface coating did prevent platelet consumption into clot when compared to the control circuit and significantly reduced the thrombus formation for NO-doped surfaces.[21] Despite this positive result, this study and others showed that there was a burst of NO release at the first day of around 10 - 30 x 10^{-10} mol min^{-1} cm^{-2}, and then the NO release on subsequent days is much less , around 0 - 5 x 10^{-10} mol min^{-1} cm^{-2}.[87,124,147,156] However, these materials all contain a defined reservoir of NO, thus limiting the duration of NO release or generation and making them insufficient for long-term applications.

1.3.4.2 Surface Generated Nitric Oxide

Device-localized anticoagulation via biomaterial-based surface NO flux can also be provided using a transition metal catalyst as a potential means of slowing device failure without increasing the risk of bleeding. In the field of artificial lungs, NO has been delivered via sweep gas or catalytically generated by copper containing materials contacting blood.[6,7,21,22,71,84,200] This approach mimics the natural endothelium, with NO fluxes into the blood ranging between 0.5-4 x 10^{-10} mol cm^{-2} min^{-1}.[23,192] For blood bearing devices, Cu can be incorporated into polymeric surfaces easily and used to

decompose S-nitrosothiols in a predetermined area. When used this way, Cu can cycle in a reduction-oxidation reaction seen in equations (1) and (2), where RSNO, RS^-, and RSSR represent a S-nitrosothiol, thiolate anion, and disulfide, respectively.

$$Cu^+ + RSNO = Cu^{2+} + RS^- + NO \quad (1)$$

$$Cu^{2+} + 2RS^- = 2Cu^+ + RSSR \quad (2)$$

As a stoichiometric reaction, the rate of NO release can be controlled with the availability of NO donor and how much Cu is exposed to the donor. This reduction-oxidation reaction can cycle indefinitely if there is a supply of the NO donor. In larger devices, such as ECMO circuits, the transition metal catalyst will quickly catalyze all endogenous sources of NO. In these settings, NO generation is maintained through intravenous delivery of NO-donors, preferably immediately upstream of the Cu containing surfaces.

1.3.4.3 Gaseous Nitric Oxide Delivery

Another means of delivering NO in an artificial lung is to use gaseous NO (gNO). Inhaled NO therapy is already used clinically as a means to induce vasodilation, decrease pulmonary vascular resistance and pulmonary arterial pressure, and improve oxygenation.[74,82] Recent data also suggests that inhaled NO can inhibit platelet aggregation. In a study by Gries *et al*, inhaled NO gas at concentrations ranging from 100 – 884 ppm inhibited platelet aggregation, p-selectin expression, and fibrinogen binding to the GPIIb/IIIa receptor.[82] Thus, if gNO can be included in the sweep gas of an artificial lung, it can also provide these antithrombotic effects to the artificial lung.

In a study by Keh *et al*, the use of 20 ppm NO in the sweep gas through a membrane based lung in an *in vitro* ELS circuit reduced platelet trapping and activation and preserved platelet function.[104] Another study by Rauch *et al*. also applied 20 ppm

NO gas in 8 silicone membrane oxygenators and found that platelets in the circuit were preserved instead of being incorporated into clot.[152] Since these are *in vitro* studies, the low dose NO gas does not get consumed or converted into other nitrogen products at the same rate as an *in vivo* circuit. The lack of hemoglobin and denitrifying enzymes in a closed system also prolong and amplify the effect of NO. Thus, delivery of gaseous NO in a single pass or *in vivo* experiment would require a higher dose of NO.

Demarest *et al* has conducted a study with various sweep gas NO concentrations, ranging from 100 ppm – 500 ppm, in an *in vivo* VV-ECMO rabbit model. Results show that the 250 ppm range is effective at both inhibiting platelet activation without causing toxic effects in this model.[50]

1.3.4.4 Risks of using NO

Nitric oxide is reactive due to its highly oxidative nature and it is dangerous in biological systems at high concentrations for its ability to diffuse through cellular membranes easily from being lipophilic. The main risk from using NO is its interaction with hemoglobin in the blood to form various derivatives. The short half-life of NO in blood may be due to the strong affinity NO has for the ferrous heme molecules in red blood cells.[26] These hemoglobin-NO reaction products influence whole blood oxygen affinity. NO combines with reduced hemoglobin 5-20 times faster than oxygen, and additionally has a half-time dissociation of the first NO molecule from Hb_4NO_4 at 19°C and pH 9 is 8 hours.[105] This bound form of NO to hemoglobin is also known as methemoglobin (metHgb), and is the most worrisome product. Once one NO molecule is bound to one of the four heme groups in hemoglobin, the remaining heme groups have a higher affinity for oxygen, thus, it is more difficult to release oxygen to tissues. This results in a shift of the oxygen dissociation curve to the left. Patients with a

methemoglobin levels above 1% are diagnosed with methemoglobinemia.[125] While levels below 10% do not show symptoms, higher methemoglobin levels result in cyanosis (>10%), tachycardia (>20%), coma, acidosis and seizures (> 50%), and eventually death (>70%).[196] Current treatment for acute methemoglobinemia is a dose of methylene blue or dextrose therapy, which reduces methemoglobin levels in less than an hour.[184,196]

Another risk from using NO at high concentrations or longer durations is lowered blood pressure.[72,74] However, in inhaled therapy, if it is kept below 100 ppm, there has been no detrimental effects. Applications of NO in systemic vasculature for anti-platelet effects have been purely experimental, and no consensus has been developed yet. This is partially due to the many ways NO is metabolized in the body.

1.3.4.5 Surface Coatings in ECLS Circuit and Artificial Lung

An anticoagulant approach that has a proven track record of success is anti-fouling surface coatings on the ECLS circuit and oxygenator. Many coatings have been commercialized, such heparin coatings. End-point covalent linkage of heparin to polymer surfaces are commercially available, such as the Carmeda Bioactive SurfaceTM, Trilium coating available on Medtronic tubing and oxygenators, and the Bioline coating found on Maquet products. Typically, heparin coatings have less anticoagulant activity when grafted than when circulating. While the ATIII/heparin complex inhibits soluble thrombin, it does not inhibit thrombin bound to fibrin. This means thrombin is being continuously generated and circulated in the ECMO system, which is not an ideal scenario.

Albumin, another successful surface coating, is a protein that provides an initial base layer of protein the delay and mitigate the biological protein adsorption onto a hydrophobic surface. An albumin coating increases the hydrophilicity of a material and is also a competitive protein that fibrinogen would have to replace on the surface.[137,145] Commercially available albumin coatings have covalently linked albumin molecules. These coatings have shown short term reduction in adhesion of platelets and fibrinogen. However, many of these effects have not been proven to last in the long-term, as applications of the albumin coating thus far have been for cardiopulmonary bypass (Safeline by Maquet).

Polymer surfaces have also been developed to increase hydrophilicity of a surface, and to create materials with a surface charge similar to that in endothelial cells. Three such polymers are phosphorylcholine (PC), polyethylene oxide (PEO), and poly 2-methoxyethylacrylate (PMEA). PC is a zwitterionic phospholipid compound that is found endogenously on cell membranes with non-thrombogenic effects. [32] In membrane oxygenators, PC has successfully been used to coat polypropylene and polymethylpentene artificial lungs and reduce fibrinogen and platelet binding.[155] The commercial name for this is P.h.i.s.i.o by Sorin. The second polymer, PEO, increases hydrophilicity and decreases fibrinogen and albumin adhesion by 90%. (36,37) While PEO has been found to reduce inflammatory markers and bleeding events, there were instances of increased stroke rates in a CPB circuit.[61,126,177] PEO is a single layer coating, and there will always be gaps in the coating which could lead to nucleation of clot. The third polymer, PMEA, is a weakly hydrophilic polymer that reduces platelet and leukocyte activation and adhesion.[183] While PMEA coated surfaces also reduce protein

adsorption and protein conformation, overall studies in vitro and in CPB circuits have been conflicting or have found little to no difference.[110,126,186,190] Surface-modifying additives have also been mixed with polymer resins or incorporated as another coating on blood contacting surfaces to provide antithrombogenic effects.[191] Unfortunately, most of these studies are small, single-center studies with variable sample collection and experiments are short-term.

1.4 Modeling Coagulation and Predicting Clot in an Artificial Lung

Clot that forms within the artificial lung is a significant complication that increases blood flow resistance and risk of thromboembolism, reduces gas transfer and device functionality, and activates blood that is flowing by that may cause more clot to form later in the circuit. In a clinical setting, the imminent change of an artificial lung is both expensive and dangerous but is difficult to predict when it is necessary since clot cannot be visualized inside the hollow fiber bundle and because blood is opaque. In order to reduce the number of device changes, engineers must design artificial lungs with longer functional lifespans by reducing clot formation. As prefaced earlier, surface coatings and anticoagulant drugs are common methods employed to reduce clot by clinicians and researchers. However, design of the artificial lung fiber bundle is not optimized and can be further explored. Current commercial and oxygenators vary widely in fiber bundle design and there is no consensus on how to best design these bundles. One way to approach this is to improve prediction of clot formation inside a membrane oxygenator. By doing so, engineers can design less coagulant devices and reduce the risks from changing out an oxygenator, such as hemodynamic instability, infection, and oxygenation failure.

1.4.1 Current Computational Methods in Artificial Lungs

Engineers use computational models to assist in the design of all medical devices, and artificial lungs are no exception. Computational models provide valuable insight to how blood moves through the fiber bundle under clinically relevant flow conditions. Solving for fluid flow in a full-scale fiber bundle is computationally expensive but achieves insight into an artificial lung that otherwise may not be possible (Figure 1-6).[129]

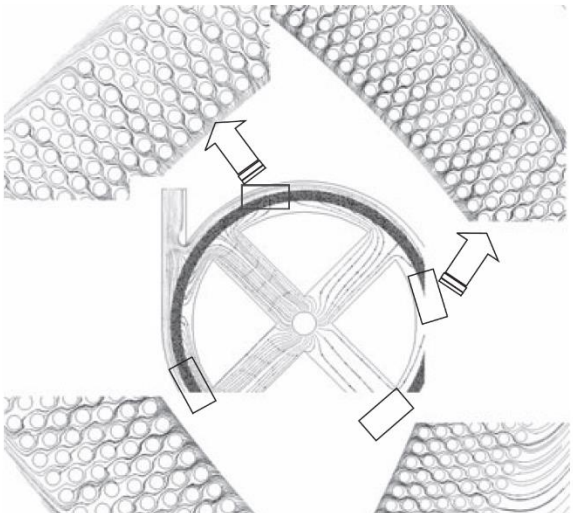

Figure 1-6. Fluid flow path lines in an oxygenator fiber bundle, flow is from the center towards the outer edge. Reproduced with permission from Ahmadi G. and Mazaheri A.R., Artificial Organs 2005, Copyright John Wiley and Sons.

In a study by the Wu group at University of Maryland, 3D computational models of three different types of hollow fiber bundles were run. These studies showed different fiber arrangements significantly impacted wall shear stress, an important factor in platelet activation. The results also showed the three dimensional effect is not negligible, as velocity and shear stress distributions varied significantly along the fiber axial direction.[206] Thus, different fiber arrangements may then result in different local blood dynamics, leading to varied regions imparting different shears and activation on cells,

leading to different patterns of clot formation. However, the details of this are still unknown as computational fluid dynamics (CFD) does not predict coagulation.

Current understanding of clot formed inside fiber bundles has been limited to two methods, (1) opening clinical and experimental devices after explantation, and (2) measuring surrogate markers for clot formation inside the artificial lung while the device is in use. After devices are removed due to failure, clot in the fiber bundles can be measured by extracting values from clot mass and dimensions. In some experimental cases, the fiber bundle is broken down into 3 or more parts, and then imaged, scanned, or weighed individually to provide clot composition.[59] Computed tomography has been used in small single-center studies to provide accurate measurement of clot formation in clinical devices such as the Quadrox Permanent Life Support membrane oxygenator.[51,52] While the second method of measuring markers related to clot formation does not directly relate to the volume of clot inside a membrane oxygenator, they can reveal in real-time some aspects of clot formation such as relative rates of deposition. However, these analysis methods do not lend much information to improve designs as these commercial and research devices vary widely and cannot be compared together.

1.4.2 Computational Models for Predicting Clot

Clot formation is a complex dance of interrelated biochemical and hematological factors that interact and cause a cascade of coagulation downstream, effects that balloon out to other feedback mechanism that span thousands of unique factors and cells. When designing a computational model to simulate clot formation, there is a tradeoff between complexity and functionality. A model that is too simple may not

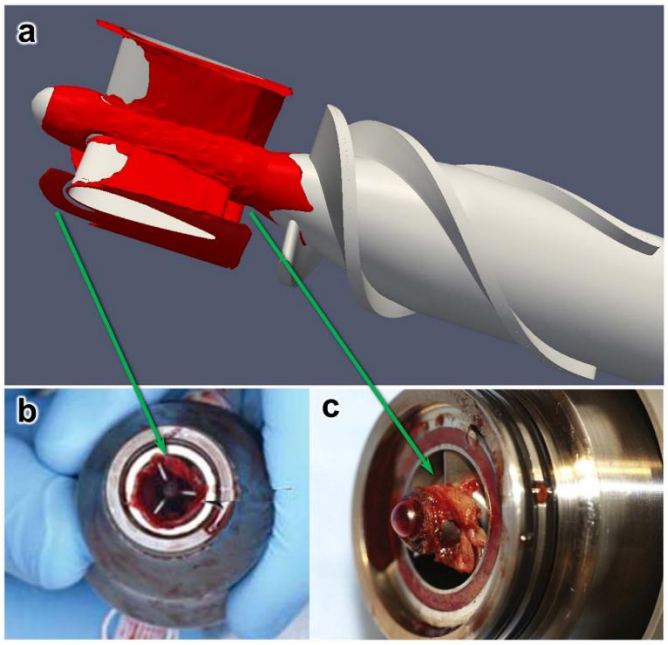

Figure 1-7. (a) Simulated thrombus in a Thoratec HeartMate II inlet straightener and clinical observations of clot in (b) and (c). Reproduced with permission under the Creative Commons License from Wu W., Yang F., “High fidelity computational simulation of thrombus formation in a Thoratec HeartMate II continuous flow ventricular assist device”, *Nature Scientific Reports* (2016).

capture the interactions that are critical to clot. On the other hand, a model that is accurate but too complex may not be feasible to compute.

The most recent thrombus deposition model by the Antaki group is a strong example of what is possible when predicting clot formation. This model developed by Wu *et al.* uses a convection-diffusion-reaction equation to simulate the transport and reactions of 10 chemical and biological species. These species are agonists ADP, thrombin, thromboxane A2, the protease ATIII, and platelets in activated and resting forms that are either free flowing or deposited in a clot.[197] This model successfully simulated three dimensional thrombus deposition in a small crevice and in a blood vessel. Results showed high fidelity to the experiments it was based off of. This model has also been applied to thrombus formation in the clinical example of the Thoratec

HeartMate II continuous flow ventricular assist device (Figure 1-7).[199] This model accurately predicts clot deposition in high shear and high flow environments and can be used to inform design changes in new medical devices under similar conditions.

So far, there has yet to be a computational coagulation model that has been applied to an artificial lung hollow fiber bundle. The challenge comes from the complex geometry within the fiber bundle, which consists of thousands upon thousands of hollow fibers that are all laid out in various shapes and have all different dimensions. In order to apply a computational model to an artificial lung, a much simpler geometry and a shorter time frame must be targeted. Once a clot formation model is applied to an artificial lung fiber bundle, experiments must be completed to validate its accuracy and to improve and optimize the model.

1.5 Infection During ECMO

Although ECMO has efficacy in many clinical scenarios, patients experience significant associated risk which include acquiring an infection during use. These cases all may induce consequences on the ECMO patient, from prolonged need for bypass support, increased risk of mechanical and patient related complications, and increased inhospital mortality.[36,53,132,144] During ECMO, patients are particularly prone to infections due to venous and arterial lines and cannulas and the host's compromised immune function, with infection rates up to 45% in retrospective studies.[36,76,88] The ECMO circuit also includes a large artificial blood contacting surface, including many areas with low blood flow velocities that aid surface bacterial colonization.[109,136] While infections are usually kept at bay with antibiotics, nosocomial infections in ECMO patients are a major complication for critically ill patients. These nosocomial infections in ECMO patients

manifest mainly as coagulase-negative staphylococci (15.9%), *Candida* (12.7%) and *Pseudomonas aeruginosa* (10.5%).[15] In a multicenter ECMO study, infected patients had a 16.1% higher chance of death.[15,47] Nosocomial infection also occurs at a higher incidence in ECMO survivors, indicating increased risk because of a prolonged in-hospital stay.[182] While the cause has not been established, it is likely due to a depleted white cells in the immune system from long-term ECMO use. Thus, antimicrobial therapy must be investigated for ECMO patients as it becomes more frequently used as a bridge to transplant or destination therapy.

The original source of infection is sometimes difficult to place, but cultures of the circuit and membrane oxygenator revealed percutaneous and transdermal support apparatus, such as central venous catheters, endotracheal tubes, and urinary catheters, were locations where bacteria were found. However, of most concern are adhered bacteria in the membrane oxygenator due to the potential for biofilm formation and further infection. These bacteria can form a protective extracellular material that envelops the bacteria colony and acts as a physiochemical barrier to antibiotics from penetrating and reaching the bacteria cells.[40,47,69] In the case of a membrane oxygenator, the coverage could also ultimately prevent gas exchange. In a study by Kuehn *et al*, bacteria were detected on the surface of 45% of the membrane oxygenators in the study, and those same species were also found in blood culture.[109] In this study, patient received antimicrobial treatments, and so the remaining bacteria found on the oxygenator fiber surfaces had adhered and potentially started colonization. This localization of bacteria on the membrane oxygenator demonstrates a need for surface-based methods for preventing adhesion.

1.5.1 Current treatment

Antimicrobial approaches for ECMO patients have mostly been restricted to infection prevention using antibiotics and cannula maintenance techniques. Based on multi-center surveys, there is no current consensus on prophylactic antibiotic use for ECMO patients, with each program independently developing their own protocol for prophylaxis and infection surveillance.[55,76,102] In many cases, the broad spectrum bundled prophylaxis has led to the emergence of antibiotic-resistant strains of bacteria and fungi.

The same causal organisms in ECMO were determined to be the same commensal species of bacteria and fungi for infection of other support apparatus, and are responsible for the majority of non-ECMO device and procedure-related healthcare-associated infections.[91] Thus, if the strategies utilized to prevent central line-associated blood stream infections, ventilator associated pneumonia can also be adopted and applied to the ECMO population, it may serve to reduce the risk of infections and their associated complications.

Experimental surface modifications to prevent bacterial adhesion for implants have been developed, but none so far for the membrane oxygenator. Research in this area in the past decade have focused on surface adsorption of, and bulk material incorporation of, one or two antimicrobial agents and increasing the hydrophilicity of a surface. Various hydrogel coatings have been created for their hydrophilic properties, and also for their ability to hold and release antibiotics as a result of the high water potential.[100] Central venous catheters (CVCs) have also been made with different antibiotics impregnated in the polymeric material, including nitrofurazone, gentamiacin,

norfloxacin, and minocycline-rifampicin (MR). This last antibiotic, MR, has significant success in reducing gram positive and negative bacteria activity on CVCs as well as catheter related blood stream infections.[47,90,117] Another approach is to create a hydrophilic coating that can resist bacterial adhesion in a wet environment. Currently, hydroxyapatite (HA) and zwitterionic carboxybetaine coatings have shown antifouling properties in short term applications by creating a hydration layer to reduce protein adhesion, and thus also bacterial adhesion. However, these have been shown to fail in long-term stability trials and have an uneven layer coating a polymer surface.[114]

One application used multiwall carbon nanotubes bound to a PVC extracorporeal circuit *in vitro* and *in vivo* as an antimicrobial surface. Unfortunately this surface modification led to platelet activation and thrombosis.[73] While these applications have reduced bacterial infection in implanted medical devices, there have only been a few that can work for an ECMO circuit, due to the densely packed fiber bundle and dynamic flows through the oxygenator.

1.5.2 Nitric oxide as an Antibacterial Agent

An alternate approach to prevent nosocomial infections is to attenuate bacterial colonization of the circuit by providing targeted therapy at the blood contacting interface of the membrane oxygenator. In the last few decades, surface nitric oxide (NO) flux has emerged as both an antithrombogenic and antimicrobial approach for implanted medical devices. Extracorporeal circuits have been experimentally tested with NO release from doped surfaces as well as from surface generation with an exogenous source of NO. Both target the large artificial surface of the membrane oxygenator that is a location of bacterial colonization.

1.5.2.1 Mechanism of Bacterial Regulation by Nitric Oxide

In vitro studies using NO donors show that NO exerts bacteriostatic and bactericidal properties against a wide variety of phyla, including bacteria, viruses, parasites, and even against tumors.[42,83,93,120,139] Since NO is also used as a signaling molecule in bacteria at low concentrations, just as it is in eukaryotes, only higher concentrations of NO exert toxic effects through oxidation. While cellular targets of NO have been identified, specific microbial targets remained unknown. This is due to the many redox forms of NO that exist biologically, and also their complex reactivity.[12,119,121] The main product formed from NO with superoxide is peroxynitrite ($OONO^-$), a highly toxic and reactive molecule that can easily oxidize a range cellular targets. NO cytotoxicity has been recorded in in neuronal cells by exogenous superoxide dismutase, heavily implicating that $OONO^-$ generation in bursts is the mechanism of killing bacteria.[119] Essential enzymes that have an iron-sulfur center can also be bound to NO which can lead to enzyme inactivation. Similarly, NO can also interact with thiols and nitrosation of primary amines on DNA bases which may lead to alterations in protein production and function through deamination.[29,142,195] NO can also interact with systemic molecules to form NO donating compounds such as RSNOs, like S-nitrosoglutathione or S-nitrosoalbumin, two endogenous NO reservoirs. Additionally, RSNOs may also exert antimicrobial effects in the vasculature.[10,96]

1.5.2.2 Nitric Oxide Delivery Platforms for Antimicrobial Effect in Medical Devices

Experimental studies delivering nitric oxide for an antimicrobial effect in medical devices have taken two routes. First is using gaseous NO to target strains such as *Staphylococcus aureus* and *Escherichia coli* from nosocomial pneumonia patients, and

from *Pseudomonas aeruginosa* strains from cystic fibrosis patients.[133] Cyclic treatment with gaseous NO at high intermittent doses successfully killed 100% of bacteria *in vitro*. A study by Sulemankhil et al. successfully used a dressing for wound healing that released gaseous NO to prevent infection *in vitro*.[181] Secondly, polymeric matrices that have doped NO are also being used to prevent bacterial activity (Section 1.2.3.3.1). Most recently, studies show that the controlled release of NO at the surface of an implanted catheter have bacteriostatic and antiplatelet effects *in vivo*.[153] These effects from surface released NO lasted for the 9 days in an in vivo ECC rabbit model, with 95% reduction in viable bacterial colonies and lower thrombus area.[23] However, so far these methods are using a limited sink of NO-donors in a material that will invariably run out, and cannot be applied to long term scenarios such as an artificial lung.

1.5.2.3 Bacterial Response to Nitric Oxide

The mechanism behind nitric oxide signaling in biofilm formation and dispersion is not understood, but investigators have proceeded to use it in applications for antimicrobial effects. Macrophages and neutrophils initiate an antimicrobial response to bacteria, viruses, and their byproducts involving the activation of the NOS2 gene and produces inducible nitric oxide synthase (iNOS). Bacteria also have homologues of both NOS and the heme domain sGC, which are the main routes of how NO influences the eukaryotic system.[10] The bacterial nitric oxide synthase (bNOS) was recently discovered and can also convert L-arginine to L-citruline and NO, just like the eukaryotic NOS can, however, this has not yet been proven *in vivo.*[9] A study by Plate *et al* showed that in *Shewanella oneidensis* bacteria, NO is used in the H-NOX signaling pathway to not only cause biofilm formation, but other protective mechanisms as well.[149] These

similarities between NO processing enzymes in prokaryotes and eukaryotes suggest that bacteria may respond to lower concentrations of NO differently than higher toxic levels. Some forms of Gram negative bacteria have NO reductase enzyme that acts to remove reactive nitrogen intermediates and reactive oxygen intermediates out of the cell. When this removal system is overwhelmed, these intermediates cause damage to DNA, lipids, and proteins.

1.5.3 Copper as an antibacterial agent

As discussed previously, transition metals, such as copper, can be used to catalyze NO generation. Copper is also a 1000-year-old antimicrobial agent that has been used to kill bacteria, and records date the use of it since the medieval times. The antimicrobial use of copper has persisted to today in wide use of copper in intrauterine devices, drinking water vessels, and even socks.[13,19,143,180] The recent ability to incorporate copper into polymeric materials has opened the door to the use of copper in many different medical applications.[35]

1.5.3.1 Mechanisms of Bacterial Regulation by Copper

Copper is an essential trace element that is tightly regulated in the biological systems due to its ability to facilitate oxidation, and thus the application of copper ions in specific conditions can become toxic. A number of mechanisms have been suggested for how copper can cause cellular damage, but it is not clear which one enacts the strongest antibacterial effect. One mechanism is the hydroxyl radical (OH•) that can be generated in a Fenton-type reaction:

$$Cu^{+} + H_2O_2 \rightarrow Cu^{2+} + OH^{-} + OH^{\cdot}$$

This hydroxyl radical can participate in numerous reactions, such as the oxidation of proteins and lipids.[202] An alternative mechanism that causes toxicity is the displacement of iron from iron-sulfur clusters by copper which disrupts the activity of many enzymatic reactions.[122] Copper has also been shown to compete with other metal ions, such as zinc, for important binding sites.[118]

Contact killing involves the direct contact between the cellular membrane of a bacterial cell and a surface that contains copper. Thus, incorporating copper into polymer biomaterials is a common and easy way to create antimicrobial and bacteriostatic materials. As copper is also utilized in bacteria, the mechanisms behind contact killing by copper surfaces seem to depend on the copper homeostasis of the bacterial cell. While not confirmed, copper has been predicted to act upon the membrane in potentially four ways: (1) copper dissolves from the material surface and causes cell damage by oxidizing lipids and proteins, (2) the bacterial membrane ruptures due to a copper stress phenomena, leading to loss of membrane potential and leaking cytoplasmic content, (3) copper ions induce more reactive oxygen species generation, causing further cell damage, and (4) these ROS can also cause genomic and plasmid DNA degradation.[81]

1.5.3.2 Bacterial Response to Copper

Bacteria can develop copper resistance or a copper response.[8] The chief mechanisms of copper tolerance are metallothionein-like copper-scavenging proteins in the cytoplasm and periplasm that round up copper ions in the cell. These proteins then actively expulse copper ions from the cell. In many bacterial membranes, a CopA copper transporting enzyme ATPase removes Cu(I) from the cytoplasm.[154] This enzyme

exists in two forms in Gram negative bacteria, such as *Pseudomonas aeruginosa*. Another mechanisms controlled by the *cueA* gene acts to control the copper level and redox states by protecting other enzymes from oxidation from copper ions.[70,77,79,168,208] These two systems, CopA and CueA, are used by multiple strains of bacteria to detoxify excess copper. Inactivation of the *copA* gene affected copper resistance most strongly.[80] Similarly, in Gram-positive bacteria where no periplasmic space exists, a CopA-type enzyme sits on the membrane and exports copper.[11,178]

1.5.4 Methods for Evaluating Antimicrobial Efficacy

Methods for testing antimicrobial efficacy commonly described in literature are mainly developed to measure the effect of antibiotics. These methods rely on the diffusion of the antibiotic, such as disk diffusion and broth/agar dilution, and do not accurately measure the effect of an antimicrobial surface.[103] In the case of a solid biomaterial surface, there are two conventional measurement methods for antimicrobial efficacy. Firstly, a coupon of the material is excised and swab of known bacteria concentration is streaked onto the surface. After drying and exposure to the biomaterial for a predetermined amount of time, the coupon is then submerged in a media and then vortexed to remove all remaining bacterial cells. Then the samples are plated onto agar plates and surviving bacteria are counted for viable colony forming units (CFUs). A wet assay is similar except there is a droplet of bacteria suspended in media that is applied as a standing droplet onto the coupon and then removed after a specified time for plating onto agar plates. These conventional methods do not reflect the local conditions of a blood contacting medical device.

The *in vitro* model used to test the antimicrobial surface of an implant must, to its best abilities, mimic the *in vivo* environment of a medical device system. Microbial adhesion is a dynamic process with an early stage when microorganisms reversibly interact with an artificial surface by van der Waals forces and H-bonds, and a second stage with irreversible microbial adhesions mediated by specific binding to host proteins (fibronectin, fibrin).[115] The gold standard and most conventional method to quantify bacteria is the viable colony forming unit (CFU) counting assay.

1.6 Summary of Study

The work in this thesis investigates the use of nitric oxide and the material Cu-PDMS to reduce biological fouling on the surface of an artificial lung. Additionally, micro- and macro- scale clot formation is studied *in vitro* to better design hollow fiber bundles. The first aim expands upon previous work using Cu-PDMS and a NO-donor for surface generation of NO to reduce clot formation in an artificial lung. Previous work successfully implemented the surface generated NO in a 4-hour in vivo experiment in a rabbit model. This study extends the duration to 72 hours and a sheep model is used due to a more similar coagulation cascade to a human.[173] Two miniature artificial lungs, one composed of Cu-PDMS hollow fibers and the other with clinical PMP fibers are studied head-to-head in parallel. This setup allows for direct comparisons between the two types of fibers and reduces the influence of animal to animal variability on results. The second aim investigates the same material, Cu-PDMS, and the potential to have a two pronged approach to prevent bacterial adhesion on the hollow fiber membrane utilizing nitric oxide as well as copper that is in the Cu-PDMS membranes. Copper and NO are well known to have antimicrobial properties, however, their ability to inhibit

bacterial adhesion and growth in artificial lungs is not known. Thus this *in vitro* study uses a flow chamber to simulate the relevant flow conditions at the hollow fiber membrane to test this potentially antimicrobial surface. The last aim in this thesis focuses on the micro-scale and macro- scale initiation, progression, and formation of clot at the hollow fiber membrane. Flow chambers are constructed to mimic a small excerpt of the hollow fiber bundle in a range of different parameters, packing density, frontal area, and path length. Overall, these studies demonstrated the feasibility of incorporating NO into artificial lungs as a localized anticoagulant and antimicrobial agent. The results from the third aim provided recommendations for designing a fiber bundle to minimize clot formation that can be applied to future designs for artificial lungs as well as experiments that can be used to validate computational clot formation models.

2 Surface Generated NO from Cu-PDMS as an Anticoagulant Agent in a Short-Term *in vivo* Sheep Experiment

2.1 Introduction

The challenge of finding a blood compatible surface for medical devices has been an issue for more than 60 years. Various biomaterials have been created to be thromboresistant, but few have functioned well in long-term *in vivo* conditions. Many successful blood compatible materials target the interface where blood and the material interact to prevent protein adsorption, or to target activation factors. Immobilized heparin coatings are a popular commercialized option, and studies have shown good short-term impacts. However, many of these experiments have yet to study longer-term effects of covalent and ionic coatings. One material that has been successfully used short-term *in vivo* experiments is a polymeric polydimethylsiloxane (PDMS) matrix that is embedded with copper nanoparticles, deemed Cu-PDMS. The main body of this material is PDMS, which is gas permeable and can be made to be as thin or thinner than commercially available hollow fiber membranes. The copper nanoparticles embedded in this material can be used as a catalyst to accelerate the decomposition of a NO-donor, such as S-nitrosothiols (RSNO), seen in Figure 2-1. This allows for the controlled release of NO in a local area, such as the surface of a hollow fiber bundle of the artificial lung. This surface generated NO from a 10 wt% Cu-PDMS hollow fiber device successfully reduced platelet activation and reduced clot in an *in vivo* rabbit model for a short 4-hour long study.[7] While this study proved the benefits of using surface generated NO from a Cu-PDMS surface, the longer-term effects have not been studied.

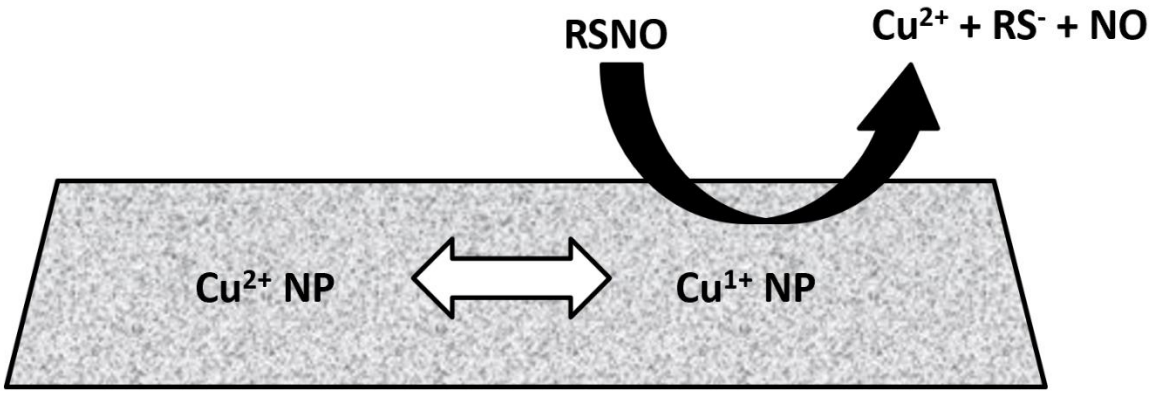

Figure 2-1. The reduction - oxidation reaction that occurs at the surface of a Cu-PDMS membrane when it is supplied with a NO donor, such as GSNO.

To address these questions, the study described below extends the initial study to a 72-hour VV-ECMO sheep model experiment to elucidate the long-term effects of surface generated NO and of the exposure of copper to blood from the Cu-PDMS hollow fibers. The goal of this study was to compare the 10 wt% Cu-PDMS hollow fibers against a clinical standard fiber, polymethylpentene (PMP), to slow clot formation in a longer 72-hour experiment. The 10 wt% copper concentration was chosen for its success in reducing clot in the previous 4-hour rabbit model. To accelerate clotting, normal clotting times were maintained rather than clinical clotting times common to ECMO. Furthermore, this study utilized two small (0.05 m^2) artificial lungs that were tested in parallel in the same circuit such that both devices always faced the same blood conditions. This conservative, head-to-head approach reduces the influence of animal to animal variability on results, giving a clear answer as to which fiber material clots more quickly. This longer study will clarify if longer term delivery of NO has negative impacts on methemoglobin levels or blood pressure from acting as a vasodilator. Similarly, this study will also look at the effect of extended copper leaching

off of the Cu-PDMS surfaces as the short-term rabbit model experiment confirmed that was occurring. In just 4 hours, the serum copper increased to 2.8 times baseline levels. Thus it is critical to study for a longer period of time. While copper is an essential trace element for mammals, in excess it can be toxic if it is not excreted and accumulates in organs such as the liver and kidneys. This study will confirm the longer-term effects of copper leaching into the system and the effect on organ function.

Device blood flow resistance was used as a measure of device performance and failure, and oxygen transfer and copper serum content were used to assess potential downsides of using Cu-PDMS fibers rather than PMP.

2.2 Cu-PDMS Surface Evaluation Methods

2.2.1 Nitric Oxide Generating Device and Circuit Components

Two types of artificial lung were tested in parallel. The first type used polymethylpentene (PMP) hollow fibers (Oxyplus, Membrana, Germany), and the second type used custom-made Cu-PDMS fibers. Cu-PDMS hollow fibers were made using a proprietary two-part silicone formulation which incorporated 10 wt% of 50 nm Cu nanoparticles within the silicone (Medarray, Ann Arbor, MI).[5] To confirm the presence of Cu particles on the surface of the fibers, electron dispersive x-ray detection (EDX) was used on both PMP and Cu-PDMS fibers (Philips XL-30, Hillsboro Oregon). The following settings were used: accelerating voltage 20 kV, beam size 3, magnification 1000x, input count rate: 1000 cps, and working distance 10 mm.

A Sievers nitric oxide analyzer (NOA, model 280, Boulder, Co) was used to characterize the release of NO from the Cu-PDMS surface. A 1 cm length of Cu-PDMS hollow fiber was introduced into a 37°C, 1 μM RSNO in a reaction chamber. Nitrogen

sweep gas was bubbled through the chamber with phosphate buffered saline (PBS, pH = 7.34) at 37°C, which carried NO gas to the chemiluminescence detection chamber in the NOA where the gas nitric oxide content was determined by measuring the peak flux.

Both types of fiber had an outer diameter of 380 µm, and the wall thicknesses of the PMP and Cu-PDMS fibers were 90 µm and 55 µm respectively. These fibers were wound into a fiber bundle with packing density of 50%. The total surface area from the fiber bundle was 0.05 m^2 for both designs. For both device types, the fiber bundles were encased in cylindrical polyethylene terephthalate-glycol modified (PETG) housings (Figure 2-2) and potted with silicone potting (Elastosil RT 625, Wacker, Germany). Polyurethane (WC-753, BJB Enterprises, USA) was added in the distal end of the blood inlet and outlet to reduce prime volume and stasis regions, as indicated by the labels in Figure 2-2 C. Each device had a prime volume of 43 ± 2 mL. The entire circuit, consisting of the two devices in parallel, and 1/4" and 3/8" ID Tygon tubing had a prime volume of 300 mL and was sterilized using ethylene oxide before surgical attachment.

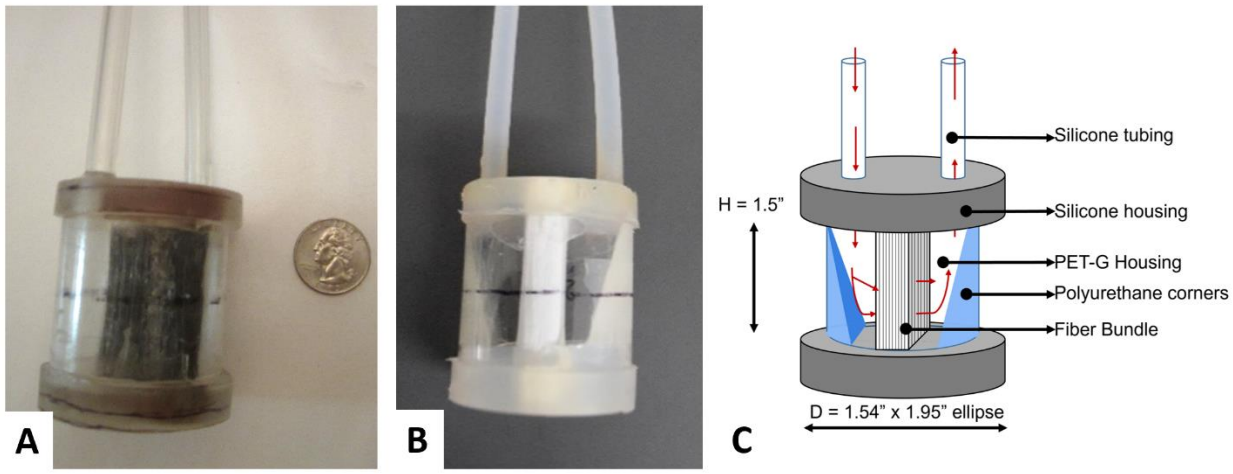

Figure 2-2. A Cu-PDMS (A) and a PMP (B) miniature artificial lung. (C) A schematic shows the flow of blood through a miniature artificial lung and the materials it will encounter.

2.3 *In Vivo* Experimental Methods

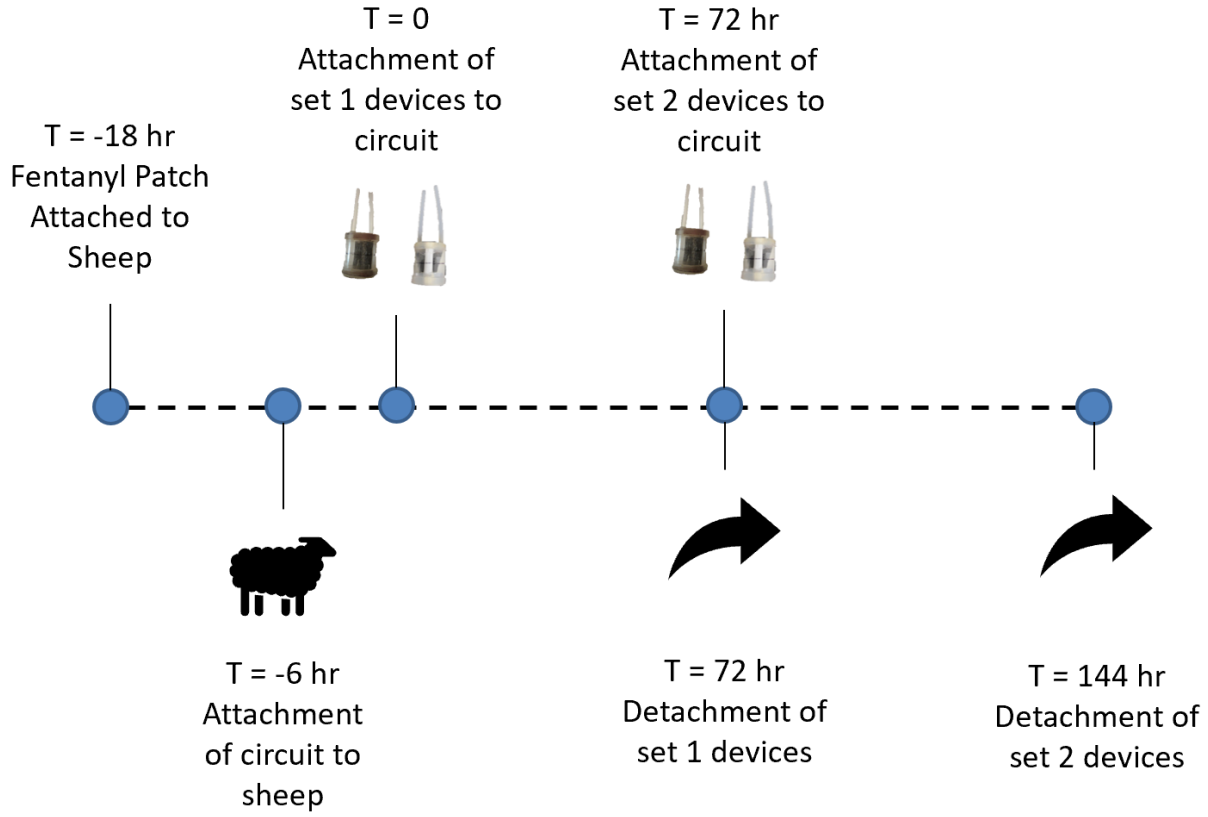

Figure 2-3. Timeline of surgical and experimental events. Two sets of Cu-PDMS and PMP devices were attached in parallel.

All methods were approved by the Allegheny Health Network International Animal Care and Use Committee, in accordance with the National Institutes of Health Guide for the Care and Use of Laboratory Animals. Nine sets of devices were attached to five Montadale sheep (Shiloh Farms, USA) with an average weight of 56 ± 2 kg. A transdermal fentanyl patch (75 – 100 µg/h, n = 5) was given 12 hours before surgical incision to provide 72 hours of analgesia. Initial anesthesia was induced with 4 – 6 mg/kg propofol and then maintained with 1-5% inhaled isoflurane for the duration of surgery. Penicillin (40,000 U/kg) and Enrofloxacin (5 mg/kg) were given every 72 and 24 hours, respectively. A beveled 24-inch long pressure tubing (Tru-Wave, Edwards

Lifesciences, USA) was placed in the carotid artery for pressure monitoring and blood sampling. Lactated Ringer's solution was administered intravenously at a rate of 10 mL/kg/hr to maintain normal blood pressure and hydration.

Baseline arterial blood samples, including blood gases (pO_2, sO_2, pCO_2, pH, total hemoglobin) and hematology (platelet count, white blood cell count, methemoglobin, activated clotting time, plasma free hemoglobin, and hematocrit), were taken immediately after the arterial line was attached. A bolus of heparin (200 U/kg) was administered arterially, and the Avalon Elite Bi-Caval Dual Lumen Catheter (Maquet, NJ) was placed in the jugular vein (Figure 2-4). The circuit was primed with a solution of 1% albumin in saline for 15 minutes prior to the experiment to slow early protein adsorption and clot formation in a similar fashion as previous work.[39,175] The circuit prime solution was also dosed with methylprednisolone sodium succinate (30 mg/kg) and heparin (100 U) before attachment. This circuit contained all the tubing and connectors but not the artificial lungs. For safety and simplicity, these devices weren't attached until the sheep was moved and stabilized in long-term housing. The circuit flow was started at 600 mL/min with a roller pump and monitored with an ultrasonic flow probe and flow meter (Transonic T402 Ithaca, NY).

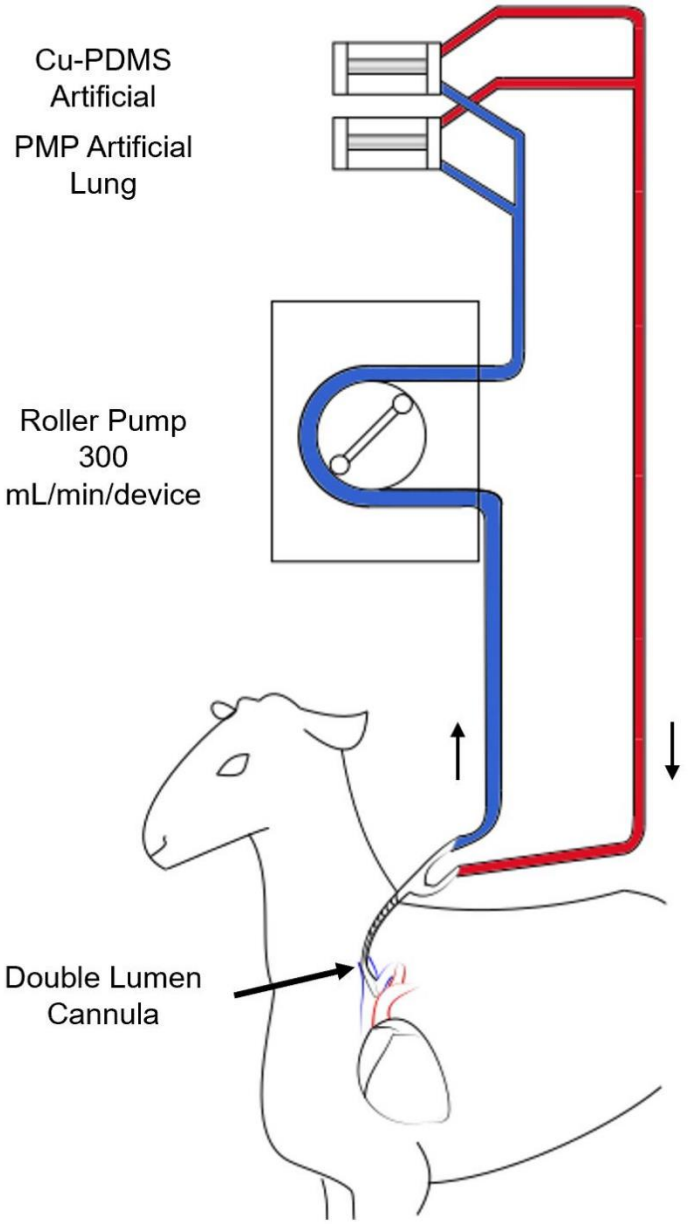

Figure 2-4. VV-ECMO circuit connecting a Cu-PDMS and a PMP device in parallel in a sheep model. The experimental timeline is as follows: T=0 Baseline samples; T=2 Circuit attachment; T=6 Device attachment set 1; Device attachment set 2 for each experiment.

After circuit attachment, the sheep were moved to a custom-built stanchion, recovered, and moved to long-term housing. One PMP device and one Cu-PDMS device were placed in parallel within the circuit after six hours of initial circuit attachment. Each device received a separate continuous infusion of a NO donor, S-Nitroso-N-acetyl-

DL-penicillamine (SNAP) (Sigma Aldrich, USA), at a rate of 0.48 µmol/min at the inlet to replace any lost NO donors in blood. This infusion rate was based on a previous *in vivo* study that used a miniature artificial lung with the same MedArray Cu-PDMS fibers as a NO generating surface.[7] Throughout the duration of the experiment, the pump speed was adjusted to maintain blood flow at 300 mL/min per device (approximately 5% of the cardiac output), while screw clamps were used at the outlet of each device to maintain even flow through both devices every half hour.[60,171] This blood flow rate was chosen to match the blood flow velocity at a relatively low 2 L/min of blood flow through an adult Quadrox HMO 70000 with a 100 cm^2 frontal area, or 20 cm/min. Although gas transfer was not necessary in these normal sheep, room air was supplied as the sweep gas through each device at double the blood flow rate to mimic the sweep gas flow rates used in the clinic. The results would thus reflect any loss of NO transferred from the surface generated NO into the sweep gas phase.

Once every 24 hours, the sweep gas was switched to 100% O_2 for gas exchange testing, while maintaining gas flow rates at twice the blood flow rates. The blood flow rates were set at 300 and then 600 mL/min, and inlet and outlet blood samples were taken at each flow rate to perform blood gas analysis using an ABL800 Flex Analyzer (Radiometer, Brea, USA). Immediately after gas exchange testing, the gas inlet was reconnected to room air flowing at 600 mL/min, and the blood flow was returned to 300 mL/min.

2.3.1 Data Acquisition and Blood Sampling

Device inlet and outlet blood pressure and flow rate were measured after the devices were first attached and every hour thereafter. Pressures were measured using

Transpac ® IV Monitoring Transducers (ICU Medical, USA) connect to a Biopac data acquisition system (manufacturer), and the flow rate (Q) was measured with a tubing flow probe (Transonic T402 Ithaca, NY, Ithaca NY). Resistance was calculated from the pressures drop and blood flow rate, according to the traditional formula:

$$R = (P_{out} - P_{in})/Q_{blood}$$

Where *R* is resistance, P_{out} is pressure at the device outlet, P_{in} is pressure at the device inlet, and Q_{blood} is the blood flow. Additionally, arterial blood samples were taken immediately after device attachment to measure activated clotting time (ACT), HCT, platelet and WBC counts. After initial device attachment, blood samples were takenevery 3 hours to measure arterial blood gases and every 12 hours to measure platelet and WBC counts. Blood samples used for blood gases and plasma free hemoglobin were drawn into heparinized syringes, while samples for platelet and white cell counts were drawn into 10% sodium citrate syringes. Arterial blood pH, pCO_2, pO_2, total hemoglobin, and metHgb were measured with an ABL800 Flex Analyzer (Radiometer, Brea CA) every 6 hours. Plasma free hemoglobin was measured with a spectrophotometer using the Cripps method, and total platelet and white blood cell counts were measured using a Z1 Coulter Counter (Beckman Coulter Electronics, Hialeah FL) every 12 hours.[43] The ACT was measured every hour until stable (three hourly samples within 100-180 s) and then every 4-6 hours. ACT was measured with a Model 801 Hemochron Blood Coagulation System (International Technidyne Corp. Edison NJ). During the entire experiment, ACT was maintained between 100-180 s, and averaged at 150 ± 9 s for all experiments. It was unnecessary to infuse heparin in 7 of

the 8 sets of circuits to maintain this range. In sheep 4, ACT dropped below 100s, and heparin was infused for a period of 30 hours. Mean arterial pressure and heart rate were monitored continuously on a patient monitor and recorded every hour to assess overall health as NO is a known vasodilator and could cause arterial hypotension.[72]

Devices were considered failed if the resistance reached three times the baseline resistance and were removed and replaced with a shunt tube. If failure did not occur, devices were removed following 72 hours. After the first set of devices were removed, a second set of devices, consisting of one PMP and one Cu-PDMS in parallel, was attached. The removed devices were immediately injected with 5 mL of heparin to prevent the stagnant blood from clotting and then rinsed with heparinized saline (2 U/mL) until the effluent was clear. These devices were then disassembled with the clear housing carefully cut away to isolate the clot on the fiber bundle for imaging. The surface at the inlet, outlet, and middle of the fiber bundle were rinsed with saline until the effluent ran clear and then each sample was fixed in 2% glutaraldehyde (Electron Microscopy Sciences, USA).

Sheep were euthanized at the end of the experiment using Fatal Plus (Vortech, USA) and necropsied tissue samples were from taken from the liver and then assayed for copper content with a quantitative colorimetric copper assay (DICU-250, Gentuar BioAssay Systems, USA). Blood samples were also taken from two sheep without circuits attached for a negative control and anticoagulated with a 1:9 ratio of acid-citrate-dextrose. Copper content was measured the same way as described above.

Following the experiment, small squares (1.5 cm^2 x 1.5 cm^2 x 1.5 cm^2) from each fixed fiber bundle were excised, dehydrated and sputter coated in platinum for scanning

electron microscopy (SEM) imaging (Philips XL-30, Hillsboro Oregon) with the following settings: accelerating voltage 10 kV, beam size 3, and working distance 10 mm.

2.3.2 Statistical Analysis

Device resistances were calculated as $R = (P_{inlet} - P_{outlet})/Q_{blood}$. Resistance data were then normalized to the percentage increase in resistance above the average of all baseline resistances. The normalized data is then averaged across 6-hour periods for statistical analysis and presentation. Devices that reached three times the baseline resistance for two consecutive hours were considered to have failed. Devices that fail are removed and thus have no further measure of resistance. For presentation and statistical analysis, the resistance of each device following failure was conservatively assumed to remain the same. This resistance value is less than the likely exponential increase in resistance that typically follows device failure and eliminates the misleading information when the device is censored from the graph thereafter. For statistical analysis, normalized resistances were compared across all devices with SPSS (IBM, Chicago USA) using a mixed model analysis with a Bonferroni-corrected confidence interval with each device set (e.g. 1-1, 1-2, 2-1, 2-2) as the subject variable, and time as the fixed, repeated-measure variable.[160,161] A p-value < 0.05 is regarded as significant.

Oxygen transfer was calculated with the following equation,

$$O_2\ transfer\ rate = Q_b(k\Delta P + 1.34 C_{Hb}\Delta S)$$

With k as the solubility of O_2 in blood ($3.56*10^{-5}$ mL O_2 /mL blood/mmHg), Q_b is the blood flow rate, C_{Hb} is the hemoglobin concentration, $\Delta p = p_{out} - p_{in}$ is the difference in O_2 partial pressure from the outlet (p_{outlet}) to the inlet (p_{inlet}), and $\Delta S = s_{out} - s_{in.}$ is the difference in oxyhemoglobin saturation between the saturation at the device outlet (s_{out})

and saturation at the device inlet (s_{inlet}). Two analyses of gas transfer were performed. In the first, only paired data from the Cu-PDMS and PMP devices from the same time point were used. This eliminates variations in gas exchange due to varying inlet conditions but includes variation in gas exchange due to clot formation. As both devices were in parallel, each would have experienced the same inlet conditions. In addition, to eliminate any potential variation in gas exchange due to clot formation on the fiber bundle, a separate analysis was performed using only the first set of gas exchange data from each device, when clot formation on the fiber bundle should not yet affect gas exchange. The data from two devices with a resistance increase of more than 5 mmHg/mL/min were excluded from data analysis, as this may have indicated a very rapid clot formation that was not due to the materials being tested. This value was chosen as it is two times the average baseline resistance, which was measured from running water through each device prior the actual experiment.

Differences between PMP and Cu-PDMS failure rates were analyzed using the Kaplan Meier method within SPSS. A t-test assuming unequal variances was used to analyze the difference between the platelet values at the start of the first and second sets of devices attached to each subject to ensure this change was minor. Lastly, all hematology variables and blood pressure were averaged for each sheep over 6-hour blocks of time, and this data was used for statistical analysis with a mixed model with time as the fixed, repeated measure. Each sheep was set as the subject variable and a p-value of < 0.05 is considered significant.[160,161] Graphs were created using Excel (Microsoft Inc. Redmond, WA).

2.4 Results

Overall, the miniature artificial lungs with Cu-PDMS hollow fibers produced NO and were able to reduce platelet adhesion and also clot formation on the bundles when compared to the control devices. Energy dispersive x-ray detector (EDX) testing revealed 26% ± 0.8 surface copper expression, shown in Figure 2-5. This is the active surface that would decompose circulating NO-donors that come in contact with the surface. The resulting peak NO flux measured from 4 separate fibers of 1 cm length is 3.43 ± 0.72 x 10^{-10} mol cm^{-2} min^{-1} and correlates well to previous work using the same Cu-PDMS fibers. [6,21,87,123]

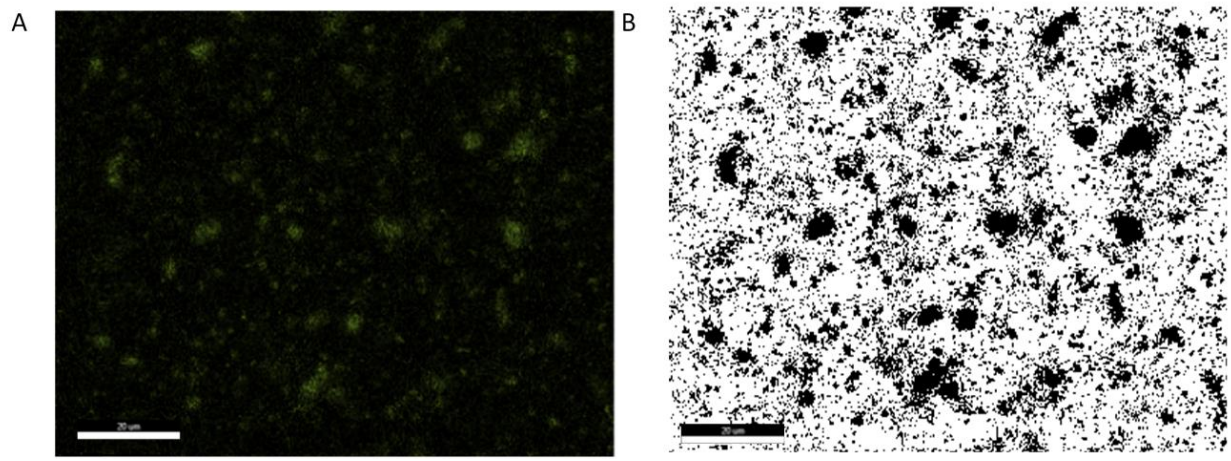

Figure 2-5. Energy dispersive microscopy is used to characterize the surface of Cu-PDMS fibers for copper exposed on the surface (A). Then, the image is converted to binary (B) and then all of the pixels representing copper are counted using ImageJ. Scale Bar 20 µm.

Five sheep had two sets of devices tested. One sheep accidentally decannulated due to inadequate cannula suturing and was euthanized at 14 hours. One set of devices was attached less than 6 hours after surgery and was outside of protocol and was not used. Thus, a total of 9 sets of devices were attached, and data from 8 were used for analysis. During testing, sheep mean arterial blood pressure and heart rate were stable and within normal ranges, averaging 91 ± 3 mmHg and 105 ± 3 bpm, respectively, from

baseline to day 6. The methemoglobin levels remained at baseline values averaging 1.9 ± 0.2%. The average ACT was 150 ± 10 s and did not vary significantly over the course of the experiment ($p = 0.43$).

2.4.1 Coagulation and inflammation

Plasma free hemoglobin counts remained at baseline values throughout each experiment and did not vary significantly over all experiments ($p=0.58$). The average white blood cell count was 9 ± 1 x 10^3 cells/µL at baseline, rose to 11 ± 2 x 10^3 cells/µl on day two after circuit attachment, and fell back towards starting values by day three (Figure 2-6). There was no response seen as a result of the second set of device attachment, perhaps due to the smaller change in surface area compared to the entire circuit and device attachment on day zero and some white cell exhaustion. There was a significant drop in platelets from baseline after the circuit was attached due to initial platelet adhesion to the oxygenators and circuit. However, platelet count returned towards baseline after day two, as seen in the minimum platelet count on day two at 149 * 10^3 μl^{-1} increasing to 381 * 10^3 μl^{-1} on day 5 (Figure 2-6). There was no significant difference ($p = 0.977$) in the platelet counts or in the white blood cell counts ($p = 0.787$) during the first and second set from a 2-tail student t-test.

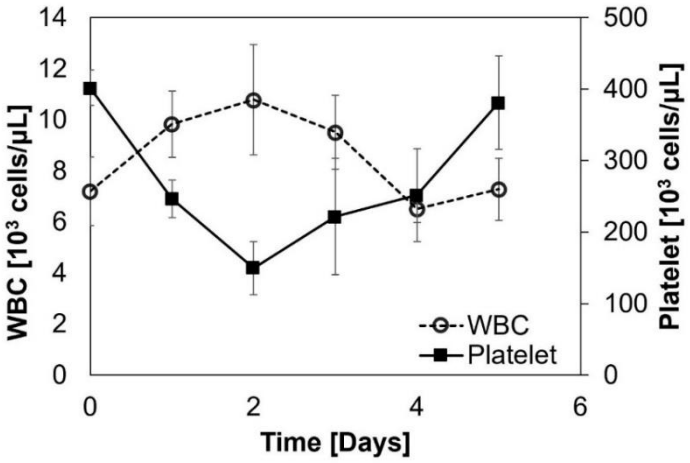

Figure 2-6. White blood cell count and platelet counts averaged over all subjects. Data are averaged over one day and presented with a standard deviation.

2.4.2 Device Function

Blood flow resistance increased from BL to 72 hours for PMP and Cu-PDMS fiber; however, the control PMP devices exhibited significantly greater resistance than the Cu-PDMS devices which indicates more clot on the fiber bundle ($p<.001$) (Figure 2-7). The failure curve (Figure 2-8) shows greater longevity for Cu-PDMS devices than PMP devices; however, using a log-rank Kaplan Meier analysis this did not reach significance ($p = 0.171$). The NO generation in the Cu-PDMS devices caused a marked reduction in clot formation and failure between the 12 to 36-hour range: by hour 36, 62.5% of control devices had failed, whereas only 12.5% of the Cu-PDMS devices had failed. At 72 hours, 87.5% of the control devices failed, while only 50% of the Cu-PDMS failed.

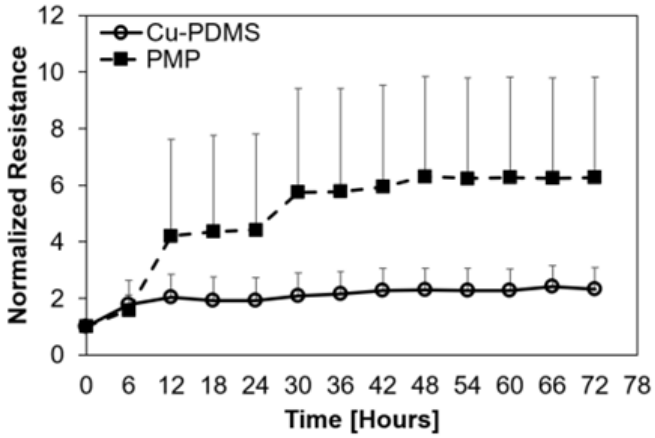

Figure 2-7. Normalized resistances to an averaged baseline show significant difference between Cu-PDMS and control devices. Data are averaged over 6-hour periods and presented with the standard deviation.

Table 1 provides the exact failure time of each set of paired devices. The first and second set of Cu-PDMS devices failed after an average of 40.5 ± 31 hours and 49.0 ± 13 hours respectively. For the PMP devices, the first set of devices lasted an average of 24.5 ± 27 hours before failing while the second set lasted an average of 32.3 ±16 hours. There was significant variation between tests with a few obvious outliers in each group, as 12.5% of Cu-PDMS devices failed before 40 hours and 12.5% of PMP devices survived the entire 72 hours. There is a censored event where a Cu-PDMS devices was removed before it had reached failure criteria due to the sheep having accidentally decannulated and the experiment ending early.

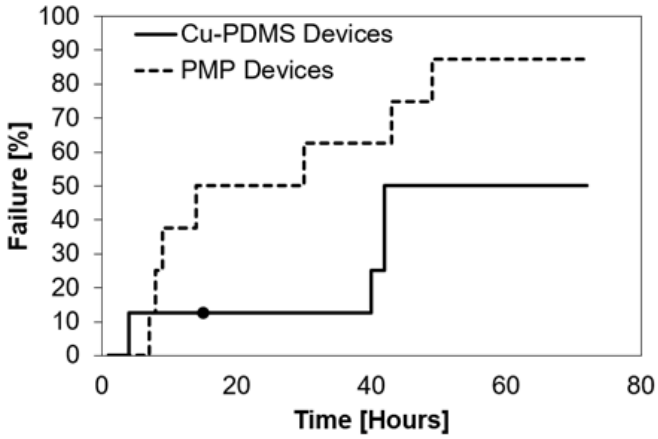

Figure 2-8. Failure of Cu-PDMS and control PMP devices over 72 hours (N = 8). The ● represents a device that was removed before it was failed, data from this was used as a censored event in Kaplan-Meier survival analysis.

Table 1. Failure times (hours) for all devices attached to each sheep.

Sheep	Set 1		Set 2	
	Cu-PDMS	PMP	Cu-PDMS	PMP
1	-	-	72	29
2	14	13	-	-
3	4	7	42	6
4	72	6	40	49
5	72	72	42	43

After the experiment, the fiber bundle removed from each device revealed that clot originated from the gas exchanging fibers or from the housing at the edge of the fiber bundle. All devices had clot on the outlet housing, but failed devices had more clot on the fiber bundle surface than on the housing. Figure 2-9 shows pictures of representative devices after failure (n = 7 PMP, n = 4 Cu-PDMS) or at 72 hours if they did not fail (n = 1 PMP, n = 4 Cu-PDMS).

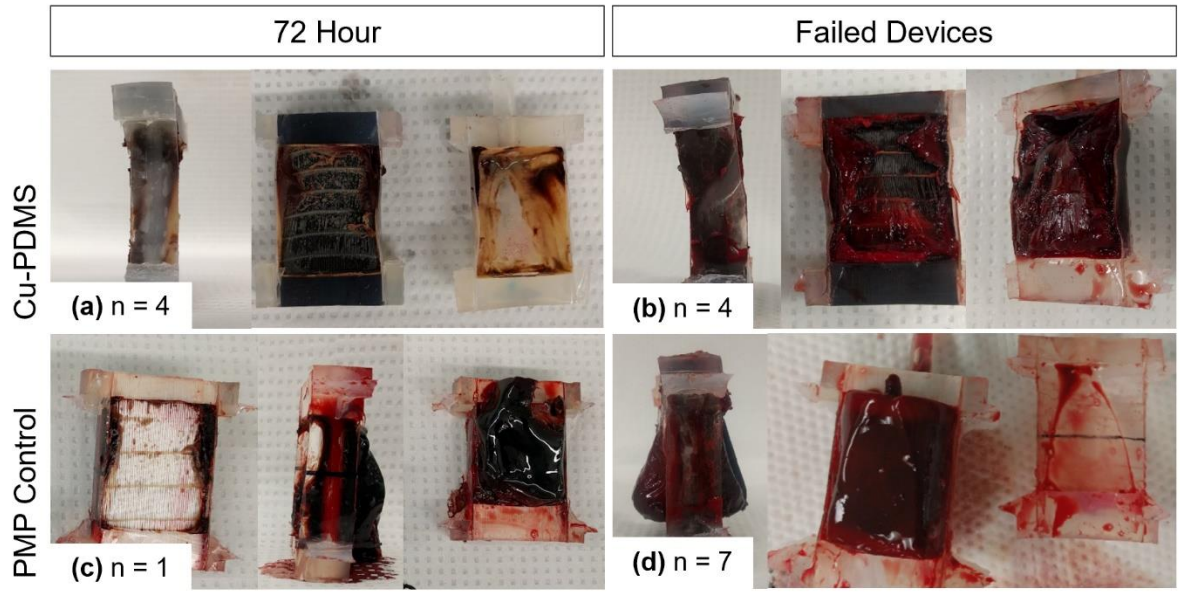

Figure 2-9. Clot formation in lungs. As expected, devices that did not reach failure (a,c) have less clot than those that fail (b,d). (a) 50% of Cu-PDMS devices had black gas exchanging fibers visible and some white clot formation on the housing and edges. The other 50% of Cu-PDMS devices (b) failed. Only one PMP device (c) survived to 72 hours, and the rest (d) 87.5% failed and had clot originating from the fiber bundle, and no gas exchanging fibers can be seen.

Average O_2 transfer of copper devices was 92 ± 17 mL O_2/min/m^2 and the average O_2 transfer of PMP devices was 106 ± 29 mL O_2/min/m^2 at a blood flow rate of 600 mL/min at the beginning of the experiment. Average O_2 transfer at 300 mL/min blood flow was 76 ± 11 mL O_2/min/m^2 for copper devices and was 91 ± 16 mL O_2/min/m^2 (Figure 2-10) (Table 2). Using a 2-tail student t-test, there was no significant difference between the Cu-PDMS and PMP gas exchange performance (p=0.65 and p=0.72, respectively). In the following days, each device's subsequent oxygen transfer measurement was lower than the previous day's measurement. Oxygen transfer is displayed in Table 2. The third day's oxygen transfer value is artificially high due to the best performing devices lasting until the end and raising the average.

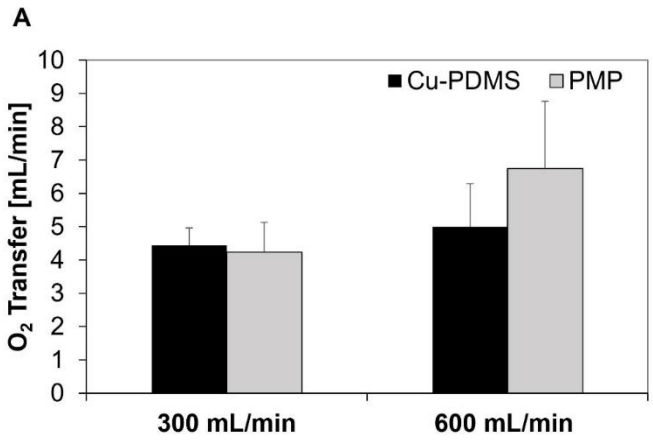

Figure 2-10. Oxygen transfer on D1 at 300 and 600 mL/min blood flow rate, and 600 and 1200 mL/min oxygen flow rate respectively (A). Data that had variable inlet conditions and high initial resistance were excluded.

Table 2. Oxygen exchange in mL/min/m2 over three days, with number of devices in each group per day.

		D1	D2	D3
300 mL/min	Cu-PDMS	76±11 N=5	29±4 N=3	47±0 N=1
	PMP	90±16 N=5	69±26 N=4	87±0 N=1
600 mL/min	Cu-PDMS	93±17 N=5	41±9 N=3	24±0 N=1
	PMP	106±30 N=5	103±39 N=3	111±0 N=1

2.4.3 Sheep Necropsy and Copper Content

SEM images were taken to assess overall clot formation on gas exchanging hollow fiber surfaces as well as on the non-gas exchanging, weaving fibers that are used to tie the fibers together. While clot filled both sides of failed Cu-PDMS and control devices, the gas exchanging fibers in these devices exhibited different surface fouling. The SEM images in Figure 2-11 were chosen as representative images since they were typical for each case. As seen in Figure 2-11, there was more protein deposition on the PMP control hollow fibers than there were on the Cu-PDMS hollow fibers. However, weaving fibers in both cases were covered with substantial clot.

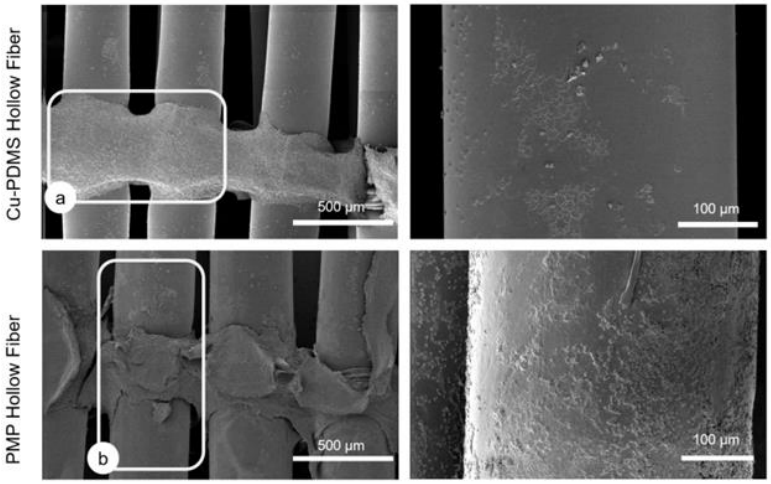

Figure 2-11. Representative SEM images of gas exchanging fibers and weaving fibers. (a) outlines a weaving fiber with pronounced protein deposition and (b) outlines a gas exchanging fiber. These are figures representing typical surfaces of failed devices looking at the middle of the fiber bundle. (87.5% of the PMP devices and 50% of the Cu-PDMS devices).

Copper content measured in serum averaged 233.72 ± 69 µg/dl, greater than the normal average sheep serum copper content of 90-160 µg/dL. Final liver copper content averaged 31 ± 11 µg/g, within the normal levels of 18-87 mcg/g).[131]

2.5 Discussion

This study assessed a Cu-PDMS NO generating hollow fiber device in a short-term, large animal biocompatibility experiment. The results indicate that catalytic generation of NO at 3.43 ± 0.72 x 10^{-10} mol cm^{-2} min^{-1} by Cu-PDMS fibers reduces clot formation when compared to standard PMP fibers. However, this benefit is not consistent across each study. The Cu-PDMS did not affect sheep health and hematology in this setting nor did it create a statistically significant reduction in gas exchange efficiency.

2.5.1 Clot Formation

As hypothesized, NO generation slowed clot formation, resulting in the reduced blood flow resistance increases, failure rates, gross thrombus (Figure 2-9), and thrombus observed via SEM. This positive effect was most pronounced in the first 36-40 hours of testing but waned thereafter in a number of the Cu-PDMS devices (Figure 2-8). This suggests that while the NO flux provides anticoagulation, this effect was eventually overcome by surface generation of clotting factors. After 36-40 hours, the accumulation of fibrin on the devices along with the increasing sheep platelet count was too much for NO generation to overcome. Furthermore, although Cu-PDMS devices had slower clot formation, on average, the results were not consistent, 12.5% of Cu-PDMS devices failed before 40 hours and 12.5% of PMP devices survived the entire 72 hours. No obvious differences in platelet counts or ACT could explain the cause of this outlying behavior. The early Cu-PDMS failure occurred with a platelet count of 382*10^3 cells/µL and ACT of 144 s vs. an average of 275 ± 50 *10^3 cells/µL and 150 s respectively, in the devices with more typical function. The slower clot forming PMP device had a platelet

count of 246*10^3 cells/µL and ACT of 157 s. This suggests other causes, such as greater concentrations of coagulation factors or device manufacturing variability.

Furthermore, the NO also caused significant reductions of fiber clot on the gas exchange fibers on SEM. However, there was ubiquitous clot formation on the polypropylene warp fibers of both Cu-PDMS and PMP bundles. These are the non-gas exchanging fibers that are knitted into the fiber every 1 cm to hold the fiber mat together (Figure 2-11). Because this requires multiple, small fiber strands, this area has multiple small interstices and a high surface area to blood volume ratio, leading to efficient generation of procoagulants. Moreover, there is no blood flow through these interstices to wash activated procoagulants from the surface, and these fibers do not contain the copper catalyst. As a result of stagnation and lack of NO flux, these fibers clot rapidly.

2.5.2 Improving the Anticoagulant Function of NO Generating Fibers

In this study, the anticoagulation function of NO was not as consistently positive as during previous, short-term studies. [7,21,152] One potential cause of this may have been the low average ACTs (150s) in this study. Nitric oxide does nothing to prevent surface adsorption of plasma proteins such as fibrinogen and the contact system of the intrinsic branch of the coagulation cascade. In fact, there is evidence that NO can enhance fibrinogen adsorption.[21,113,123,124] Platelet adhesion to fibrinogen causes platelet activation, while protein adsorption and activation of the intrinsic branch of the coagulation cascade generates thrombin that can further enhance platelet activation.[113] Because of this, anti-adsorptive surface coatings could be combined with NO generation to limit the amount of platelet agonists present and thus enhance the ability of NO to inhibit platelets. Previous research has shown that anti-adsorptive surface

coatings work synergistically with NO surface flux to further decrease platelet surface adhesion.[7,84] However, these studies created NO flux by delivering NO within the oxygenating gas of the gas exchanger. For catalytic NO generation, surface coatings could potentially reduce Cu interactions with SNAP and thus reduce NO flux rates.

NO generation from fibers should also be optimized to improve its function. First, the ideal rate of NO donor infusion is not known. The infusion rate for this study, 0.48 µmol/min, matches that provided when testing a similar but slightly larger surface area artificial lung during a 4-hr rabbit study.[7] It is unknown if this rate of delivery generates the maximum NO flux without also causing systemic vasodilation and hypotension or elevated metHb. Lastly, much of the ECMO circuit wasn't coated with Cu nanoparticles in this study. In future studies, the entire ECMO circuit could be coated with Cu nanoparticles, including the warp weaving fibers, to catalytically generate NO at every surface.

2.5.3 Side-Effects – Oxygen Transfer and Serum Copper

A secondary goal of this study was to examine if there are differences in the gas transfer efficiency of the two fiber types due specifically to differences in fiber wall oxygen permeability. Isolating the role of the permeability requires significant control over the other variables affecting oxygen transfer in these devices. In addition to fiber wall oxygen permeability, oxygen transfer in any artificial lung fiber bundle is a function of blood composition and chemistry, blood flow velocity, and fiber bundle geometry.[134] During a long-term study, clot formation will also reduce gas exchange by reducing the amount of fiber exposed to flowing blood and changing blood flow patterns and velocity

within the open portions of the fiber bundle. Therefore, to isolate the effect of fiber wall permeability, the study sought to do the following:

1. Each device was constructed with the same methodology in order to construct fiber bundles with identical geometries.
2. Blood inlet chemistry and composition is the same for each paired PMP and Cu-PDMS fiber bundle, and
3. Devices were only analyzed if their initial resistance was very close to the typical starting resistance for these devices (15 ± 5 mmHg/mL/min), to eliminate outliers with significant clot formation.

Following these methods, results of this analysis indicate a small, statistically insignificant reduction in gas exchange efficiency with the Cu-PDMS fibers when compared to the PMP fibers. Examination of each specific pair of devices showed that there was no consistent trend in superior gas exchange for the PMP or Cu-PDMS fibers.

Although this suggests similar gas exchange, these results were confounded by variations in gas exchange efficiency within both the Cu-PDMS and PMP groups. These differences cannot be explained by differences in blood inlet chemistry or composition. Each paired device was tested at the same inlet conditions, pO2 at 45 ± 4 mmHg, sO2 at 65 ± 7%, and hematocrit 21 ± 3% for all samples. Clot formation is also not the source, as this has been controlled for the results in Figure 2-10Figure 2-9. The cause of these differences is also unlikely varying amounts of Cu present in the fibers, as the distribution of Cu in the membrane was found to be homogenous and largely uniform in the SEM images from the sampled Cu-PDMS fibers. Thus, the cause of this variation is likely differences in device construction. While each of the miniature artificial lungs were

produced with the same methodology, they are hand-made and likely to vary by some degree. This is common in prototype artificial lungs.[38,39] Fiber bundle frontal areas and path lengths, potting depths, and/or the percentage of fibers open for gas flow can vary slightly in these devices. Furthermore, blood flow can shunt around the fiber bundle to some degree. To address this, devices used in this study had been first measured for gas resistance and only those with resistances less than 2 mmHg/mL/min were used. However, stricter criteria could be applied. These differences affect blood flow patterns and the amount of fiber surface area available for gas exchange.

In addition to assessing the negative effects of Cu on gas exchange, care must also be taken that leaching copper does not lead to systemic toxicity during long-term support. Copper toxicity manifests mainly as liver cirrhosis and damage, as non-reabsorbed copper is mainly excreted in bile produced by the liver. Mammal blood has endogenous copper that is mainly bound to albumin and transcuprein as a reservoir, before it is transported to the liver.[118] The kidney also receives copper through the blood and may have increased copper concentrations as a result of enhanced tubular reabsorption of circulating copper. Therefore, the copper toxicity exhibits itself as liver cirrhosis first and then with episodes of hemolysis and damage to renal tubules, the brain, and other organs.[19,34] In sheep specifically, the tolerance for copper is low and some are unable to increase biliary copper excretion in response to increased copper intake, making it a conservative model.[20] In this study, copper concentration taken from the liver remained low, 31 ± 11 μg/g of tissue compared to averages seen in sheep which range from 18-87 μg/g.[27,49,135,185] On the other hand, copper serum content was

elevated above normal levels. Together, this suggests active leaching into the blood but no toxic build-up within the liver.

Although these results are positive, this device was undersized purposely so that systemic hematology would be less affected by the attached devices (see section 4.4). As a result, the hollow fiber surface area of this device is $1/26^{th}$ of a typical full-sized ECMO oxygenator. Therefore, it grossly underestimates the amount of copper that would leach using commercial oxygenators. Moreover, those devices are likely to be used for longer periods. Therefore, further long-term testing is also required to study Cu-PDMS biocompatibility.

2.5.4 Effect of Study Design and Test Devices on Clot Formation and Study Conclusions

Extrapolation of these results to performance of full-scale oxygenators during clinical ECMO must be done with caution due to the size of the tested devices in this study, their relatively low flow rate, the use of two devices at one time, and the withholding of heparin anticoagulation and the resulting low ACT (150 ± 10 s). In particular, this latter condition created an aggressive test of the ability of NO to reduce clot formation. If heparin had been used to generate a more clinically applicable ACT of 180-220s, there would have been reduced thrombin formation and thus lower levels of platelet activation and fibrin formation. This would, in turn, increase the time to failure for each device. Therefore, to judge the true clinical impact of the technology, future studies will need to test full-scale devices in single animals with ACTs ranging from 180-220s.

2.6 Conclusion

This study assessed the effect of Cu catalyzed NO generation on clot formation in a low-ACT, accelerated clot formation model of VV ECMO. This is the first study to investigate this effect in a long-term, large-animal model. The NO-generating, Cu-PDMS fibers significantly slowed clot formation and maintained fiber bundle patency. However, this effect was not consistent for each pair of devices tested. The effect of Cu on oxygen transfer was small but confounded by device to device variability. Leaching of copper led to elevated copper serum content but no build-up in the liver. Future studies should investigate blood clotting and serum Cu levels in studies with full scale oxygenators and normal levels of heparin anticoagulation over a period of weeks.

3 Two-Pronged Method for Preventing Bacterial Adhesion using Nitric Oxide and Copper

3.1 Introduction

Between 9-18% of adults on ECMO experience a blood stream infection.[28,76] Bacteria typically enter ECMO circuits through connections between the inner and outer surfaces of the circuit, such as stopcocks and injection ports, are dispersed in the flowing blood, and eventually adhere to and colonize circuit surfaces exposed to the blood. Frequently, the bacterial infection results in the colonization of the oxygenator in the ECMO circuit due to the low blood flow velocities on its gas transfer membrane surface.

Artificial lung hollow fibers composed of Cu-PDMS have the potential to inhibit bacterial colonization. As shown in Chapter 2, Cu-PDMS surfaces reduce local platelet activation due to surface generation of nitric oxide (NO), and thus reduce clot formation. In addition, Cu-PDMS could reduce bacterial adhesion by concurrently providing NO flux *and* copper exposure at the hollow fiber membrane surface. As outlined in Chapter 1, copper has been used for centuries for its antibacterial properties for water vessel and household applications. In medical devices, copper has been incorporated into polymers for its antimicrobial effects in intrauterine devices, respiratory masks, bedding, and more recently in catheters.[13,19,143] The use of NO in medical device applications is a more recent development, with controlled release from polymeric materials used to reduce both thrombosis and bacterial infection.[17,23,33,65,201] Several studies have specifically examined the use of surface NO flux to reduce platelet activation and clot

formation in hollow fiber artificial lungs, but the effect on bacterial colonization has not been tested alone or in combination with a copper surface.

The purpose of this study is to examine the antimicrobial function of Cu-PDMS surfaces with and without their accompanying NO flux. As both have antibacterial effects separately, this study looked at both of these antibacterial agents individually and in combination to reduce adhesion in an ECMO oxygenator setting. This study was performed under dynamic conditions mimicking the blood flow within and oxygenator in order to simulate convection of copper ions and NO away from the surface and bacteria to the surface.

Conventional methods to study the antimicrobial effects of a new biomaterial or drug typically involve a static environment.[103] When studying a potentially antimicrobial material, the testing is based on submerging a small coupon of the material in a bath of bacteria (petri dish or well plates) in static or shaking conditions in an incubator for a predetermined period of time and examining the extent of bacterial colonization.[147,159,193,201,205] However, blood flows constantly over artificial lung hollow membranes, transporting cells and proteins to and from the surface, and conventional static testing is unlikely to accurately predict their function. Thus, this study examines the effects of the antimicrobial function of Cu-PDMS surfaces using flow chambers. These flow chambers have been used previously to study the effects of shear rates on bacterial adhesion, but are not typically applied bacterial colonization in the presence of antimicrobial surfaces.[115]

3.2 Study Design and Methodology

3.2.1 Bioreactor and Cellulose Membrane Preparation

A custom-made polycarbonate flow chamber was constructed to provide the interface for simulated blood flow, a permeable membrane for gases, and gas flow (Figure 3-1). This design provided the ability to replicate artificial lung delivery of NO in both a gas form and surface generation in one device, while providing accurate convection to and from the surface. The chamber features included a 1/16" barbed inlet and outlet for simulated blood and gas flow past the membrane, a total volume of 2.5 mL, and an exposed membrane surface area of 1.75 cm^2.

A custom-made PDMS or Cu-PDMS membrane was used to separate the fluid and gas sides of the flow chamber. A circular cellulose membrane with a 0.025 μm pore size (VSWP04700, EMD Millipore, USA) was cut to a 24 mm by 47 mm rectangle to serve as the gas permeable, base membrane. These membranes were then attached to a glass coverslip with dimensions of 24 mm by 50 mm to apply a layer of PDMS or Cu-PDMS. PDMS (SYLGARD® 184, Dow Corning, USA) was mixed in a THINKY Planetary Centrifugal Mixer (ARE-250, THINKY, USA) in a 10:1 ratio of polymer to cross-linking agent. Cu-PDMS was similarly mixed with a 10:1:0.3 ratio of polymer, cross-linking agent, and acetone (A18-4, Fisher Scientific, USA). Additional 10% wt copper (II) oxide nanoparticles (544868, Sigma Aldrich, USA) were combined with this mixture and incorporated using a THINKY Planetary Centrifugal Mixer (ARE-250, THINKY, USA).

A spin coater was used to apply a uniform 50 μm layer of PDMS or Cu-PDMS onto the membranes (Spincoat G3p-8, SCS, USA) to mimic the wall thickness of

standard PDMS hollow fibers used in prototype artificial lungs.[62,112] These modified membranes were placed in an oven and cured at 65°C for 3 hours. These membranes were then individually placed in sterilization pouches and sterilized via ethylene oxide.

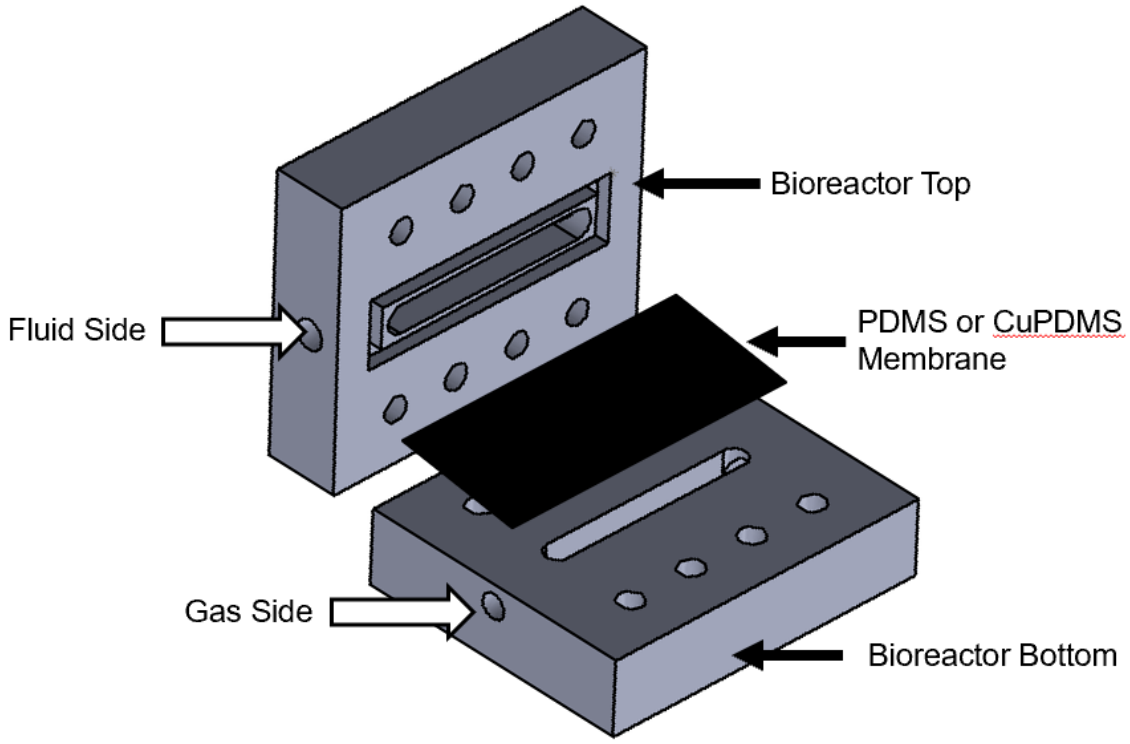

Figure 3-1. A schematic of the bioreactor setup that simulates the conditions of a gas exchanging membrane of a hollow fiber of an oxygenator. There is a gas side and a fluid side and a membrane that is sandwiched between the two bioreactor pieces.

3.2.2 Surface Characterization

Scanning electron microscopy (SEM) and energy dispersive spectroscopy (EDS) were used to verify the surface Cu composition. The membrane was cut into 1 cm by 1 cm pieces and each piece was sputter coated in platinum in preparation for SEM imaging (Philips XL-30, Hillsboro Oregon). To achieve a penetration depth of 10 nm, the following settings were used: accelerating voltage 10 kV, beam size 3, and working distance 10 mm.

To characterize the nitric oxide flux from Cu-PDMS and PDMS (control) membranes using a NO-donor, a 1 cm by 1 cm coupon of the membrane was introduced into a 37ºC reaction chamber with 1 µM GSNO. Nitrogen sweep gas was bubbled through the chamber with phosphate buffered saline (PBS, pH = 7.34) and carried the generated NO gas to the chemiluminescence detection chamber in the Sievers nitric oxide analyzer (Model 280, Boulder CO). The gas NO content was determined by measuring peak flux for 4 separate membrane pieces.

3.2.3 Strains and Media

The antibacterial effects of Cu and NO were analyzed using *Staphylococcus aureus* (*S. aureus*) and *Pseudomonas aeruginosa* (*P. aeruginosa*), Gram-positive and Gram-negative bacterium, respectively, commonly found in blood stream infections.[1] Strain ATCC25923 of *S. aureus* and strain ATCC27853 of *P. aeruginosa* were used. Before experimentation, a growth curve for each bacteria strain was produced by transferring cells from a -80°C frozen stock, streaking 10 µL on a Luria-Bertani (LB) (LB Agar Lennox L, Invitrogen, Carlsbad, CA) agar plate, and incubating it overnight at 37°C. The next day, cells from four colonies were inoculated into 10 mL of Tryptic Soy Broth (TSB) (Remel Tryptic Soy Broth, Thermo Scientific, Waltham MA) plus 1% glucose media and incubated at 37°C with aeration. After a 6-hour incubation, optical density readings were taken at 600 nm with a spectrophotometer (Nanodrop 2000C, ThermoFisher Scientific, USA) every 30 minutes based on growth curves in previous literature[4,6,9,147]. At each 30 minute time point, a 100 uL sample was also serially diluted and then plated on an LB agar plate and then incubated for 18 hours overnight at 37°C to quantify the viable cells at that time point, as described by previous literature.[174] A

curve to describe the relation between optical density and CFU/mL was created for each strain and used to inoculate media to use during experimentation.

3.2.4 Preliminary Flow and Conventional Shaking Experiments

The main methodology in literature to measure bacterial adhesion on a potentially antibacterial biomaterial uses coupons of the material that are inoculated with a known concentration of bacteria in a petri dish or micro-well plate in a near static environment or agitation with orbital shaking.[18,159,193] However, these conditions do not mimic the local environment of a hollow fiber bundle oxygenator. Thus, this conventional method was compared to the novel bioreactor setup to observe differences in bacterial adhesion. For the conventional, shaking method, 1.75 cm^2 PDMS membrane coupons were placed in a petri dish with 5 mL of a starting media with a concentration of $10^{4.5}$ CFU/mL of *S. aureus* in a shaking incubator for 4 hours. This starting media is a low nutrient media with 1:5 ratio of sterile TSB and 1% glucose to water. For the revised method under flow, the previously described bioreactor was used. All chamber and connector components were sterilized prior to the experiment using an autoclave. The same starting media that was in the petri dish was pumped through the bioreactor at a flow rate of 1.81 mL/min for 4 hours using a peristaltic pump (Watson Marlow 505U, Wilmington MA). This flow rate sets the bioreactor media velocity equal to the blood flow velocity through an adult Quadrox oxygenator with 2 L/min flow and a 100 cm^2 frontal area.

After four hours of testing, membrane-adhered bacteria and planktonic bacteria in both experimental setups were compared for viability by quantifying viable colony forming units on agar plates. To assess the bacterial viability of the cells adhered to the

membrane, the bioreactor membrane was removed under sterile conditions and gently rinsed in sterile Hank's Balanced Salt Solution to remove unattached bacteria. To ensure the adhered bacteria on the membrane were accurately measured, bacteria were removed by vortexing. Under sterile conditions, the membrane was transferred to a 50 mL Falcon tube containing 10 mL sterile TSB and 1% glucose. It was then vortexed at the highest setting on the Vortex Mixer (Vortex-Genie 2, Scientific Industries, Bohemia, NY) for 3 minutes to shear off all attached bacteria into the media. This membrane was then transferred to a second 50 mL Falcon tube with 10 mL TSB and 1% glucose and vortexed a second time for 3 minutes to ensure all adhered bacteria were removed from membranes. The resulting bacterial suspension samples were plated on LB agar plates to assess viability of the membrane-adhered bacteria. This process was completed as discussed in previous literature.[2,3] In brief, the bacterial suspension was serially diluted (10^{-1} – 10^{-6}) and then 50 µL of each diluted sample was plated on LB agar plates. Agar plates were then covered and placed in a sterile incubator at 37°C for 18 hours. Post incubation, colony-forming units (CFUs) were counted three times and averaged for a final colony count. Similarly, to measure the viability of the planktonic bacteria 1 mL of residual media was taken from the fluid side of the flow chamber and from the media in the petri dish and transferred to separate microcentrifuge tubes for serial dilution and plating onto agar plates. The same growth and quantification process was used here. To ensure consistency between trials, CFU counts were obtained with serial dilutions and cells from the initial bacterial suspension that was pumped through each experiment was also quantified. If the initial bacteria concentration did not fit in the range of $10^{4.5 \pm 0.5}$ CFU/mL then that trial was not used.

3.2.5 Experimental Setup: Role of Copper and Nitric Oxide Flux on Bacterial Viability

In this next phase, the ability of a NO-generating Cu-PDMS surface to limit bacterial colonization was evaluated using the same bioreactor system. A “decisive period” of 4-6 hours following ECMO circuit placement has been identified for being critical in preventing infection.[5,8] Thus, an experimental time of 4 hours was chosen for the experiment. As in the previous experiment, a low-nutrient medium was pumped through the circuit for the duration of the experiment, with constant flow provided by a peristaltic pump as seen in Figure 3-3A. The media was made by sterilely combining TSB with 1% glucose and water in a 1:5 ratio. A blood stream infection was simulated by inoculating the entire circuit volume with bacteria to a concentration of $10^{4.5 \pm 0.5}$ CFU/mL by using the previously made growth curves. This concentration was chosen from previous literature values of blood stream infections[25,54,76,157] and was verified by growing the inoculated media on agar plates and counting the viable colonies for each experiment.

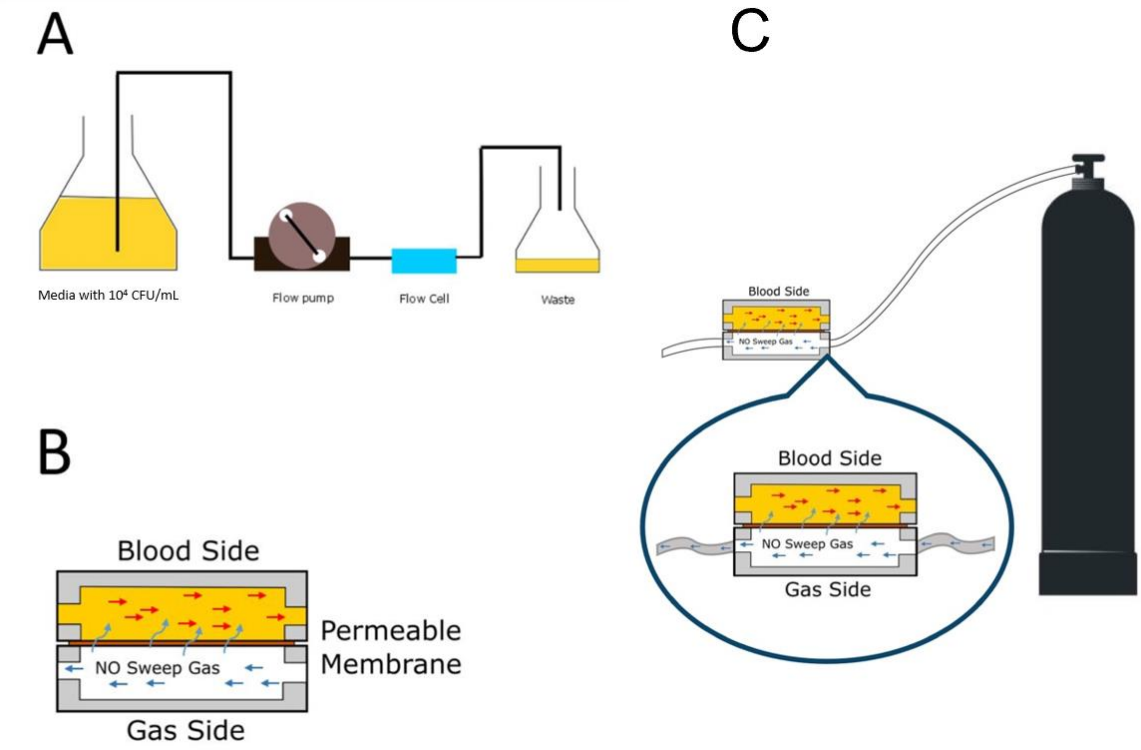

Figure 3-2. Experimental setup with a single direction of flow (A). The bioreactor chamber has a blood side and a gas side, divided by a permeable membrane which represents the hollow fiber membrane (B). Gas is provided at the same rate as in a hollow fiber membrane oxygenator (C).

Each experiment utilized a different combination of Cu exposure, presence of the NO donor GSNO, and NO flux to best evaluate the separate and combined effects of each aspect of the NO-generating Cu-PDMS surface on surface bacterial colonization and growth. Table 1 summarizes the six combinations of Cu expression and NO delivery: (1) PDMS membrane only (negative control); (2) Cu-PDMS membrane only; (3) PDMS membrane with a GSNO infusion at 1 µM, (4) Cu-PDMS membrane plus GSNO infusion at 1 µM; (5) PDMS membrane plus 250 ppm gNO; (6) Cu-PDMS membrane plus 250 ppm gNO. These groups were chosen to distinguish between the individual and combined effects of nitric oxide and copper. Groups 1 and 2 showed the antibacterial effect of copper alone at the blood contacting surface, without any sort of

nitric oxide. Group 3, while not an accurate representation of a real NO delivery platform, showed the effect of GSNO on bacteria growth. Group 4 showed the combined effect of surface generated NO and copper at the blood-material interface. Group 5 showed the individual effect of gaseous NO delivery at 250 ppm, and group 6 showed the combined effect of gaseous NO with copper at the blood-material interface. The concentration of gaseous NO used was 250 ppm for its known antibacterial effects at this range, as lower ranges may actually induce biofilm growth and signalling.[9,95,133] Additionally 250 ppm was chosen since it was used in an *in vivo* rabbit study and successfully inhibited platelet function without causing methemoglobin toxicity.[50]

Table 3. Testing Matrix reflecting PDMS surface conditions.

	Copper Expression	Cu-Mediated NO Generation via GSNO	NO Flux from Sweep Gas
1. PDMS membrane only			
2. Cu-PDMS membrane only	✓		
3. PDMS membrane with GSNO		✓	
4. Cu-PDMS membrane with GSNO	✓	✓	
5. PDMS membrane with gNO			✓
6. Cu-PDMS membrane with gNO	✓		✓

All chamber and connector components were sterilized prior to the experiment using an autoclave. Media was pumped through the blood side of the bioreactor at a rate of 1.81 mL/min using a peristaltic pump (505 U, Watson Marlow, USA) as in the previous experiment. When NO was delivered via the sweep gas, 1.81 mL/min of 500 ppm NO in N_2 was mixed with 1.81 mL/min of oxygen just prior to the device inlet, to

provide 250 ppm of NO at a flow rate twice the blood flow rate. After 4 hours, media and gas flow were stopped, and the inlet and outlet were closed to prevent further flow and keep the entire circuit sterile. The membrane was then removed under sterile conditions for quantifying the adhered bacteria. All samples were tested in replicate (n = 5). The viability assessment of adhered bacteria was conducted in two ways: (1) change in broth turbidity following 6 hours of culture and (2) CFU counts on LB agar plates. In the first assessment, the antimicrobial effect of the tested conditions is measured by quantifying the membrane adhered bacteria. The bacteria that were removed from each membrane after the 4-hour experiment were immediately inoculated into 10 mL of fresh TSB with 1% glucose and turbidity was measured at 600 nm using a spectrophotometer (Nanodrop 2000C, ThermoFisher Scientific, USA). Then, the sample mix was placed in a shaking incubator with aeration at 37°C for 6 hours. Afterwards, turbidity was measured again. Measurements were taken three times per sample and then averaged and the change in optical density was graphed. The second assessment measures the extended antimicrobial effect of the tested conditions after the source has been removed from the bacteria. These bacteria adhered to the membrane were quantified by removing all cells adhered to the membrane, plating them onto plates, and counting the CFUs after 18 hours of growth as described above (Section 3.2.4). This data was graphed for the 6 cases described above.

3.2.6 Statistical Analysis

Statistical analysis was performed using SPSS software by using a two-way ANOVA. The two independent variables are presence of copper, and presence of nitric oxide, and the dependent variable was the change in optical density after 6 hours, or viable

CFU/mL after 18-hour growth on LB plates. The tests for between-subjects effects, and simple effects analysis, and pairwise comparisons can also determine if there is an interaction between nitric oxide and copper, such as when NO is generated from a Cu-PDMS surface and if these factors have effects individually. A Tukey post-hoc test was performed on these results. Statistical significance was confirmed for $p < 0.05$.

3.3 Results

3.3.1 Membrane Characterization

Using EDS, the PDMS membranes were determined to have 0 ± 0% Cu expression on the fluid interface and the Cu-PDMS membranes had 15 ± 1% copper expression at the fluid interface (Figure 3-3).

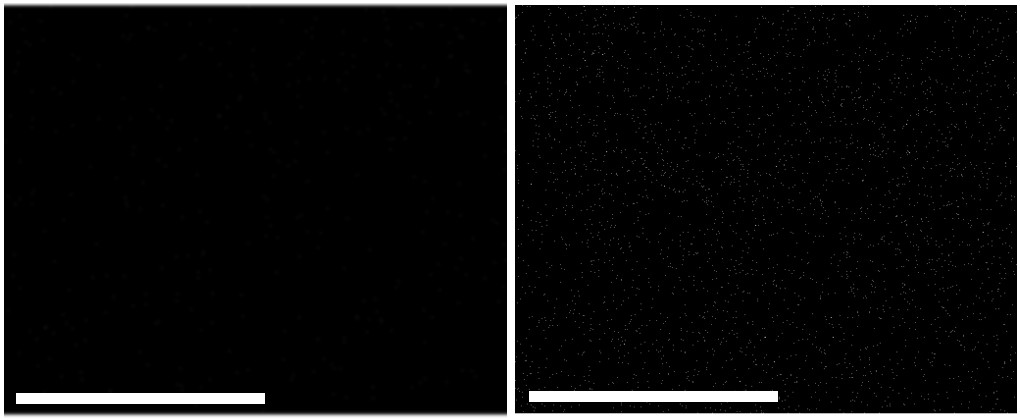

Figure 3-3. The EDS image shows 15 ± 1% Cu-PDMS copper expression at the surface representing the active area available to catalyze the NO release from GSNO. The copper is seen in white. SB = 900 µm

Using chemiluminescence, the NOA detected that the Cu-PDMS membranes have a NO-flux rate of $2.02 \pm 0.13 * 10^{-10}$ mol cm^{-2} min^{-1}. This correlates well with previous work that related surface copper expression to NO flux with the following equation:[6]

$$J_{NO} = (0.16\,(\%SA_{Cu}) + 0.34\,) \times 10^{-10}$$

3.3.2 Growth Curves

Equations for the growth curves were created as outlined in section 1.2.5 and used to estimate the preliminary mix of bacteria in media to simulate a nosocomial infection. The relationship between optical density and viable colony forming units for *S. aureus* was estimated with the equation:

$$y = (4 \cdot 10^8)x + (3 \cdot 10^6)$$

And the growth curve for *P. aeruginosa* was estimated with the equation:

$$y = (5 \cdot 10^8)x + (3 \cdot 10^7)$$

Based on these values, the starting concentrations of bacteria in the experimental studies were made to be 10^4 colony forming units per milliliter (CFU/mL) by inoculating a known concentration of bacteria into a larger volume of fresh media. The actual concentration of bacteria in starting media was $10^{4.02 \pm 0.01}$ CFU/mL and $10^{4.46 \pm 0.03}$ CFU/mL for *S. aureus* and *P. aeruginosa*, respectively.

3.3.3 Bacterial Adhesion Under Flow and Conventional Shaking Conditions

The concentration of bacteria in the media and on the membranes was determined under static and flowing incubation. The media had 4.54 ± 0.04 and 4.14 ± 0.03 log CFU/mL in the static and flow cases, respectively ($p = 0.03$). Thus, there was a small, but statistically significant reduction in bacterial growth under flowing conditions. The membrane had 3.98 ± 0.09 log CFU/mL and 2.60 ± 0.04 log CFU/mL in the static and flow cases, respectively. Thus, flow significantly reduced bacterial adhesion on the membrane ($p = 0.009$) and to a greater extent than what was seen in the media. While these two cases are not directly comparable since the static case was not also

conducted inside a bioreactor chamber and circuit, it provides a more conservative scenario for the static case. Because the bioreactor chamber volume is less than the petri dish, there would have been a more concentrated and overestimate of the bacteria inside a static bioreactor case. However, a closer look at the bacteria attached to the membrane could be taken to observe only the effect of flow on adhesion. Most likely under flow, the reduced residence time each bacteria cell had to contact and form adhesions to the membrane was a contributing factor to the lowered adhesion.

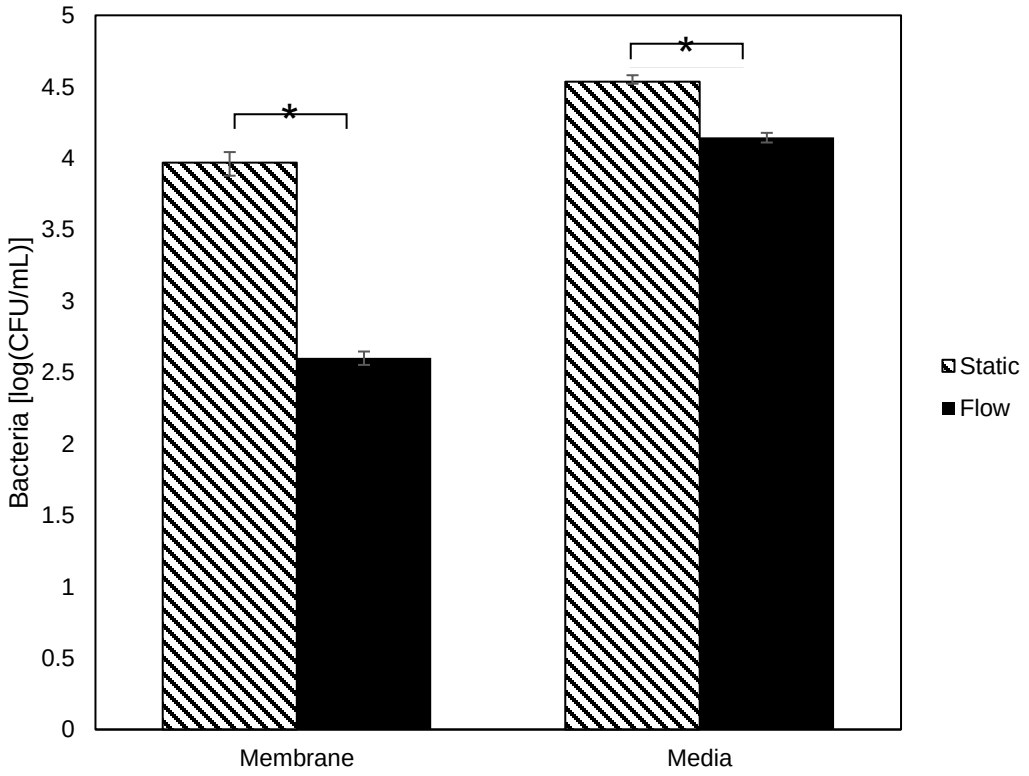

Figure 3-4. A reduction of S. aureus bacteria can be seen in the experimental bioreactor circuit case under flow when compared to the conventional coupon method in both the number of bacteria adhered to the membrane and in the media surrounding the membrane.

3.3.4 Inhibition of P. aeruginosa Bacteria Adhesion by Cu-PDMS Membranes

Results show that a Cu-PDMS membrane minimally reduces adhesion of *P. aeruginosa* bacteria when compared to a PDMS membrane. Bacterial viability measured with optical density showed that there was less bacteria in the Cu-PDMS case when compared to PDMS membrane, however it was not significantly less (Figure 3-5A) ($p = 0.454$). Without looking at the effects of NO, a Cu-PDMS membrane reduced bacteria growth by 0.014 ± 0.005 when compared to the control PDMS membrane. Even after the bacteria were removed from the membrane, the antibacterial effect of the Cu-PDMS membranes persisted as seen from the agar plates (Figure 3-5 B). These results showed significantly less viable CFUs adhered to Cu-PDMS membranes than on PDMS membranes ($p = .00018$), with a reduction of 0.72 log(CFU/mL).

Bacteria that were exposed to 250 ppm gaseous NO (gNO) flux had reduced growth. The independent effect of gNO delivered through a PDMS membrane had an average OD_{600nm} decrease of $0.025 \pm .007$ ($p = 0.049$). When combined with a Cu-PDMS membrane, gNO had decreased the reading by 0.014 ± 0.001 when compared to the no NO case. The inhibitory effect of gNO did not extend to the bacteria grown on plates with $3.27 \pm .03$ log(CFU/mL) on control PDMS membranes and $2.97 \pm .05$ log(CFU/mL) in the Cu-PDMS case and were not significantly different from the no NO cases ($p = 0.105$ and $p = 0.111$, respectively).

P. aeruginosa that was exposed to surface generated NO had significantly stunted growth. Cu-catalyzed surface NO generation from GSNO reduced bacteria growth by 0.012 ± 0.001 OD_{600nm}. When GSNO was supplied with a PDMS membrane,

it reduced growth by 0.027 ± 0.002 OD_{600nm}. In this scenario, minimal amounts of GSNO decomposed into NO, and means that the effect of GSNO on its own was able to reduce bacteria adhesion. The NO released from catalyzed GSNO by the Cu-PDMS membrane had a lesser inhibitory effect. The growth of bacteria on plates showed that the inhibitory effects did not last when the NO source was removed. There was no difference between GSNO delivered with a PDMS membrane or Cu-PDMS membrane, with 3.44 ± .06 log(CFU/mL) and 3.07 ± .08 log(CFU/mL) respectively ($p = 0.279$).

These results show that while both means of NO delivery provided an antimicrobial effect on *P. aeruginosa*, it did not last when the bacteria were removed from the system and grown on plates. On the other hand, copper from the Cu-PDMS membranes did not significantly affect the growth of *P. aeruginosa*, but the effects were consistent and seen in reduced cell viability when grown on plates.

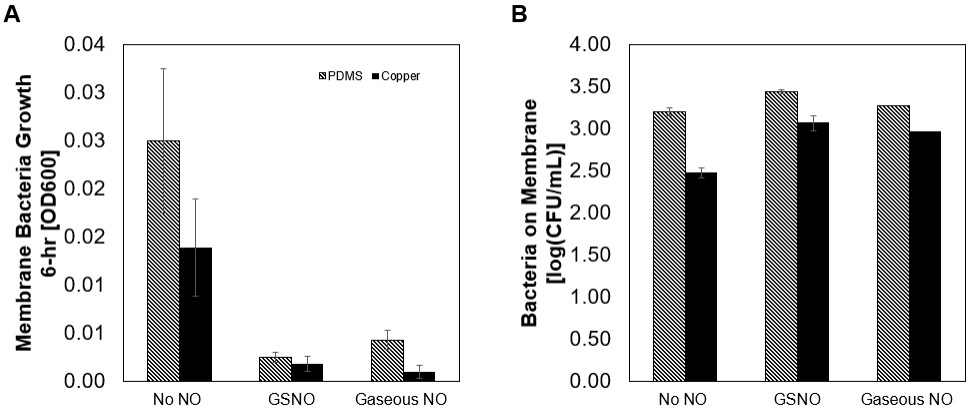

Figure 3-5. P. aeruginosa bacterial adhesion on membrane after exposure to copper, surface generated nitric oxide (NO), or gaseous NO. (A) The short-term viability of adhered bacteria, measured in optical density after incubation in TSB for 6-hr. (B) The effects of these antibacterial agents after 18-hr growth of bacteria on an agar plate in log(CFU/mL).

3.3.5 Inhibition of S. aureus Adhesion Under Oxygenator Conditions

Bacterial adhesion of *S. aureus* bacteria was inhibited by the addition of NO flux and copper individually, but the combination of copper and NO flux did not result in a greater antimicrobial effect. Copper on its own inhibited bacterial growth, with a 0.332 OD_{600nm} decrease when compared to the bacterial growth from the control PDMS membrane. However, this effect was not significant ($p = 0.569$). The Cu-PDMS membrane affected bacteria that was adhered to it even after it was no longer in contact as shown from growth on agar plates. These results showed that a Cu-PDMS membrane decreased the number of viable bacterial cells by 0.332 log(CFU/mL) when compared to the control PDMS membrane, and approached significane ($p = 0.066$).

On the other hand, 250 ppm of gNO delivery did not have a significant reduction in bacterial adhesion after 4-hour exposure. When independently exposed to bacteria with a PDMS membrane, gNO only mildly reduced the 6-hour growth ($p = 0.749$) and did not reduce much more when combined with a Cu-PDMS membrane ($p = 0.830$). The growth on plates revealed similarly that the effect of gNO on the growth of bacteria was mild and actually increased the number of viable colonies ($p = 0.018$).

The infusion of GSNO, on its own, decreased the growth of bacteria on both the PDMS membrane and the Cu-PDMS membrane, but did not significantly affect the growth of bacteria on plates after the GSNO source was removed. Independent 4-hour GSNO exposure reduced bacteria growth significantly by 0.0225 OD_{600nm} ($p = 0.032$). When combined with Cu-PDMS, the release of NO from the membrane surface also significantly reduced bacterial growth when compared to the Cu-PDMS membrane independently ($p = 0.011$). This reduction in bacterial growth did not persist after the

bacteria was removed from the GSNO source, and there was no significant difference between both membranes with or without GSNO infusion ($p = 0.165$).

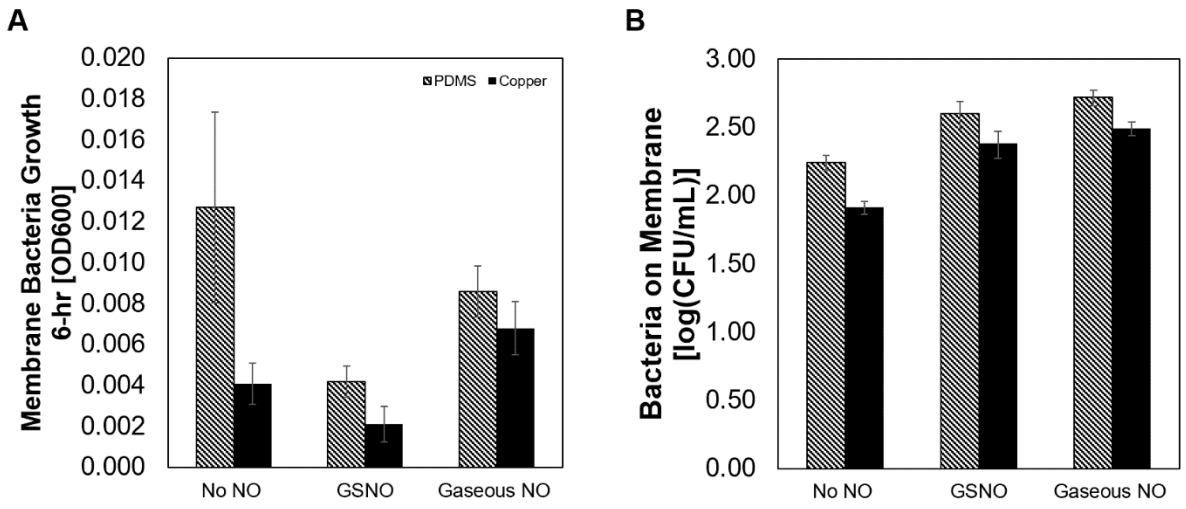

Figure 3-6. S. aureus adhesion on the membrane after a 4-hr flow experiment. (A) The short-term viability of adhered bacteria that is measured after incubation and 6-hr growth with turbidity at OD_{600nm}. (B) The long-term viability of bacteria adhered to the membrane grown on agar plates.

These results show that there is inhibition of *S. aureus* bacteria growth from both delivering NO at the surface and from gas. These results are not enhanced when combined with a Cu-PDMS membrane.

3.4 Discussion

3.4.1 Effects of Flow Chamber on Gaseous Nitric Oxide and Surface Generated Nitric Oxide Delivery

This study modeled the local conditions of a membrane oxygenator using a unique flow chamber that enabled Cu expression and NO gas delivery through its permeable membrane. It simulated the constant transport of fluids to and from the surface of a hollow fiber permeable membrane in order to more accurately depict transport of bacteria, Cu ions, and NO gas.

The initial hypothesis that nitric oxide is antimicrobial in this setting was proven, and these inhibitory effects were seen after 4 hour exposure. These inhibitory effects may be milder than seen in previous literature due to the following reasons. For one, the amount of NO flux the bacteria experienced may have been lower than what was found to be bactericidal. In a study by Jardeleza et al, *S. aureus* biofilm was exposed to a low and a high level of NO, 0.9-2.0 µM and 125-1000 µM respectively. At the higher NO concentrations there was decreased biofilm biomass, and at lower concentrations of NO the biomass was increased significantly ($p < 0.001$).[99] In another study by Neufeld et al., GSNO was applied to *P. aeruginosa* biofilms in a range from 5-25 mM.[141] This study found that 10 mM of GSNO provided the critical amount of NO for 90% bacterial killing, or 1.49 mM of NO. The flow circuit for my study received an infusion of 1 µM GSNO, reflecting the infusion of NO-donor in previous experiments for anti-platelet activity. The GSNO infused directly into the bioreactor chamber resulted in a surface generated NO concentration of 73.7 nM. The delivery of 250 ppm of gaseous NO case translates to a concentration of 8.2 µM. These lower concentrations do not provide the same antimicrobial effect that higher concentrations do, and instances of low NO concentrations have been recorded to provoke combative mechanisms from the bacteria. This response continues to protect the bacteria after it has been removed from the membrane and then plated (see Section 3.4.3) and may be why the growth on bacterial plates do not appear impeded as seen in Figure 3-5 B and Figure 3-7 B.

In addition, the NO flux that was experienced by the bacteria on the other side of the membrane may have been lower than the concentrations that were delivered due to convection and transport away from the surface. Nitric oxide provided either through

surface generation or from the gas side of the chamber is constantly being removed from that interface due to fluid flow. Thus, even though we supplied NO at concentrations known to be antimicrobial, bacteria on the other side of the membrane most likely experienced a lesser concentration. However, both strains of bacteria experienced short-term bactericidal effects when exposed to NO flux on the membrane surface. This suggests that a longer period of higher concentrated NO delivery from gas and surface generation could further reduce adhesion and viability. In a medical device that experiences flow at the blood material interface, NO flux can be used to deter bacterial adhesion, and standard antibiotics can be used to target the planktonic bacteria.

The bacterial growth on agar plates show the effect of 4-hour exposure to NO after the bacteria have been removed from the surface that is releasing NO. Agar plates are an ideal environment to grow, and thus, the CFU counts reflected the bacteria response to the oxidative stimulus and recovery. Thus, the turbidity measurements conducted after the experiments are more representative of the antimicrobial effects of NO flux and copper exposure at the membrane. If the experiment had been extended past 4-hours, the antimicrobial effect might be more pronounced during a long-term incubation study.

3.4.2 Bacterial Mechanisms to Counter Antimicrobial Therapeutics

From growth and transcriptional studies, bacteria have been shown to have the ability to sense and respond to exogenous NO. In particular, *S. aureus*, among other gram-positive bacteria, have shown to have a metabolic adaptation to nitrosative stress.[41,94] For one, *S. aureus* itself produces NO endogenously for metabolic use through synthesis of bacterial nitric oxide synthase (bNOS), which is only found in gram-

positive bacteria. In a study by Gusarov *et al.*, endogenously produced NO has been shown to protect *S. aureus* from broad spectrum antimicrobial therapy, and thus it is possible that an exogenous NO source could also provide this mechanism.[85] Additionally, NO-inducible lactate dehydrogenase in *S. aureus* provides it with the ability to replicate under nitrosative stress, and may have also played a role in the improved growth seen on the agar plates in this study.[158]

Similarly, *P. aeruginosa* also has mechanisms that respond to NO and nitrosative stress. *P. aeruginosa* has mainly been reported to have NO mediated dispersive events, in which mature biofilms slough off small aggregates of bacteria to travel elsewhere and colonize another location. In this same vein, NO has also been found to modulate the ratio of biofilm to planktonic bacteria. The motility of *P. aeruginosa* is enhanced after exposure to low concentrations of GSNO (1 μM) for 24 hours, increasing swimming by 39% and swarming by 116%.[10] These dispersive effects can be seen more clearly in the current study with *P. aeruginosa* than with *S. aureus* using the optical density readings, as there was a larger reduction in growth in *P. aeruginosa* than with *S. aureus*. However, these effects may not carry over to the agar plate may be due to the denitrifying abilities of *P. aeruginosa*. *P. aeruginosa* produces endogenous NO at a steady state concentration of 2-4 nM and also has the ability to metabolize NO with two enzymes bound to the inner membrane of each cell, NO reductase and the copper containing N_2O reductase.[44] These are a few of potentially many combative mechanisms these bacteria activate when exposed to sublethal NO concentrations to counteract antimicrobial agents.

3.4.3 Bacterial Response to Copper on Cu-PDMS Membranes

Copper consistently reduced bacterial growth and adhesion on the Cu-PDMS membranes when compared to the control PDMS membranes, albeit to a small degree. The mechanistic action of copper on bacterial cells is not fully understood, but part of the toxicity is inferred to come from the oxidative stress through contact killing imparted by a copper surface on the cell membrane. Copper can cause redox potentials across the membrane, from +200 mV to +800 mV, and cause cellular membrane damage.[193] Further, cells removed from copper have shown loss of cell integrity, which translates to the observed lower viable cell counts.[159] Thus, the antibacterial effect from the Cu-PDMS membranes may have not been strong enough to completely kill bacterial due to the low surface exposure, around 15%. In addition, contact killing would work more effectively if the residence time was long enough between the bacteria cell and the Cu-PDMS membrane.[81] Cu-PDMS provides an antimicrobial effect on adherent bacteria due to the proximity the cells and the membrane have.

Another reason why Cu-PDMS did not prevent more bacteria adhesion is that bacteria have the potential to develop a copper tolerance. Copper transporting ATPases are present in some bacterial cytoplasmic membranes and are expressed more when under stresses and when copper tolerance is developed.[8] Responses to copper can occur in less than 2 hours.[122,154] Increasing the surface composition of copper on the membrane would most likely increase the killing as well as the surface generation of NO. In literature, between 1-10% wt Cu NP have been incorporated into polymer matrices for NO generation, and incorporation of more Cu could also be used.[21,71,123] However,

this is limited as the percentage of copper is increased the membrane also becomes less permeable to gas transfer.

3.4.4 Minimal Effect on Planktonic Bacteria

Under the flow chamber conditions, there is also minimal exposure from the oxidative and nitrosative stress on bacteria that are flowing by. As bacteria suspended in the fluid were quickly moved away through convection, they experienced less NO flux and minimal contact to the Cu-PDMS membranes and received small bacteriostatic effects for both *P. aeruginosa* and *S. aureus*. As seen in Figure 3-7 A, there is an antimicrobial effect from both surface generated NO ($p = 0.048$) and gaseous NO delivery ($p = 0.054$) that killed planktonic *S. aureus* bacteria in both membrane groups. However, these inhibitory effects did not extend to the bacterial growth on plates, again proving that proximity to the NO flux is required for the antimicrobial effects.

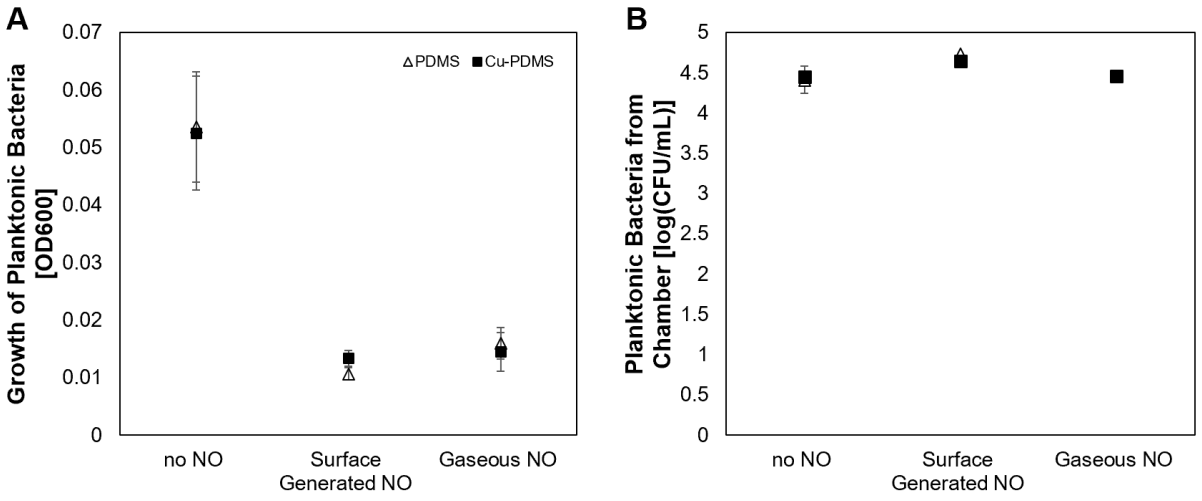

Figure 3-7. The planktonic *S. aureus* bacteria was affected negatively by both NO delivery mechanisms in the short-term when compared to the negative control (A). The viable bacteria on membranes showed that those effects from NO did not persist after growth on agar plates, and in fact had a slightly positive effect (B).

Just like the Gram-negative bacteria, the effects of the surface generated NO, gaseous NO, and Cu-PDMS membrane on planktonic *P. aeruginosa* bacteria in the chamber

were similarly inhibitory (Figure 3-8 A). Only the surface generated NO significantly decreased the growth of planktonic *P. aeruginosa* bacteria ($p = 0.021$) when compared to the no NO case. The inhibition of bacteria growth did not translate to the inhibition of growth on agar plates after the NO source had been removed. As seen in Figure 3-8 B, there is not a clear effect on planktonic bacteria from the groups that received NO, nor from the use of a Cu-PDMS membrane. Overall, effects of NO on inhibiting bacteria growth existed, however, these effects did not persist once the bacteria were removed from the NO containing environment. The main benefit of releasing NO flux and exposure of Cu at the hollow fiber membrane is the focused effect at the surface that reduces adhesion and growth of bacteria.

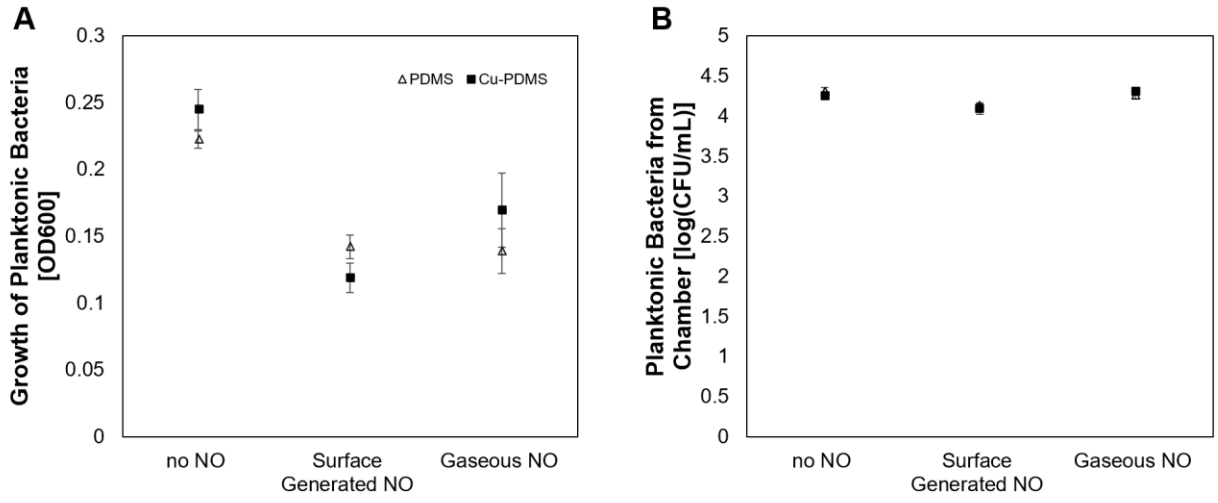

Figure 3-8. Effect of surface generated NO, gaseous NO, and a Cu-PDMS membrane on planktonic P. aeruginosa bacteria. (A) The short-term effects of NO are antibacterial but mild. (B) The effects of NO and copper from the Cu-PDMS membrane are not seen in the planktonic *S. aureus* bacteria.

3.5 Conclusion

To summarize, this study suggests that there are inhibitory effects from 4-hour exposure to surface generated NO and gaseous NO, and that bacteria adhered to Cu-PDMS membranes have inhibited growth. While there were no additional beneficial enhancements of the antimicrobial therapies by combining NO delivery with copper, these therapies can be individually applied as an initial burst therapy, then followed up with an antibiotic drug, such as tobramycin, as the initial antimicrobial effect could weaken the adhered bacteria. Nitric oxide flux from the surface and Cu-PDMS materials can be employed to prevent bacterial adhesion and biofilm formation, and systemic antibiotics can be used to kill bacteria in the blood until the circuit is removed or replaced. This combined treatment could remove all of the adhered bacteria from the hollow fiber membrane without increasing the risk of bacterial resistance from using multiple broad-spectrum antibiotics.

4 Macro- and Micro-scale Evaluation of Clot Formation in an Oxygenator Hollow Fiber Bundle

4.1 Introduction

Currently, it is not known how fiber bundle design parameters affect clot formation. This includes the fiber bundle frontal area, path length, and packing density. It may be that designs that have similar gas exchange have different degrees of clot formation, and this may, ultimately, cause significant differences in long-term function. To date, there are only CFD models for simulating blood flow velocities and shear stresses through a fiber bundle.[56,66,164,165,206,207] Those CFD models offer limited information on where clots might form in the device due to low blood velocity or high shear stresses. However, they cannot predict the complex interplay between blood flow velocity, shear stress, and transport and activation of clotting factors, platelets, and platelet agonists such as thrombin. Long-term experiments can be used to indicate the most likely regions of clot formation, but these experiments are time consuming, require large animal numbers due to animal to animal variability, and thus expensive. Correction of excessive clot formation also requires repetitive trial and error testing, including device redesign and prototyping.

Research is thus needed to study the initiation and progression of clot in a fiber bundle under controlled conditions. The results of these studies could then be used to validate mathematical models of clot formation, and these models could then be used to design artificial lungs that clot more slowly and thus a longer functional life. To resolve this gap, this study examines the effects of fiber bundle path length, packing density, and blood flow velocity on the initiation of clot formation and the initial localization of

platelets and fibrin at the blood-material interface. To do this in a low cost, high throughput manner, a 3D-printed flow chamber that mimics the fluid mechanics of the fiber bundle was used. The design of these devices could be adjusted easily to replicates fiber bundles with different geometries. Human blood at clinically relevant activated partial thromboplastin times (aPTTs) was pumped through these devices for 15-minutes, and the extent of clot monitored using a combination of blood flow resistance testing and post-experiment imaging. The microfluid channel material could not be constructed from polymethylpentene, the typical fiber material used in long-term artificial lungs. However, the urethane acrylate resin that the chamber is made of is similar to the polyurethanes that are used in many artificial lung housings.

4.1.1 Hollow Fiber Parameters That May Affect Coagulation

There is no standard artificial lung fiber bundle geometry. Some fiber bundles are rectangular, such as the Maquet (Getinge) Quadrox, while others are cylindrical, such as the Medtronic Affinity or Terumo's Capiox. Despite this, the shape and dimensions of these fiber bundles can be simplified to factors that were mentioned earlier, the packing density and the path length and frontal area. Assuming a certain surface area fiber bundle is needed for gas exchange, the fiber bundle shape could also be characterized by a surface area and aspect ratio equal to the frontal area divided by the path length. Fiber bundle packing densities range from around 30-60% in research and commercial devices, and some experimental devices have packing densities as low as 25%. Path lengths in commercial devices range from 2 to 4 cm and frontal areas can range from 80 to 100 cm^2. All of these factors contribute not only to how the fiber bundle transfers

oxygen, but also to blood flow velocities, shear stresses, and potentially how clot may initiate and grow inside the fiber bundle.

4.2 Methodology

4.2.1 Experimental Design of the Flow Chamber

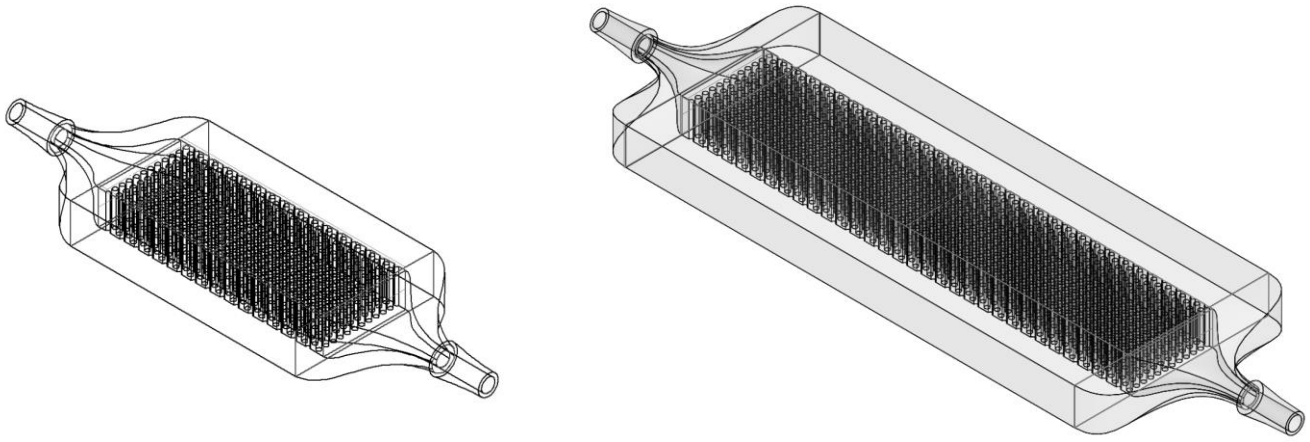

Figure 4-1. A CAD of the flow chamber for 2 cm long (A) and 4 cm long (B) path lengths.

To simulate the local conditions of an artificial lung hollow fiber bundle, miniature flow chambers (Figure 1-2) were first created in computer aided design (Solidworks, MA). This bench top model of a fiber bundle represented a small excerpt of a clinical oxygenator with various combinations of the physical fiber bundle parameters: packing density and path length. Each flow chamber was 7.3 mm wide by 3 mm tall and was 20 or 40 mm long and had a barbed inlet and outlet for 1/16” tubing. Rods with a 380 µm diameter were spaced evenly inside the device and spaced to create packing densities of 40%, 50%, or 60% (Figure 4-2). These rods spanned the entire 3 mm height of the chamber and create blood flow patterns

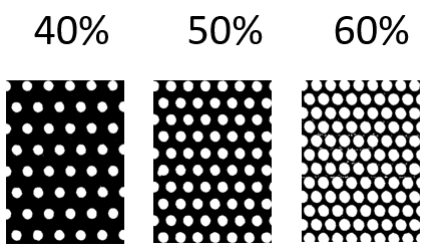

Figure 4-2. The various tested packing densities of hollow fibers in the flow chamber.

similar to the hollow fibers of an oxygenator. The 3 mm height of these devices are smaller than the thickness of a full-sized fiber bundle, limiting clot formation in the flow chamber in the z-direction. A taller flow chamber would have more realistic flows. However, this height must be maintained in order the quantify clot inside the chamber with different imaging modalities.

Each chamber designed in CAD was then manufactured using a DLP 3D printer (Ember Autodesk, San Rafael, CA) for ease of repeatability and uniformity. A clear acrylate resin was used (PR-48, Colorado Polymer Solutions, CO), which is most similar to urethane acrylate plastic. After printing, the flow chamber was rinsed with 60 mL of isopropyl alcohol from both the inlet and outlet to remove uncured resin. The device was then post-cured with a UV lamp for 20 minutes and then sterilized using UV-ozone for 15 minutes.

Devices were thus designed and printed to simulate differences in fiber bundle packing density and path length. Rather than create devices with different frontal areas, the frontal areas were translated into the resulting fiber bundle blood flow velocity. These were set at 16, 20, and 25 cm/min, which corresponded to blood flowing through a full sized adult artificial lung at 2 L/min with 80, 100, and 120 cm^2 frontal areas. For each of the experiments, the devices were run in triplicate, with a standard device with parameters of 50% packing density and 2 cm path length in each set. For example, one donor's blood would be used for three flow chambers of 40%, 50%, and 60% packing density, all with a 2 cm path length, and with a flow rate of 4.38 mL/min. A second set would be run with the next donor's blood for three flow chambers that were all 50%

packing density and 2 cm long, but have different flow rates of 3.65, 4.38, and 5.46 mL/min.

Table 4-1. The tested parameters in the benchtop flow experiments.

Testing Parameter	Testing Range	Experimental Parameter
aPTT	25-55 seconds	Heparin Concentration
Packing Density	40%, 50%, 60%	Fiber Spacing
Velocity	16, 20, 25 cm/min	3.65, 4.38, 5.46 mL/min
Path Length	2 cm, 4 cm	Distance (x) through device

Baseline resistance was measured for each type of device using a glycerol water mixture. This mixture was set to a 3.4 cP viscosity using a viscometer (9721-B56, Cannon-Fenske, USA) and was pumped through at a rate of 3.65, 4.38, and 5.46 mL/min using a syringe pump. Pressure drop was measured with a manometer and used in the following equation to calculate resistance:

$$R = \frac{\Delta P}{Q}$$

Where R is resistance, ΔP is the pressure drop across the device, and Q is the flow rate. Pressure measurements were made in triplicate for each flow rate and then averaged.

4.2.2 Experimental Setup of Benchtop Experiment

Bench top experiments were conducted using human blood from consenting donors under an approved CMU Institutional Review Board protocol. Between 250-550 mL blood is drawn from each participant through the median cubital, basilic, or cephalic vein with an 18 G catheter, as per standard venipuncture procedures using a gravity drain. The blood was anticoagulated to 0.1 U/mL with heparin. After the full volume of blood has been collected in a sterile blood bag, it was moved to 60 mL syringes for the

experiment less than 10 minutes after the blood draw. A syringe pump (NE-300, New Era Pump Systems, Inc., NY) was used to pump blood through 1/16" Tygon tubing (E-3603, Saint-Gobain, Malvern, PA) (Figure 4-3) connected to the device in a single pass. Each donor's blood is used in triplicate, so each condition is tested with the same blood, reducing experiment to experiment variability.

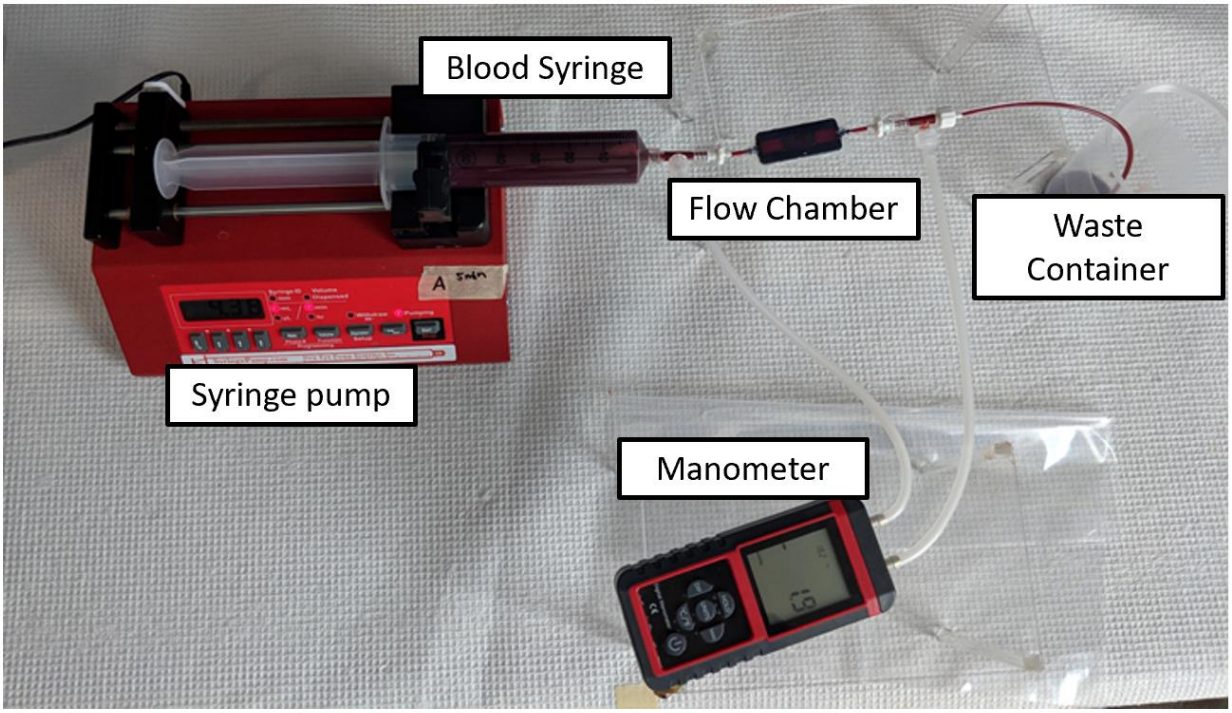

Figure 4-3. The experimental flow circuit invovles one-way flow from a syringe pump, connected to the flow chamber and then to a waste container. A manometer measures the pressure drop across each experimental device.

In this circuit, a manometer (CR410, Ehdis, China) was used to measure the differential pressure across the device every 3 minutes for a total of 15 minutes, and then used to calculated resistance using the standard equation mentioned above. Blood samples were taken at the inlet and outlet for the following tests: 2 mL in K_2EDTA purple top tubes for hematology and 3 mL in 1:9 citrate for aPTT and PT measurements (Diagnostic Stago Start 4, Siemens, Germany). If aPTT was not between 20-50

seconds, the experiment data was not used. After 15 minutes of flow, the pump was stopped, and the device was detached from the circuit and immediately rinsed with heparinized saline (2 U/mL) to halt the progression of clot formation. The flow chamber was then filled with 4% (v/v) paraformaldehyde and fixed overnight at 4° C.

4.2.3 Micro-Computed Tomography Scans

Micro-Computed Tomography (µCT) scans are used to quantify the clot volume inside the flow chambers. Prior to the µCT scan, the fixative inside the flow chambers are rinsed out using 10 mL of saline. Three flow chambers at a time are placed inside a custom built holder and then scanned using a Skyscan 1172 (Bruker-Skyscan, Contich, Belgium) µCT system that has a 3 µm voxel resolution and the following conditions: 40 Vp, 175 µA, 300 ms exposure, 0.4 degrees rotation step, 8 frame averaging. Then, the scans were reconstructed into a 3D volume using the software NRECON (Bruker-Skyscan, Contich, Belgium) with a 60% beam hardening correction and a ring artifact correction of 20. These volumes were then converted to ND2 files (FIJI, ImageJ 1.51H, NIH Bethesda, MD) and imported into the software Slicer 3D (Slicer 4.10.2) to be transformed, segmented, and cropped. To avoid artifacts from increased blood activation from the wall, the volume was cropped 0.4 mm from the top and bottom, 1.3 mm from each side, and 1 mm from the inlet side. The cropped volume was then imported as a DICOM image back into FIJI and then two analysis steps are done. First, a 3D probability map was created for each type of device by averaging all the clot volumes from the scans µCT (n = 6) for each parameter. Three-dimensional masks were created from scans of clean empty devices and subtracted from the experimental scans, so the volumes only consisted of clot (Figure 4-4 B).

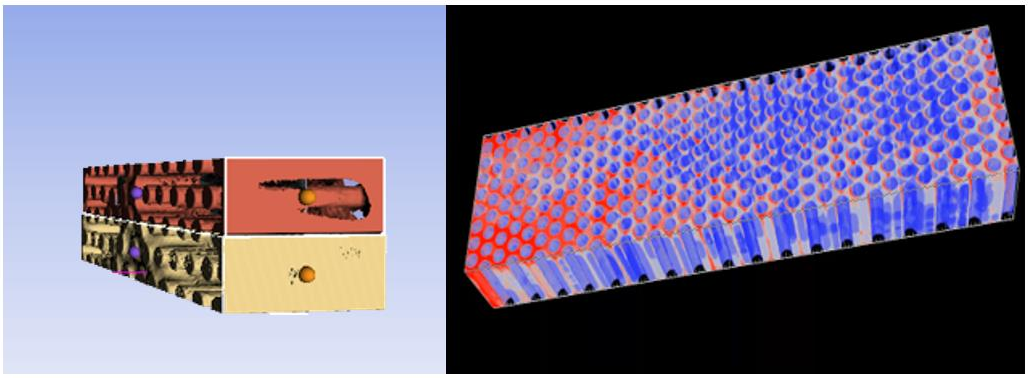

Figure 4-4. An image of the 3D reconstruction of a µCT scan in Slicer 4 software (A). These are then averaged with other scans, and the rods in the chamber are subtracted to create the 3D probability map of where clot is most likely to form, red being more likely and blue less likely (B).

Secondly, the resulting 3D volume was then sliced transversely from the inlet to the outlet and the clot at each slice was extracted using a custom macro (Appendix 7.1). Clot volume at 5 locations through the length of the device were summed for 2 mm segments and then graphed. Results were normalized based on the space available for clot to form in each type of chamber. In this chapter, the 3D probability maps are represented with a 2D image that is the 3D map that has been averaged through the z-direction for ease of displaying.

4.2.4 Equivalent Surface Area to Volume Distance

To relate the raw clot volume data back to full scale devices, clot is measured at a distance from the inlet that equates the volume to surface area ratio in a certain time. In other words, blood at this point should have been encountered the same surface area and been activated and prone to clotting the same amount across differently shaped devices under different flows. This allows for the raw data to be compared across fiber bundle parameters. For instance, in the various velocity conditon experiment which devices were run at 16, 20, and 24 cm/min, clot volume was measured at 6.8, 5.7, and 4.5 mm from the inlet, respecively, since each device had a 2 cm long path length with

50% packing density. And for the 40%, 50%, and 60% packing density devices, clot is measured at 10.0, 5.7, and 3.2 mm from the inlet, respectively.

4.2.5 Immunofluorescent Staining and Imaging of Clot Inside Flow Chamber

Separate experiments were run to specifically obtain microscale understanding of clot at the interface of the rods, using platelet and fibrin staining. The experiments were exactly the same as those in the previous section except for the introduction of a glass coverslip on one side of the flow chamber for visualization. This glass coverslip was not included in the previous studies, as it is more procoagulant than the urethane acrylate housing, leading to regional variability in clot formation.

In these experiments, packing densities of 40% and 60% and velocities of 16 cm/min and 25 cm/min were compared. After the 15-minute experiment, the chamber was rinsed with 10 mL of 2 U/mL heparin-saline and fixed overnight in 4% (v/v) paraformaldehyde. This was followed by six rinses with 1 X PBS (BP24384, Fisher Scientific, USA). Blocking with 1% (w/v) bovine serum albumin with 5% (v/v) goat serum in PBS for 2 hours at 4°C. For platelet and fibrin staining, 1:400 diluted CD61 stain (Tyr773 44-876G, ThermoFisher, USA) and a mouse monoclonal anti-human fibrin(ogen) (F9902, Sigma-Aldrich, USA) was incubated inside the flow chambers overnight at 4°C. The following day, after six rinses with 1 X PBS, the flow chambers were subsequently incubated with the secondary antibodies, goat anti-rabbit IgG (H+L) Alexa Fluor 555 (A-21428, ThermoFisher, USA) and goat anti-mouse IgG1 CF633 (SAB4600335, Sigma-Aldrich, USA), in a 1:250 ratio for 1 hour at room temperature.

These flow chambers were then rinsed with 1 X PBS three times and imaged on a confocal microscope (A1 R+ HD25 Nikon) using a 16 X NA water immersion objective.

Confocal z-stack images for each condition were obtained for 5 different fields for three different blood donors, resulting in n = 15 analyzed stacks per condition. Images were taken 100 µm past the coverslip for a 100 µm tall stack, for 20 slices, each 5 µm apart. For each field, the number of pixels above a predetermined threshold were counted for platelets and fibrin in three locations in the field, representing the front side of a fiber, back side of a fiber, and center spot between two fibers. This will reveal differences in platelet and fibrin deposition around the rods due to the various flow paths that can be used to validate computational models in the future.

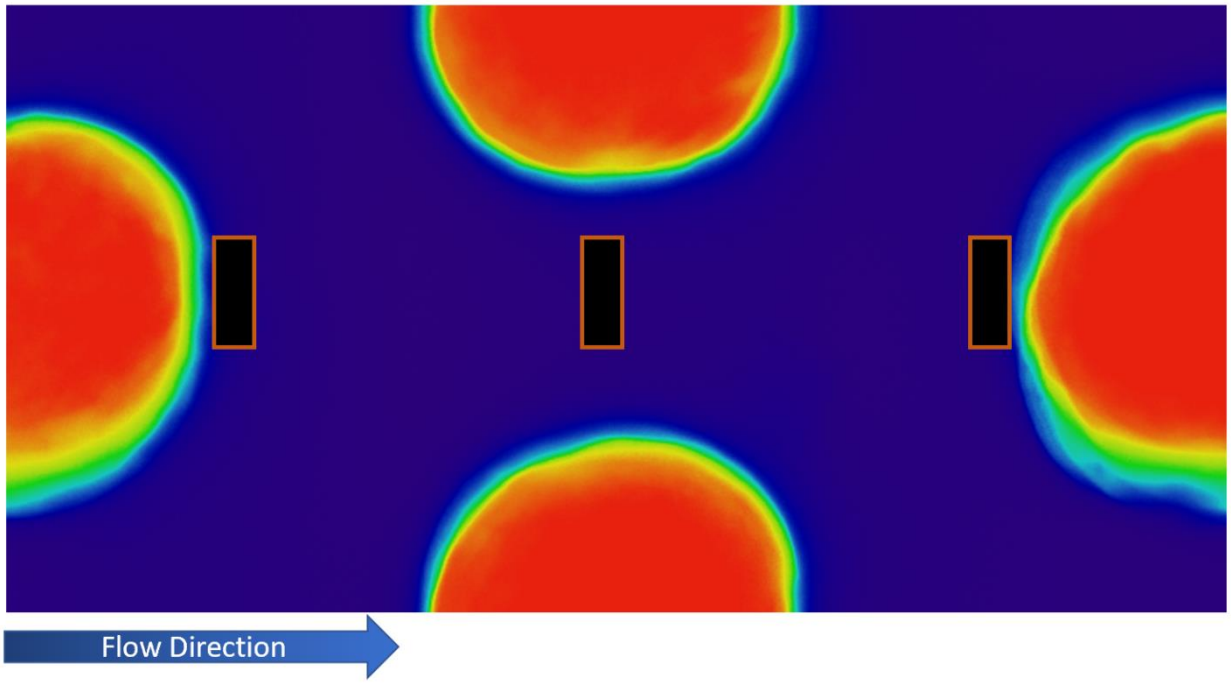

Figure 4-5. Three regions of interests are indicated here in black outlined in red, representing the back side of the fiber (left), the middle flow region (middle), and the front side of the fiber (right). Fluorescent intensities were quantified in these three regions.

For visualization, an average image for each condition was created by using a pixel per pixel plugin: Image Expression Parser.

4.2.6 Effect of Temperature on Clot Formation

Hypothermic conditions are known to increase platelet activation, but the exact manner in which it affects platelet function remains controversial.[58,128,150] For the purpose of this study, a preliminary experiment was conducted to compare the clot formation in a circuit heated to 37ºC and one at room temperature. A donor's blood was pumped through two circuits (Figure 4-3) that each featured a 2 cm long path length, 50% packing density device, at a flow rate of 4.38 mL/min. On device was kept at 37C using a heating pad (Zoo Med, San Luis, USA) that covered the circuit and device and the other remained at room temperature. This was completed for a total of 5 sets and then each device was imaged using the µCT methods as described in Section 4.2.3.

4.2.7 Statistical Analysis

All µCT clot volume and resistance values were analyzed for statistical significance using mixed model analysis with a Bonferroni corrected confidence interval using SPSS (IBM, Chicago USA). For a tested parameter, clot volumes were compared across all devices, with the blood donor ID as the subject variable. The independent variables were the condition being tested (e.g. velocity or packing density) and distance from the inlet, and the dependent variable was volume of clot at that distance. The aPTT was used as a covariate. For resistance analysis, the blood donor ID was used as a subject variable, the repeated-measure variable was time, and the independent variable was the condition being tested (e.g. velocity or packing density). The dependent variable was ln(resistance). The aPTT was set as a co-variate. Using SPSS,

a one-way ANOVA compared the clot volumes at an equivalent distance through the device for the packing density and velocity groups. For path length groups, clot volume for a 1 mm thick segment was compared at 10 mm and 20 mm from the inlet for both devices. This equivalent distance takes into account the surface activation of blood from each device. Post-hoc tests were completed using Tukey's test to find the difference between groups. In all cases, a p-value of < 0.05 was regarded as significant.

4.3 Results

4.3.1 Baseline and Inlet Conditions

The donor blood collected in this study was all within normal clinical ranges, albeit slightly on the low end (Table 4-2). However, the variation between groups was not large.

Table 4-2. Hematology of each donor group. All results are within normal clinical ranges. N = 6 for each group

	aPTT, s	***PT, s***	***HCT (%)***	***Hgb (g/dL)***	***PLT (k/uL)***
Flow Rate	36.9 ± 3.5	8.8 ± 0.3	38.8 ± 0.9	13.7 ± 0.3	237 ± 8
Path Length	36.0 ± 3.8	9.1 ± 0.3	39.5 ± 1.9	13.4 ± 0.7	275 ± 17
Porosity	41.2 ± 3.8	8.4 ± 0.1	40.9 ± 1.6	13.8 ± 0.4	240 ± 21

The baseline resistances for each device condition was measured using a glycerol and water mix and seen in Table 4-3. The longer path length device had a higher resistance to flow compared to the shorter path length devices. These values could be compared to the initial resistance measurements to inform us of immediate clot formation.

Table 4-3. Baseline resistance values for each packing density and path length condition.

	2 CM			4 CM
	40%	50%	60%	50%
RESISTANCE (mmHg/(mL/min)	0.333 ± 0.003	0.365 ± 0.008	0.379 ± 0.005	0.615 ± 0.010

4.3.2 Effect of Temperature on Clot Formation in Flow Chambers

There was no difference found between the clot formed in devices at 37ºC and room temperature. After five sets of experiments, resistance measurements showed that there was no difference in the rate of clot formation in the 15 minutes ($p = 0.921$). Additionally, there was no significant difference after comparing the clot volumes through the device ($p = 0.898$) as seen in Figure 4-6. Due to the insignificant differences between a heated and room temperature circuit, the experiments were conducted at room temperature for feasibility. Since the experiments were only 15 minutes long, the temperature may be a concern in future longer experiments.

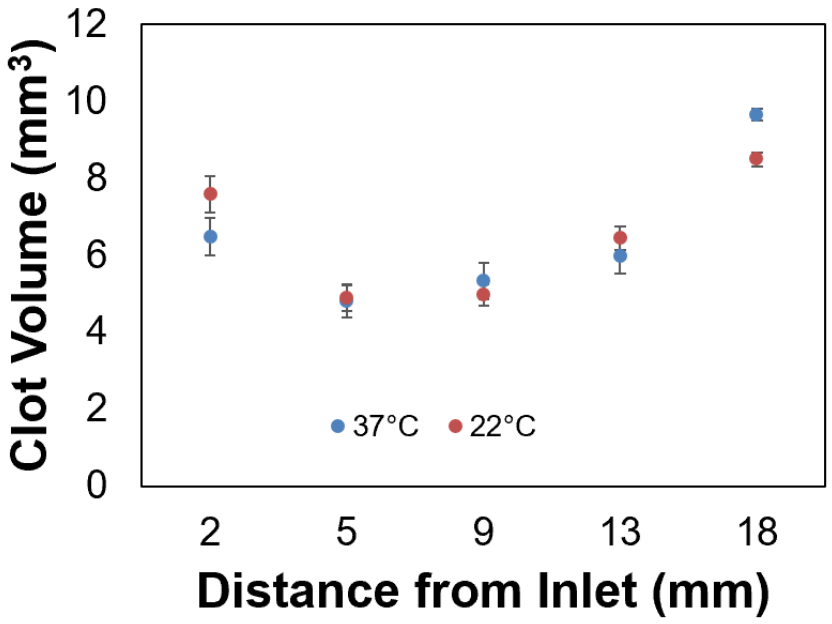

Figure 4-6. Clot volume through a 2 cm device at 37°C and one at 22°C. There is not a significant difference between the two sets.

4.3.3 *Macroscale Effects from Various Hollow Fiber Bundle Parameters*

Device shear rates and Reynolds Numbers for each flow chamber and condition were calculated and remained in the clinical range as seen in artificial lungs. This data is seen in Appendix 7.1.

4.3.3.1 Effects of Packing Density

There was more clot found in densely-packed (high packing density) flow chambers than loosely-packed chambers (low packing density). As seen in the probability maps created from multiple μCT scans (Figure 4-7), there is more clot at the

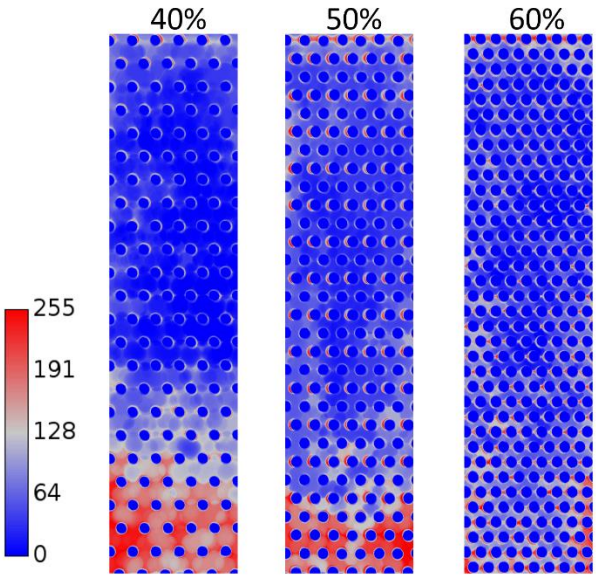

Figure 4-7. Probability map of clot formation in devices with various packing densities. Blood flow is from top to bottom.

outlet as visualized in red in all the cases and less in the center of the channel. There is also noticeable capture of clot at the inlet of each device, likely from clot breaking off from upstream locations and becoming trapped in the simulated fiber bundle. This effect is greater at the 60% packing density, as this denser packing may be more effective at catching small clots. This is reflected in the

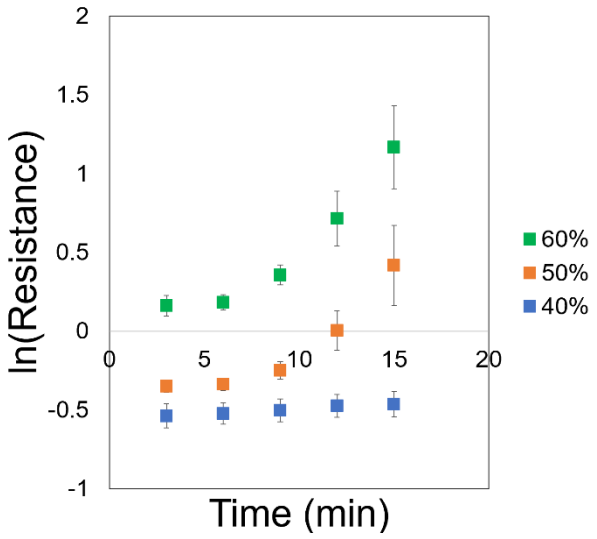

Figure 4-8. The change in resistance in natural log over the 15-minute experiment. A higher packing density correlates with a higher resistance.

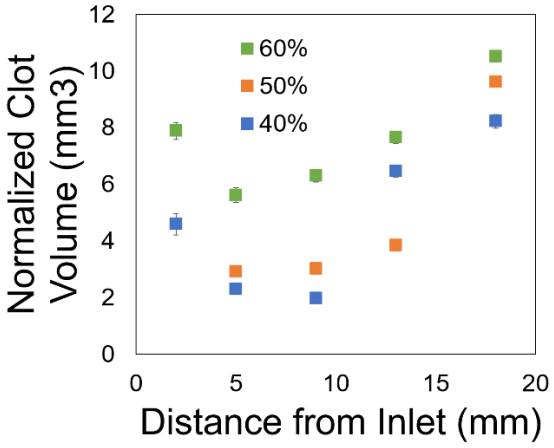

Figure 4-9. Clot volume in flow chambers with various packing densities. The 60% packing density device had more clot than the 40% or 50% packing density devices in the entire length of the flow chamber.

quantification of the normalized clot volume as seen in Figure 4-9. There was a significant difference between the 40% and 60% clot volumes through the device ($p = 0.024$), but no significant difference between the 50% and 60% ($p = 0.243$) or 40% and

50% (p = 0.272). Blood flow resistance values showed the rate of clot formation was fastest in the 60% packing density devices, slower for the 50% and slowest for the 40% devices (Figure 4-8). Additionally, the rate of clot formation tended to be exponential, with clot formation in the 50% and 60% devices accelerating around 8 minutes. The 60% ln(resistance) was found to be significantly higher than that of both the 50% (p = 0.00001) and the 40% device ($p = 7.6 \times 10^{-13}$). The difference between the 40% and 50% ln(resistance) was also significant (p = 0.0002). To compare across the different flow chambers, an equivalent distance from the inlet was obtained for each type of device based on the total surface area it had encountered (Figure 4-10). For the 40%, 50% and 60% packing density devices, they were 10.0, 5.7, and 3.5 mm from the inlet, respectively. These results showed that the 60% packing density flow chamber had more clot than the 40% device (p = 0.047). The 40% packing density device also had less clot than the 50% device, and the 50% had less than the 60% device, but these differences were not significant (p = 0.652 and p = 0.236, respectively). These results all suggest a loosely packed fiber bundle could reduce clot formation.

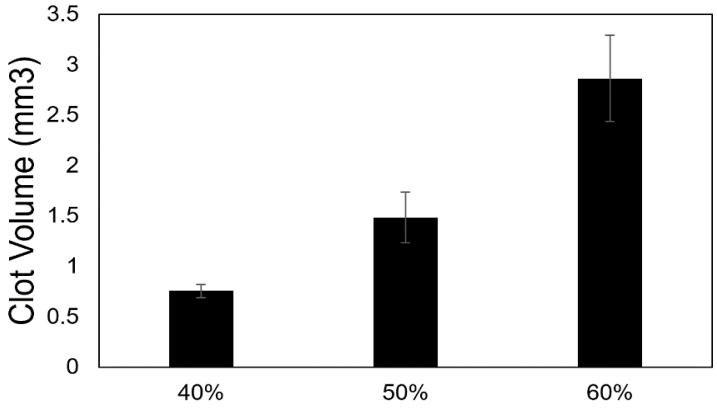

Figure 4-10. The clot volume in a 1 mm slice at equivalent distances from the inlet in flow chambers with various packing densities after a 15-minute experiment.

4.3.3.2 Effects of Blood Flow Velocity

A lower blood flow velocity resulted in more clot formation than a higher flow rate in the miniature flow chambers. As can be seen in the probability maps in Figure 4-11, there is more clot formation throughout the entire length of the slowest flow device as depicted by the light pink coloring. As seen previously, there was more clot localized at the outlet of each flow chamber, regardless of the condition being tested.

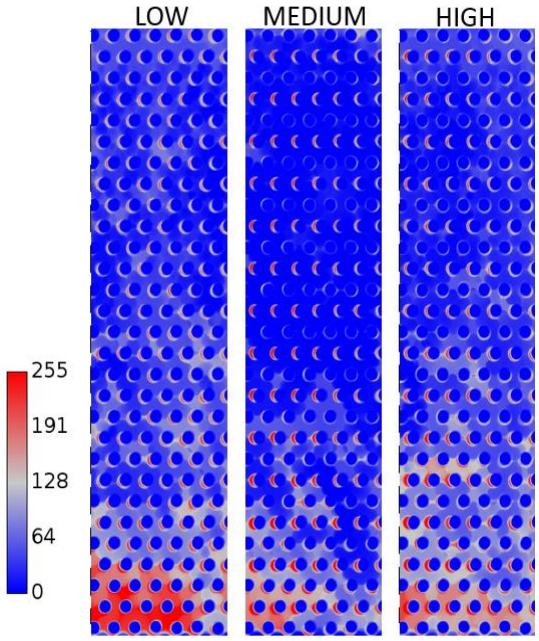

Figure 4-11. Probability maps for clot formation in low (3.68 mL/min), medium (4.38 mL/min), and high (5.46 mL/min) velocities. Pink is higher probability of clot, and blue is least probability of clot.

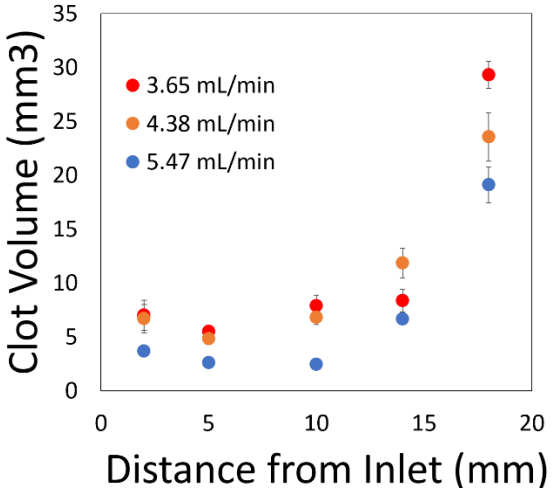

Figure 4-13. Clot volume from CT scans show a trend of more clot at the outlet side of the flow chamber, as well as slightly more clot in the devices experiencing lowest flow.

The µCT clot volumes (Figure 4-12) were significantly greater under the lowest flow when compared to the highest flow ($p = 0.014$). This was potentially due to less convection of activated clotting factors away from the material surface and thus greater

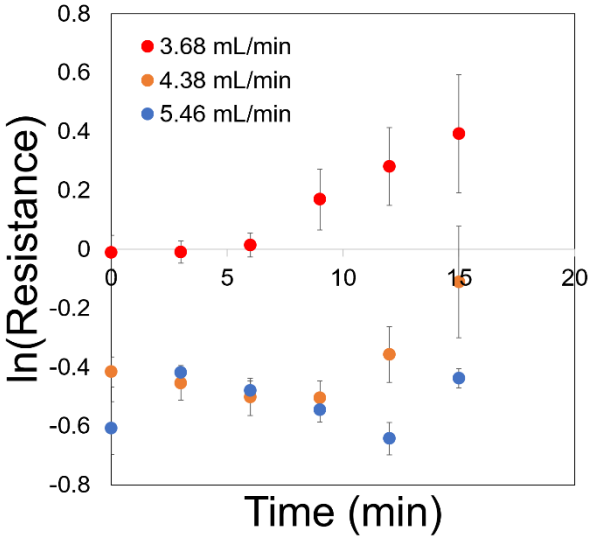

Figure 4-12. Resistance of flow chambers experiencing various flows for a 15 minute experiment.

local concentrations. Under higher flow, the coagulation activation factors should be rinsed away more quickly, lowering clot production in the device. Figure 4-12 shows the natural log of resistance, ln(resistance), increases at each velocity vs. distance from the device inlet. Similar to clot volumes, blood flow resistance is significantly higher in the lowest velocity devices when compared the medium velocity ($p = 0.008$) and high velocity ($p < 0.001$). In the medium and high velocity devices, there is a decrease in resistance from three to 10-12 minutes and then an increase in resistance thereafter when compared to the baseline resistances (Table 4-3). This may be due to clot being sheared off or enzymatically degraded initially, and then clot building up and being stabilized in some way so that it cannot be sheared off. This may be due to fibrin crosslinking or clot formation in areas that are shielded from high shear, which can be seen in Section 4.3.4. These results suggest that a higher velocity will delaying the initiation of clot formation in a hollow fiber bundle.

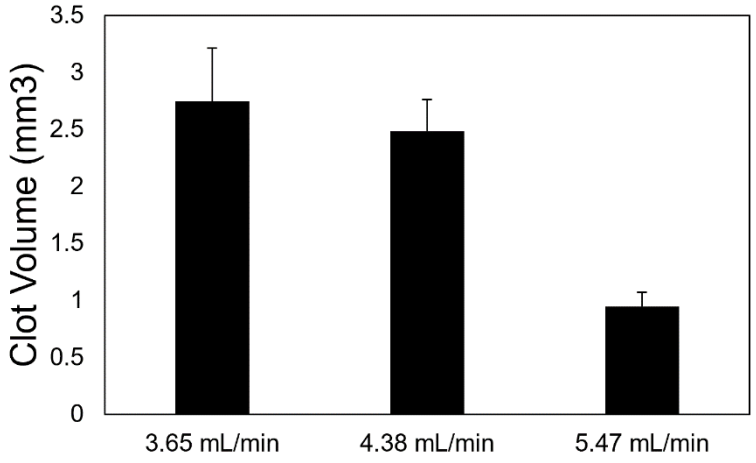

Figure 4-14. Clot in a 1 mm segment of experimental devices at the same equivalent distance based on surface area for different flow rates after a 15-minute experiment.

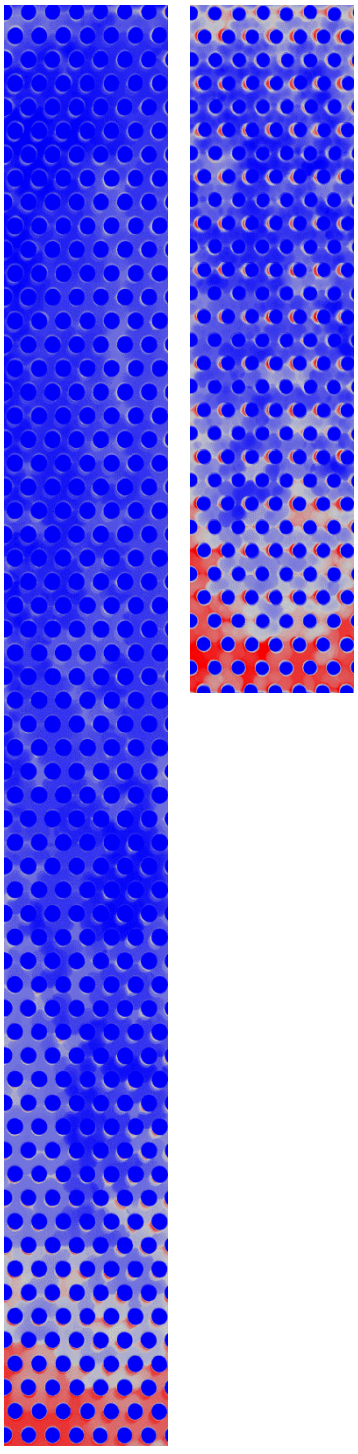

Figure 4-15. Probability map of clot formation in 4 cm (left) and a 2 cm (right) device. Flow is from top to bottom and higher probability is represented with pink and least probability is represented in dark blue.

To translate these results back to fiber bundle parameters, clot was evaluated at a different distance from the inlet for each case, based on an equivalent surface area to volume of blood that had flowed past (Figure 4-14). At these points, the fastest flow had reduced clot when compared to the medium flow ($p = 0.313$) and slowest flow ($p = 0.213$). The slowest flow also had more clot than the medium flow ($p = 0.965$). These results support that faster flow, which corresponds to a smaller frontal area would result in less clot.

4.3.3.3 Effects of Path Length

Figure 4-15 shows the clot density probability maps for two and four cm long devices. The shorter path lengths of 2 cm resulted in overall more clot than the 4 cm device. Although the 2 cm device had higher resistances through the 15-minute experiment as well as more total clot volume, the quantified results were not significant after the mixed model analysis. As seen in the probability map (Figure 4-15), the shorter device had more condensed clot through the length of the flow chamber, whereas most of the 4 cm path length device was clear. When quantified at the

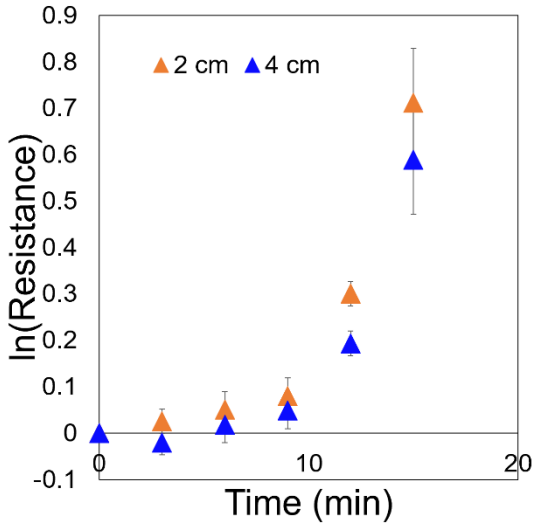

Figure 4-16. Resistance change through the flow chamber over a 15-minute experiment.

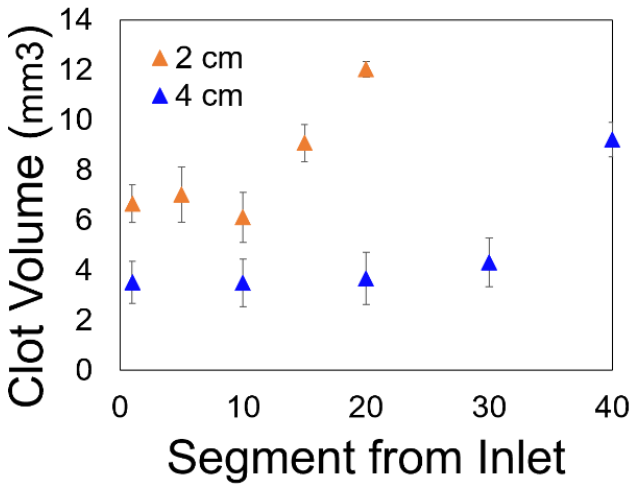

Figure 4-17. The clot volume quantified from CT scans show more clot overall in the shorter 2 cm devices than in the 4 cm devices.

entrance, first quartile, middle, third quartile, and end, the clot volume was overall higher in the 2 cm device and approached significance when compared to the 4 cm flow chambers ($p = 0.08$) (Figure 4-17). The ln(resistance) increases exponentially over 15 minutes (Figure 4-16) for both devices and did not differ significantly ($p = 0.396$).

To account for the effect of surface area on the two path lengths, clot volume was compared at the same point from the inlet (10 mm and 20 mm) for both path lengths. Blood that was pumped through the two devices would have been activated by the same surface area at each distance x. Doing so also reduces the outlet effect of clot that grows retrograde from the outlet. At the 10 mm location there was more clot in the 2 cm devices than in the 4 cm devices ($p = 0.393$) as well as at the 20 mm location ($p = 0.004$). Taking into account this equivalent location from the inlet, and the total clot volume data, these data suggest that using a shorter path length will contribute to a more concentrated and denser clot than in a fiber bundle with a longer path length. While a longer path length fiber bundle would also develop clot at the outlet, the majority of the fiber bundle would have less clot and provide gas exchange.

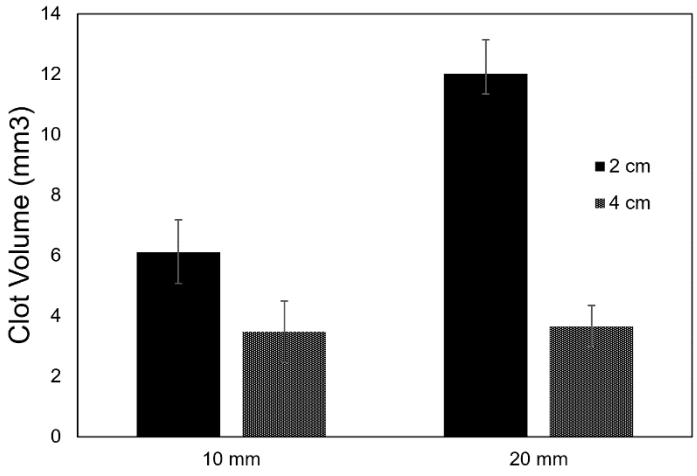

Figure 4-18. Clot volume in a 1 mm slice at an equivalent distance from the inlet after a 15-minute experiment in a 2 and 4 cm path length flow chamber.

4.3.4 Microscale Effects from Various Hollow Fiber Bundle Parameters

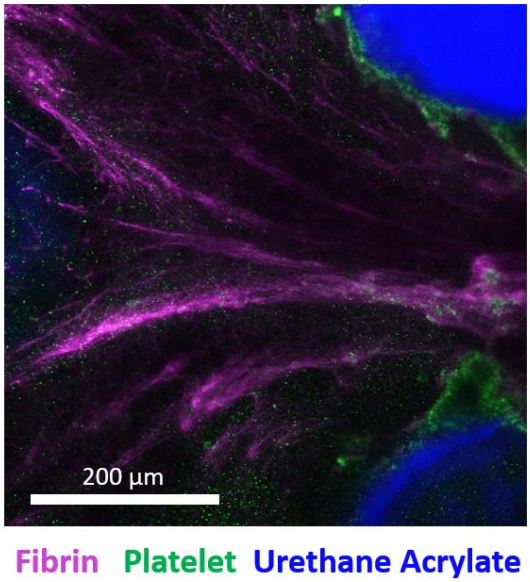

Figure 4-19. Fluorescent staining of fibrin and platelets showed clot depositing in the direction of flow (left to right) and colocalization of platelets close to the rods.

The internal clot structure, 100 µm away from the coverslip, was assessed using fluorescent staining of fibrin and platelets, and these results mirrored the results from the µCT scans. There was generally more fibrin and platelets at the outlet side of the flow chambers, in the 60% packing density flow chambers when compared to the 40% packing density devices, and when there was a low velocity compared to high velocity.

Since the flow chamber plastic was autofluorescent, images taken for each field had separate z-stacks for fibrin, platelets, and plastic. (Figure 4-19). Each individual fluorescent image consistently showed the fibrin network forming in the direction of flow,

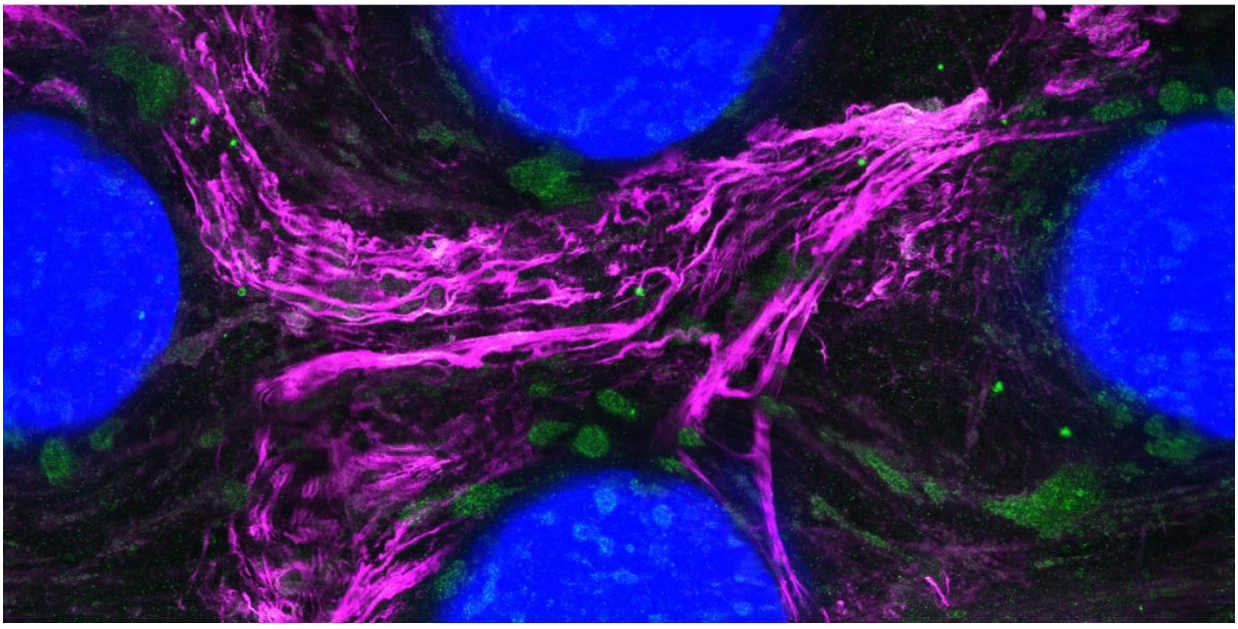

Figure 4-20. Maximum intensity projection of one representative field at the outlet. Fibrin is in magenta, platelets in green, and the plastic rods are in blue.

with strands of fibrin forming a network between the plastic rods. Based on the intensity of fluorescence, there tended to be a slightly higher density of fibrin and platelet on the inlet side of the rods (facing flow) than on the outlet side. There was a denser fibrin network at the outlet ends of all devices and also featured thicker fibrin strands, an example can be seen in Figure 4-20. There was also some fibrin webbing between adjacent fibers observed, however this was only apparent in flow chambers that had aPTTs less than 30 seconds. This suggests that by keeping aPTT above 30 seconds, one could prevent the formation of fibrin networks between hollow fibers, thus reducing the chance of clot completely blocking the fiber bundle.

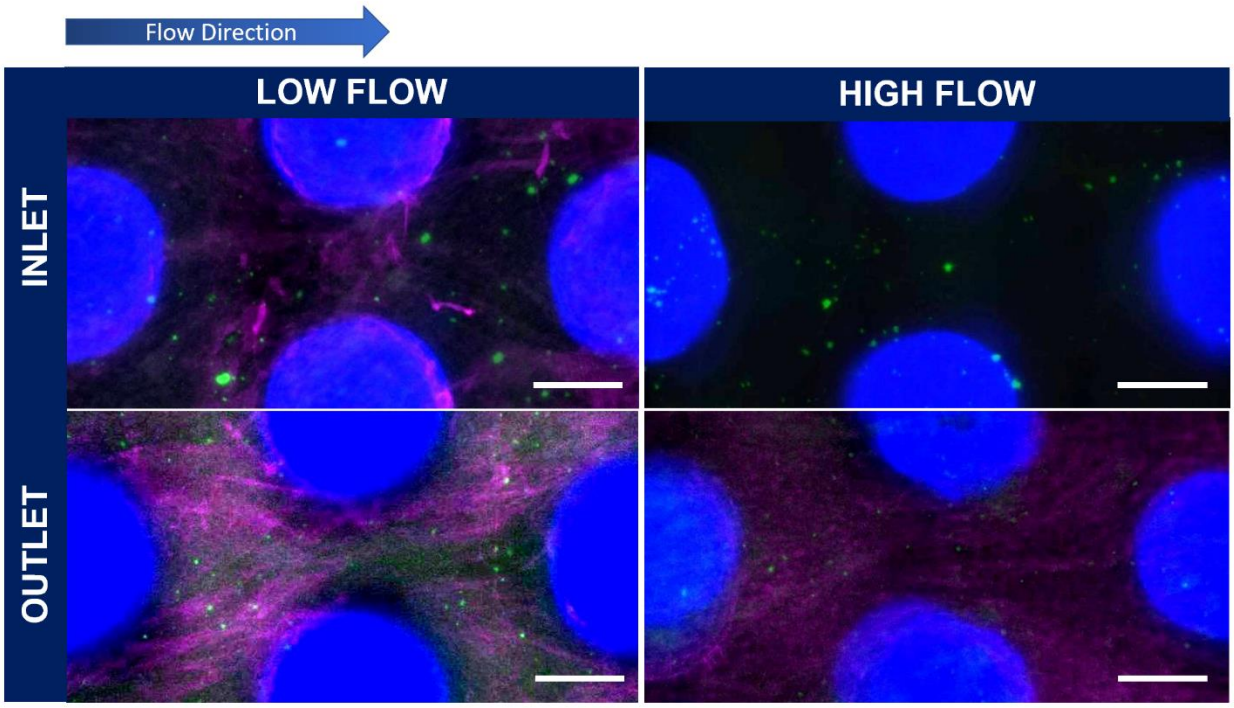

Figure 4-21. Averaged fluorescent images of low flow (3.65 mL/min) and high flow (5.46 mL/min) conditions at the inlet and outlet of a 2 cm long flow chamber. Fibrin (magenta), platelets (green) and the plastic rods (blue) are seen in each field. SB = 200 µm

Fluorescent intensity images show that there was qualitatively more fibrin and platelet deposition at the outlet than at the inlet of the both the flow experiments (Figure 4-22 and Figure 4-23). Separating out platelets and fibrin into individual images reveals there is both fibrin and platelets localized on the back side of the hollow fiber rods (Figure 4-22). Quantification of the number of pixels with fibrin and platelets indicates that the higher flow chambers had less deposition of fibrin and platelets.

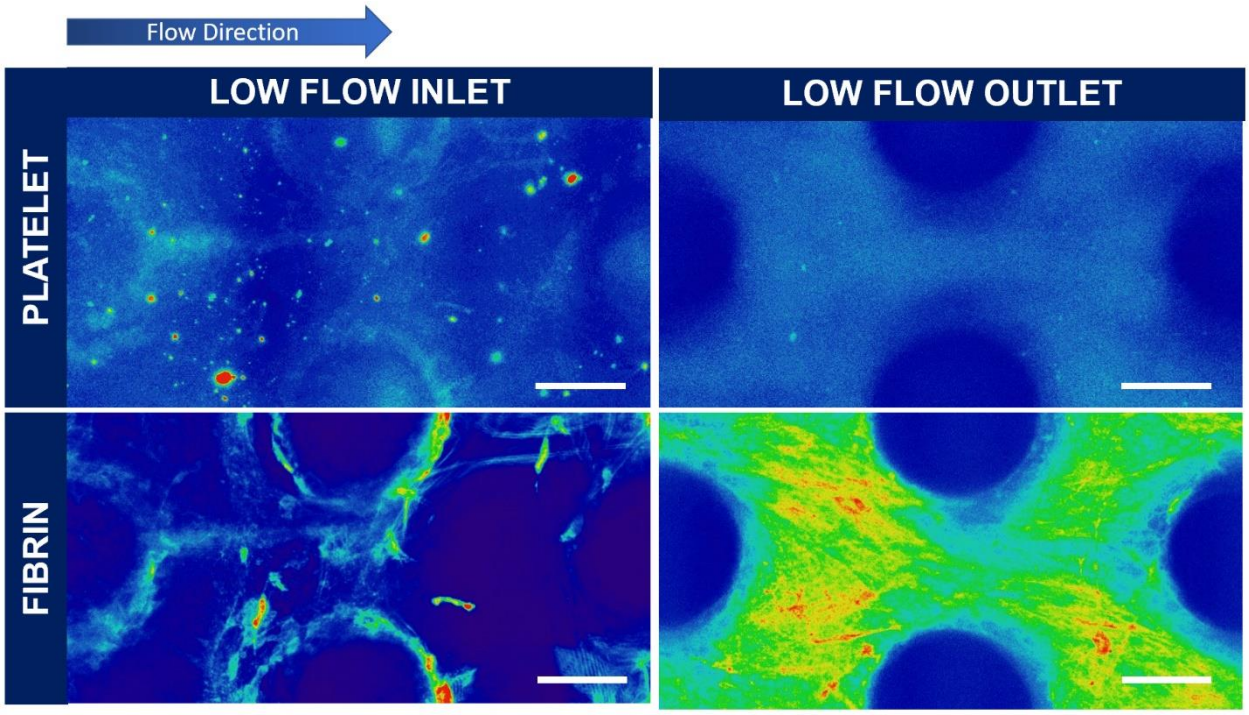

Figure 4-22. The platelet and fibrin probability of depositing in certain areas between hollow fibers under low flow(16 cm/min blood velocity). The outlet reflects the higher clot volume that was also seen in the µCT scans. Scale bar is 200 µm.

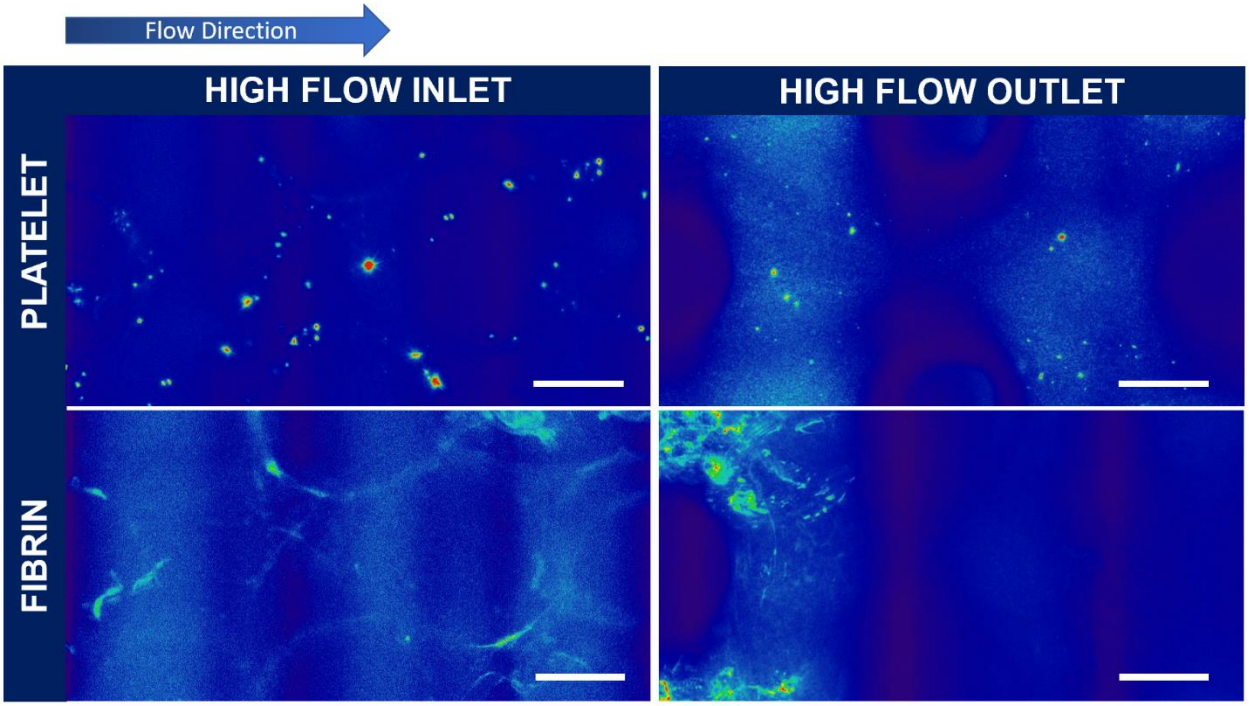

Figure 4-23. The platelet and fibrin deposition map on an area between hollow fibers at high flow (25 cm/min blood velocity) through a fiber bundle. Scale bar is 200 µm.

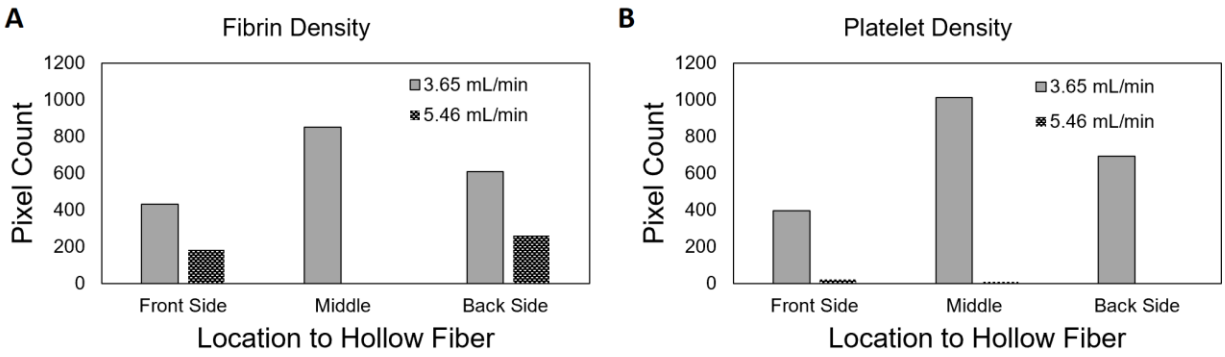

Figure 4-24. Change in total pixel count of fibrin and platelets from the inlet to outlet. In all cases, there was more signal detected at the outlet of the flow chamber. These cases show that there was more fibrin and platelet deposition in the low flow experiments when compared to the faster flow.

The total pixel values show that there is more fibrin and platelets detected in the lower flow scenario than in the higher flow (Figure 4-24). These values also reflect the trend of more clot volume at the outlet.

Fluorescent imaging of 40% and 60% packing density flow chambers resulted in similar conclusions to those found from µCT scanning. Namely, the higher density packing fiber resulted in more detected fibrin and platelets. This can be seen qualitatively in Figure 4-25, where the 60% packing density column has a more fibrin in purple and platelets in green.

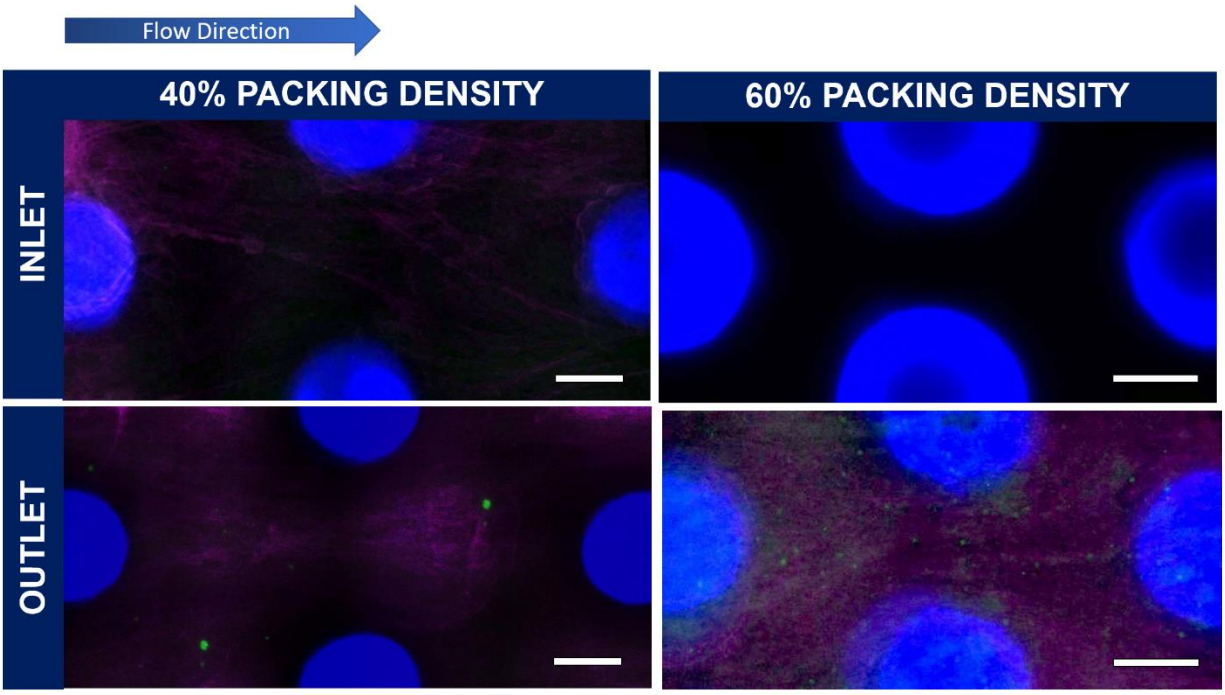

Figure 4-25. The averaged fluorescent images for a 40% packing density and 60% packing density conditions at the inlet and outlet of a 2 cm long flow chamber. Fibrin (magenta), platelets (green) and plastic 3D printed rods (blue) are in each field. SB = 200 µm.

This is also quantitively supported after separating the fibrin and platelet fluorescent images, as seen in Figure 4-26 and Figure 4-27. These images show there is a higher chance of fibrin and platelet deposition on the hollow fibers, especially on the outlet side of these devices. Theo overall pixel counts confirm that there is more clot in the 60% packing density devices than in the 40% (Figure 4-26).

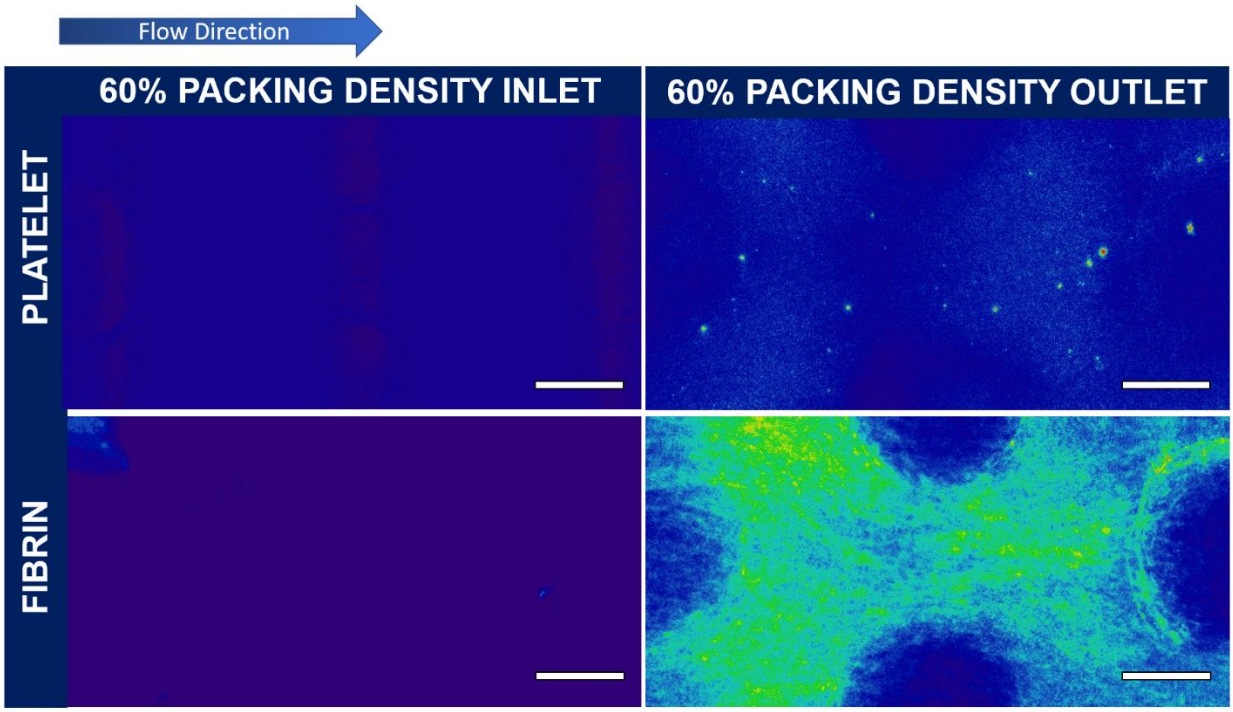

Figure 4-26. Platelet and fibrin average deposition in a 60% packing density flow chamber after 15 minutes of blood flow.

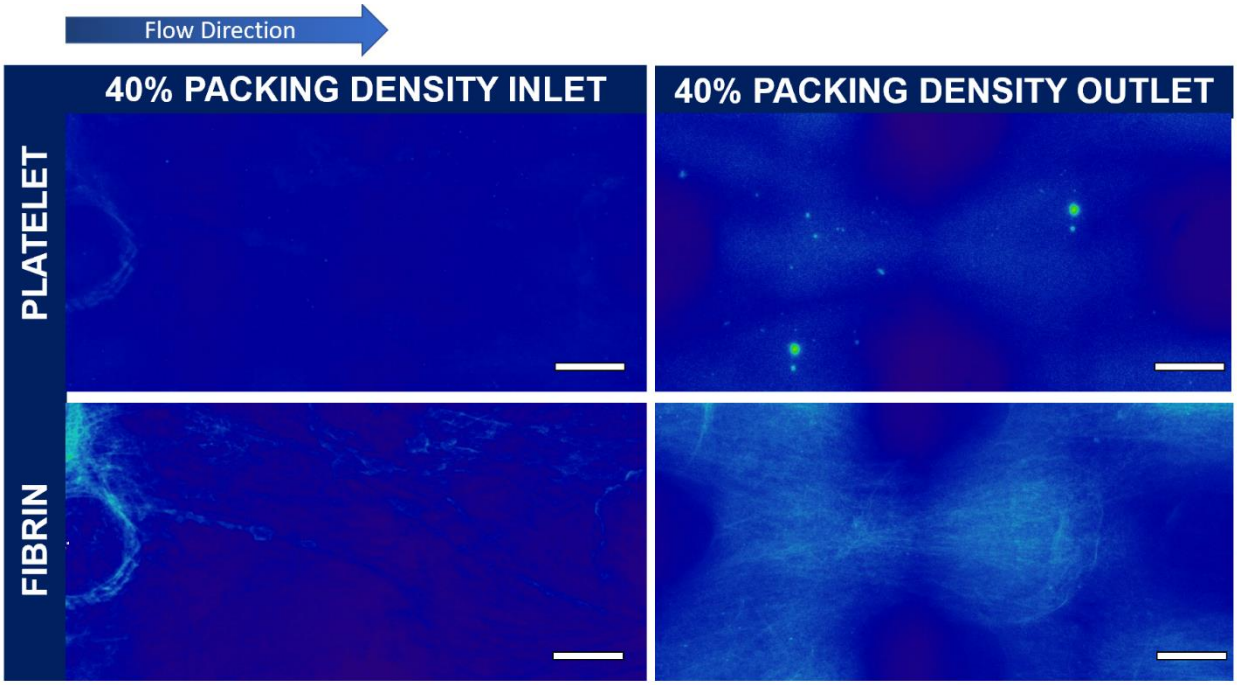

Figure 4-27. Average platelet and fibrin deposition in a 40% packing density flow chamber after 15 minutes of flow. There is more deposition at the outlet than at the inlet. Additionally, the wide spacing between fibers do not have much fibrin tendrils bridging between adjacent rods. However, they can still be seen growing in the direction of flow. SB is 200 µm.

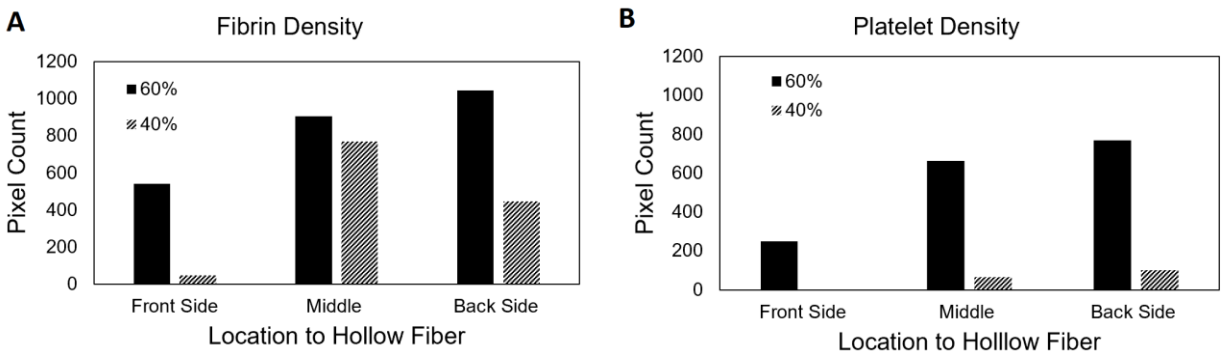

Figure 4-28. Total pixel count of the 15 imaged regions of interest increased from the inlet to outlet in all packing density devices. This means more platelets and fibrin were adhered to the outlet end of each device. Also, there were more fibrin and platelets adhered to the back end of the hollow fiber rods. In particular, the 60% packing density devices had more clot than the 40% ones.

4.4 Discussion and Conclusion

From this study, it is clear that clot formation varies significantly with fiber bundle packing density, path length, and frontal area. First, these results showed that a loosely packed fiber bundle reduced clot formation. Second, a longer path length unexpectedly had around the same clot volume as in a shorter path length, but it was dispersed over a larger length. Thus, there was more of the fiber bundle that was not covered with clot and remained patent. Third, a faster velocity through the bundle reduced clot formation, and thus devices with smaller frontal areas will develop less clot. The findings from these devices reflected known clinical and experimental trends towards more clot forming at the outlet end of the devices, no matter the condition being tested.

In addition to these findings, at lower aPTTs, there was a trend of clot being captured at the inlet, which may be due to clot coming from an upstream part of the circuit such as the syringe. In the statistical analysis, aPTT as a covariate was found to significantly correlated with resistance measurements. With lower aPTT values, the corresponding experiments experienced more clot formation.

While the intentional cropping of the scanned volumes was meant to minimize the effect of the clotting initiated from the outlet, it is possible to further reduce these effects be creating an outlet that does not narrow down to one small tube, but instead have an open end or multiple outlet ports at the outlet of an oxygenator. Potentially a manifold could be added to separate the outlet port from the fiber bundle. A way to test this in the future is to use another flow chamber with an open outlet, with the parameters being tested further away from outlet tube (Figure 4-29).

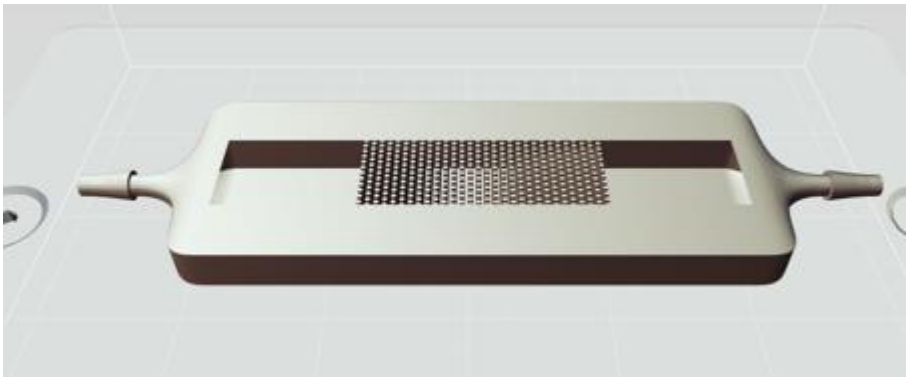

Figure 4-29. Potential future flow chamber with a centered array of fibers to avoid flow effects from the inlet and outlet. The flow through this chamber would be fully developed.

4.4.1 An Ideal Artificial Lung Fiber Bundle

These results indicate that an artificial lung fiber bundle should be designed with low packing density, a small frontal area, and a long path length. Each hollow fiber has a small dead space on the back side of it where procoagulant molecules, proteins, and platelets may accumulate. As reinforced by the fluorescent imaging, it is an area of a fiber bundle where fibrin and platelets localize and adhere to the hollow fibers and can initiate clot growth and propagation. In a couple cases of the higher packing density flow chamber, fibrin strands were seen connecting adjacent fibers, potentially acting as a net

to capture platelets, fibrin, and other activation factors. If present, this clot could then propagate to nearby regions over a longer test period to generate an expanded effect. This was not seen in the low packing density chambers.

The clot volume analysis for the path length and velocity experiments suggested that the general shape of the fiber bundle should be long and thin. The µCT scans showed more diffuse clot through the flow chambers with a longer path length, however, the same approximate clot volume was at the outlet end of both 2 cm and 4 cm flow chambers. This is likely due to the change in flow pattern as blood exits the fiber bundle portion and into the narrow outlet channel. As seen in similarly shaped flow chambers that have a narrow outlet, there is possibly turbulent flow and the creation of vortices.[48]

4.4.2 Informing a Computational Model of Clot Formation

Despite the flow chambers being much smaller than a clinical oxygenator, they were able to capture the effects of various fiber bundle parameters with both µCT scans and fluorescent imaging. Fluorescence imaging results showed a higher concentration of platelets and fibrinogen, major components of clot, at the outlet end of the flow chambers, which also reinforce the results from the µCT scans. This work matches well with Demarest *et al* and other works where artificial lung outlets displayed more clot than the inlet side.[50,160,161,188]

In addition to suggesting improvements in artificial lung design, these results can be used to update and improve current computational models for clot formation for a wide variety of blood contacting medical devices. A recent model from the Antaki group (Tao et al.) attributes the bulk of clot volume to platelets adhered to device surfaces.[98,198] This coagulation model is based on the activation of platelets from shear

forces and local concentrations of agonists which can lead to a couple of issues when applying it to predict clot formation in an artificial lung. For one, the flows and shear stresses in an artificial lung fiber bundle are lower in the local environment of the hollow fiber bundles than what is currently being modeled by the Wu model. The Zhang et al. computational model showed that shear stress on hollow fibers ranged between 0.1 to 34.0 Pa, which is much lower than what the model has been used for.[158] Secondly, by disregarding the contact activation pathway, the model does not capture the largest source of activation in an artificial lung fiber bundle. The large blood contacting surface area is the most impactful parameter for clot formation in an oxygenator and using the current Wu model might predict underwhelmingly less clot than there is experimentally. To improve upon this computational model, the inclusion of fibrin may be beneficial. While platelets play a major role in clot formation, the other proteins (e.g. fibrinogen) and cells that constitute the clot are excluded in the current model. In a system without platelets, clot still forms, as seen in coagulation tests using only spun down, platelet free plasma. From the fluorescent images, fibrin plays a large role in forming connections between platelets and the artificial surface and are also a large part of the clot that is formed. This suggests that the formation of fibrin should also be modeled.

Compared to the blood flow through a ventricular assist device, lower velocity flow environment in an artificial lung fiber bundle has a tendency to form clots with more fibrin and red blood cells, and fewer platelets. As the artificial surface activates the intrinsic branch of the coagulation cascade, the activated clotting factors are convected slowly from the material surfaces. Therefore, they are not diluted in the bulk flow, leading to more rapid conversion of fibrinogen to fibrin. Higher shear, in contrast,

washes these activated factors away from the surface rapidly, slowing fibrin formation. Additionally, high shear stress can dislodge long fibrin strands. This reduces lateral aggregation and protofibril extensions.[140] In the simulated fiber bundles, long fibrin strands were captured by the fluorescent images in this study, indicating new regions for future platelet adhesion and activation. Thus, artificial lung clot models should model fibrinogen conversion to fibrin and subsequent platelet deposition.

4.4.3 Experimental Limitations

While the methods of this study have successfully quantified clot in a benchtop hollow fiber bundle model, it has some limitations. Firstly, while blood flow in the device resembles that within a clinical artificial lung fiber bundle, the blood was pumped from a syringe that is at risk of clotting during the 15-minute experiment. There may be some build-up of procoagulant factors from blood contacting the bag as it is drawn and from the upstream, feed syringe as well. This could lead to the formation and transport of small clots into the test device. Clinically, procoagulant cannulas and circuit components upstream of the artificial lung also generate clot that may shear off and end up in the inlet of the device. Thus, these events are no unrealistic. Such embolization was observed in a couple cases where aPTTs were less than 30 seconds.

Additionally, blood was fed in a single pass, rather than recirculated around the body as during clinical ECMO. This eliminated any build-up of procoagulant factors or loss in clotting factor zymogens or platelets. Overall, to achieve a more realistic model, , a small animal (i.e rat) model could be connected to 3D printed flow chambers . Secondly, as mentioned in the discussion, the flow chamber itself had outlet flow patterns and wall effects that may have impacted the analyzed clot volume. The depth

and width of the flow chamber had to be limited due to the restricted imaging platforms that were available for the µCT and confocal microscope. To target this effect, the outlet path could be reduced more gradually from the rectangular chamber to the 1/16” barbed outlet, a wider outlet could be created, or an outlet manifold could be created that distances the simulated fibers from the outlet.

Thirdly, it will be difficult to scale the results of this experiment up to a full-scale artificial lung fiber bundle. These results were used to make recommendations for a large device based on the total surface area to volume ratio of blood contact during the experiment, however, these results may need some translation due to different materials and other fiber orientations. These results were standardized between the conditions being tested thus can be compared between donors and sets. These flow chambers did not encompass the vast variety of fiber bundles that are out there, such as ones with a cross-angle, or double woven mats. However, the flow chambers can be easily modified and 3D printed to test those other conditions. A limitation with this is that the material of the flow chamber is not polymethylpentene (PMP), what standard oxygenator hollow fibers are made of. Although these materials are all similar, the extent of protein adsorption and coagulation cascade activation might be different.

A couple limitations from fluorescent imaging also occurred. Since the confocal microscope can only reach a couple hundred microns deep due to each objective’s working distance, it is unable to capture the entire 3D clot. We were able to capture a 100-300 µm deep range into the flow chamber that could give an idea of how the formation of clot started. The clot that has formed inside the chamber may also impede the penetration of antibody stains, limiting their fluorescence. Since the stain is

completed by flowing through the antibody mixture, a flow chamber that is packed with clot may have less effective staining.

These limitations mean the fluorescent images may not truly representative of the clot that has formed inside. For example, in the devices that had high resistance measurements and visible clot through the device after an experiment that were so filled with clot had lower fluorescence detected. By keeping future experiments within a tighter aPTT range may prevent too much coagulation that reduces staining efficiency. Additionally, the flow chambers used in the fluorescence experiments have a wall made of glass for confocal imaging. However, glass is a known activator of the coagulation cascade and thus the results from the fluorescent studies most likely overestimate clot formation. Despite this, these results still mirror the results that were found from the uCT scans which were conducted in flow chambers that were completely plastic. Lastly, the fluorescence imaging imaged 15 fields for each condition, from 3 different donors (45 total images), so expanding the study to include more experiments would create an improved, more accurate average. Additionally, analyzing the 3D scans from the sagittal or axial planes may also reveal other trends. Ultimately, this overall experimental design remains very flexible, enables high-throughput testing, and addresses many of the challenges hinder coagulation experiments with full-scale oxygenators. Namely, a simple, repeatable, and adaptable methodology that can be used to test a wide variety of device design and hematological factors, such as surface coatings and anticoagulant drug dosing, for their effect on coagulation in an artificial lung fiber bundle. This method can act as a bridge between benchtop coagulation assays and in vivo studies, allowing study optimization and reduction in animal usage.

5 Conclusion

This work investigated different methods for reducing biofouling on the surface of artificial lung hollow fiber membranes and improved understanding of coagulation initiation and progression on these surfaces. A novel material, Cu-PDMS hollow fibers, was tested in a in a 72-hour *in vivo* experiment for surface generated NO's ability to reduce platelet activation and clot formation. Then, the effects of surface generated NO, gaseous NO, and copper were tested for their individual and combined antimicrobial effects on a Gram-positive and Gram-negative bacteria in an *in vitro* experiment. Lastly, the micro- and macro-scale formation of clot was studied using a new bench top model of flow through a membrane fiber bundle. These studies led to the following conclusions:

5.1 Surface Generated NO from Cu-PDMS Hollow Fibers as an Anticoagulant in Short-term in vivo Sheep Experiment

Cu-PDMS hollow fibers reduce clot formation in artificial lungs and improves the functional lifespan of devices it is used in. Its antithrombotic effects can be combined with low dose anticoagulant drug therapy for long-term effects.

1. Surface generated NO using Cu-PDMS hollow fibers produced physiological NO fluxes at $3.43 \pm 0.72 \times 10^{-10}$ mol cm^{-2} min^{-1} and correlated well to previous work using the same Cu-PDMS fibers.
2. Cu-PDMS fibers reduces clot as measured through significantly lower blood flow resistances over 72-hours ($p < 0.001$) and markedly reduced failure rates between 12-36 hours.
3. The benefits of using Cu-PDMS in the long-term may be more beneficial when used with another antithrombotic therapy.

4. Copper leached off of Cu-PDMS surfaces in the 72-hour study which led to elevated serum Cu levels but no build-up in the liver. Longer term studies are needed to capture the Cu levels and potential toxicity.

5.2 Two-Pronged Method for Preventing Bacterial Adhesion using Nitric Oxide and Copper

Cu-PDMS membranes, surface generated NO, and gaseous NO all reduced the adhesion and short-term growth of S. aureus and P. aeruginosa bacteria under the flow conditions of an artificial lung. This benchtop study determined each of these three methods exhibited short term antimicrobial effects but did not show enhanced effect when combined.

1. A custom-made bioreactor simulated the dynamic environment of a hollow fiber bundle, mimicking the convection of antibacterial agents away from the surface, a phenomenon that is not captured in conventional antimicrobial surface tests
2. Bacterial adhesion was reduced after 4-hour exposure to surface generated NO from an infusion of 1 uM GSNO on both Cu-PDMS and PDMS membranes, however these effects affected bacteria growth only in the short-term.
3. Bacterial adhesion and growth were also reduced after 4-hour exposure to gaseous NO delivered at 250 ppm both membranes types in the short term growth experiments. Again, these inhibitory effects were short lived and did not persist after the bacteria were removed from the location of concentrated NO.
4. Planktonic bacteria growth was also reduced after exposure to GSNO and gNO when compared to the negative control, suggesting that the convection of GSNO

and produced NO from the interface mildly deterred growth of the bacteria suspended in solution.

5. Bacterial exposure to copper consistently reduced bacteria adhesion and growth on 10% wt Cu-PDMS membranes. Inhibitory effects were seen in both the short-term growth and the long-term growth on plates but were not significant. These results suggest that increasing the copper composition of the material may induce more antibacterial effect.
6. The combination of Cu-PDMS and surface generated NO did not enhance the antimicrobial effect.
7. These results suggest that individually applying copper exposure, gaseous NO, or GSNO in an artificial lung can inhibit bacterial adhesion and biofilm formation at the blood contacting surface. Combined with an antibiotic drug, Cu-PDMS or NO delivery can target both adhered and planktonic bacteria.

5.3 Macro- and Micro-scale Evaluation of Clot Formation in an Oxygenator Hollow Fiber Bundle

A longer path length, smaller frontal area, and a loosely packed fiber bundle reduced clot formation in an artificial lung fiber bundle. MicroCT scans quantified clot volume in the complex geometries of a fiber bundle, revealing that there was more clot at the outlet of all flow chambers. Fluorescence staining of platelets and fibrin revealed the inner clot structure that had varying fibrin networks that webbed between fibers in the direction of flow.

1. A high throughput, repeatable experiment was designed with custom 3D printed flow chambers that mimicked the flows through artificial lung hollow fiber bundles

of various parameters, based on 2 L/min flow through an adult Quadrox oxygenator with a 100 cm^2 frontal area.

2. The volume of clot formed in flow chambers with a shorter path length (2 cm) was not different than the volume of clot in the longer chamber (4 cm). However, since the longer chamber had more prime volume, the clot was more diffuse and spread out, leaving the majority of the fiber bundle patent.
3. A smaller frontal area fiber bundle, scaled to higher flow rates, displayed less clot than in a flow chamber with larger frontal areas.
4. Clot formed at the outlet may be caused by flow patterns from the narrowing of the chamber to the outlet, and by an accumulation of activation factors that have been generated from the large surface area upstream.
5. A design recommendation for less procoagulant fiber bundles is to have a long and thin fiber bundle, rather than a wide and short one.
6. An increase in packing density was correlated with an increase in clot formation. Thus, a lower packing density is recommended to increase the functional lifespan of a fiber bundle.

5.4 Limitations and Future Work

5.4.1 Antimicrobial and Anti-platelet Effect of Surface Generated NO form Cu-PDMS

The effects of Cu-PDMS are capable of reducing clot formation as well as bacterial adhesion in the dynamic environment of an ECMO circuit, however, the effects are quite mild and may be easily overcome. This is partially due to the conversion and uptake of the surface generated nitric oxide into less oxidative forms. Future studies could implement a burst delivery system as to provide intense antimicrobial or antiplatelet

effects in critical times. Additionally, the use of copper in the circuit is essential for NO release, but also leads to the question of toxicity. The 72-hour *in vivo* experiment found copper leaching into the system and in the blood plasma, but none could be found in the excretory system. Thus, to confirm the long-term use of copper, longer copper leaching study should be performed in a full-size artificial lung.

Additionally, these studies were run to test the effects of Cu-PDMS and nitric oxide independently. Despite being conducted at low ACTs and in a conservative environment, surface generated NO from Cu-PDMS fibers reduced clot significantly over 3 days. For this methodology to be relevant, future studies will need to test it in combination with a low dose anticoagulant therapy to further improve device longevity. Similarly, the antimicrobial effects of the Cu-PDMS, gNO, and surface generated NO prevented bacterial adhesion at the membrane interface but did not affect the bacteria in solution as much. Thus, these antibacterial agents could be combined with other antibiotic drugs to reduce fouling and infection in blood contacting devices.

5.4.2 Computational Model of Clot in Hollow Fiber Bundle

Application of a computational model to predict clot formation in a hollow fiber bundle remains a challenge due to the expensive computational power that is needed for the complex process and flow patterns. The experiments completed in this study were short, only 15 minutes long. However, how clot formation may progress hours, or even days later, is yet to be explored. There may be retrograde clot growth from outlet casings or circuit components as seen in clinical devices. This phenomenon needs to be studied and modeled so future artificial lung designs can be optimized to support patients in the long-term.

6 References

1. Adrian, K., M. Skogby, L. G. Friberg, and K. Mellgren. The effect of S-nitroso-glutathione on platelet and leukocyte function during experimental extracorporeal circulation. *Artif. Organs* 27:570–575, 2003.

2. Al-Sa'doni, H. H., I. Y. Khan, L. Poston, I. Fisher, and A. Ferro. A novel family of S-nitrosothiols: Chemical synthesis and biological actions. *Nitric Oxide - Biol. Chem.* 4:550–560, 2000.

3. Alquwaizani, M., L. Buckley, C. Adams, and J. Fanikos. Anticoagulants: A Review of the Pharmacology, Dosing, and Complications. *Curr. Emerg. Hosp. Med. Rep.* 1:83–97, 2013.

4. ALung Technologies Inc. The Science of ECCO2R. , 2019.doi:10.1017/CBO9781107415324.004

5. Amoako, K. A. Nitric Oxide Therapies for Local Inhibition of Platelets' Activation on Blood-Contacting Surfaces. , 2011.

6. Amoako, K. A., and K. E. Cook. Nitric oxide-generating silicone as a blood-contacting biomaterial. *ASAIO J.* 57:539–544, 2011.

7. Amoako, K. A., P. J. Montoya, T. C. Major, A. B. Suhaib, H. Handa, D. O. Brant, M. E. Meyerhoff, R. H. Bartlett, and K. E. Cook. Fabrication and in vivo thrombogenicity testing of nitric oxide generating artificial lungs. *J. Biomed. Mater. Res. Part A* 101:3511–3519, 2013.

8. Argüello, J. M., D. Raimunda, and T. Padilla-Benavides. Mechanisms of copper homeostasis in bacteria. *Front. Cell. Infect. Microbiol.* 3:73, 2013.

9. Arora, D. P., S. Hossain, Y. Xu, and E. M. Boon. Nitric Oxide Regulation of Bacterial Biofilms. *Biochemistry* 54:3717–3728, 2015.

10. Barraud, N., D. J. Hassett, S. H. Hwang, S. A. Rice, S. Kjelleberg, and J. S. Webb. Involvement of nitric oxide in biofilm dispersal of Pseudomonas aeruginosa. *J. Bacteriol.* 188:7344–7353, 2006.

11. Barré, O., F. Mourlane, and M. Solioz. Copper induction of lactate oxidase of Lactococcus lactis: A novel metal stress response. *J. Bacteriol.* 189:5947–5954, 2007.

12. Beckman, J. S., and W. H. Koppenol. Nitric oxide, superoxide, and peroxynitrite: the good, the bad, and ugly. *Am. J. Physiol.* 271:C1424–C1437, 1996.

13. Bilian, X. Intrauterine devices. *Best Pract. Res. Clin. Obstet. Gynaecol.* 16:155–168, 2002.

14. Billings, P., G. Ewart, W. Liao, A. Malarcher, D. Mannino, R. Pleasants, A. Punturieri, E. Storey, J. Walsh, and D. Weissman. Public Health Strategic Framework for COPD Prevention. Atlanta, GA: 2011.at <http://www.cdc.gov/copd/pdfs/framework_for_copd_prevention.pdf>

15. Bizzarro, M. J., S. A. Conrad, D. A. Kaufman, and P. Rycus. Infections acquired during extracorporeal membrane oxygenation in neonates, children, and adults. *Pediatr. Crit. Care Med.* 12:277–281, 2011.

16. Bjork, I., and U. Lindahl. Mechanism of the anticoagulant action of heparin. *Mol. Cell. Biochem.* 48:161–182, 1982.

17. Bohl, K. S., and J. L. West. Nitric oxide-generating polymers reduce platelet adhesion and smooth muscle cell proliferation. *Biomaterials* 21:2273–2278, 2000.

18. Boles, B. R., and A. R. Horswill. agr-mediated dispersal of Staphylococcus aureus biofilms. *PLoS Pathog.* 4:, 2008.

19. Borkow, G. Safety of using copper oxide in medical devices and consumer products. *Curr. Chem. Biol.* 6:86–92, 2012.

20. Bremner, I. Manifestations of copper excess. *Am. J. Clin. Nutr.* 67:, 1998.

21. Brisbois, E. J., H. Handa, T. C. Major, R. H. Bartlett, and M. E. Meyerhoff. Long-term nitric oxide release and elevated temperature stability with S-nitroso-N-acetylpenicillamine (SNAP)-doped Elast-eon E2As polymer. *Biomaterials* 34:6957–6966, 2013.

22. Brisbois, E. J., T. C. Major, M. J. Goudie, R. H. Bartlett, M. E. Meyerhoff, and H. Handa. Improved hemocompatibility of silicone rubber extracorporeal tubing via solvent swelling-impregnation of S-nitroso-N-acetylpenicillamine (SNAP) and evaluation in rabbit thrombogenicity model. *Acta Biomater.* 37:111–119, 2016.

23. Brisbois, E. J., T. C. Major, M. J. Goudie, M. E. Meyerhoff, R. H. Bartlett, and H. Handa. Attenuation of thrombosis and bacterial infection using dual function nitric oxide releasing central venous catheters in a 9 day rabbit model. *Acta Biomater.* , 2016.doi:10.1016/j.actbio.2016.08.009

24. Broniowska, K. a, A. R. Diers, and N. Hogg. S-nitrosoglutathione. *Biochim. Biophys. Acta* 1830:3173–3181, 2013.

25. Brown, K. L., D. A. Ridout, M. Shaw, I. Dodkins, L. C. Smith, M. A. O'Callaghan, A. P. Goldman, S. Macqueen, and J. C. Hartley. Healthcare-associated infection in pediatric patients on extracorporeal life support: The role of multidisciplinary surveillance. *Pediatr. Crit. Care Med.* 7:546–550, 2006.

26. Brune, B., and K. Hanstein. Rapid Reversibility of Nitric Oxide Induced Platelet Inhibition. *Thromb. Res.* 90:83–91, 1998.

27. Buck, W. B., and R. M. Sharma. Copper Toxicity in Sheep. *Iowa State Univ. Vet.* 31:4–8, 1969.

28. Burket, J. S., R. H. Bartlett, K. Vander Hyde, and C. E. Chenoweth. Nosocomial infections in adult patients undergoing extracorporeal membrane oxygenation. *Clin. Infect. Dis.* 28:828–833, 1999.

29. Burney, S., J. L. Caulfield, J. C. Niles, J. S. Wishnok, and S. R. Tannenbaum. The

chemistry of DNA damage from nitric oxide and peroxynitrite. *Mutat. Res. - Fundam. Mol. Mech. Mutagen.* 424:37–49, 1999.

30. Camboni, D., A. Philipp, M. Arlt, M. Pfeiffer, M. Hilker, and C. Schmid. First Experience With a Paracorporeal Artificial Lung In Humans. *ASAIO J.* 55:304–306, 2009.

31. Chambers, J., L. Manley, J. E. Nolen, K. Pruitt, T. Weaver, and D. Maple. Lung Disease Data : 2008. *Am. Lung Assoc.* , 2008.at <http://action.lung.org/site/DocServer/lung-disease-data-2008-report.pdf>

32. Chan, V. H. T., P. Monagle, P. Massicotte, and A. K. C. Chan. Novel paediatric anticoagulants: A review of the current literature. *Blood Coagul. Fibrinolysis* 21:144–151, 2010.

33. Charville, G. W., E. M. Hetrick, C. B. Geer, and M. H. Schoenfisch. Reduced bacterial adhesion to fibrinogen-coated substrates via nitric oxide release. *Biomaterials* 29:4039–4044, 2008.

34. Chen, Z., H. Meng, G. Xing, C. Chen, Y. Zhao, G. Jia, T. Wang, H. Yuan, C. Ye, F. Zhao, Z. Chai, C. Zhu, X. Fang, B. Ma, and L. Wan. Acute toxicological effects of copper nanoparticles in vivo. *Toxicol. Lett.* 163:109–120, 2006.

35. Cioffi, N., L. Torsi, N. Ditaranto, G. Tantillo, L. Ghibelli, L. Sabbatini, T. Bleve-Zacheo, M. D'Alessio, P. G. Zambonin, and E. Traversa. Copper nanoparticle/polymer composites with antifungal and bacteriostatic properties. *Chem. Mater.* 17:5255–5262, 2005.

36. Coffin, S. E., L. M. Bell, M. Manning, and R. Polin. Nosocomial Infections in Neonates Receiving Extracorporeal Membrane Oxygenation. 18:93–96, 1997.

37. Collaud, S., C. Benden, C. Ganter, S. Hillinger, I. Opitz, D. Schneiter, R. Schuepbach, I. Inci, and W. Weder. Extracorporeal Life Support as Bridge to Lung Retransplantation: A Multicenter Pooled Data Analysis. *Ann. Thorac. Surg.* 102:1680–1686, 2016.

38. Cook, K. E., A. J. Makarewicz, C. L. Backer, L. F. Mockros, H. J. Przybylo, S. E. Crawford, J. M. Hernandez, R. J. Leonard, and C. Mavroudis. Testing of an intrathoracic artificial lung in a pig model. , 1996.

39. Cook, K. E., C. E. Perlman, R. Seipelt, C. L. Backer, C. Mavroudis, and L. F. Mockrost. Hemodynamic and gas transfer properties of a compliant thoracic artificial lung. *ASAIO J.* 51:404–411, 2005.

40. Costerton, A. J. W., P. S. Stewart, and E. P. Greenberg. Bacterial Biofilms : A Common Cause of Persistent Infections Published by : American Association for the Advancement of Science Linked references are available on JSTOR for this article : Bacterial Bioflims : A Common Cause of Persistent Infections. 284:1318–1322, 1999.

41. Crane, B. R., J. Sudhamsu, and B. A. Patel. Bacterial Nitric Oxide Synthases.

Annu. Rev. Biochem. 23:, 2010.

42. Craven, M., S. H. Kasper, M. J. Canfield, J. A. Hrabie, and N. C. Cady. Nitric oxide-releasing polyacrylonitrile disperses biofilms formed by wound-relevant pathogenic bacteria. , 2016.doi:10.1111/jam.13059

43. Cripps, C. M. Rapid method for the estimation of plasma haemoglobin levels. *J. Clin. Pathol.* 21:110–112, 1968.

44. Cutruzzolà, F., and N. Frankenberg-Dinkel. Origin and impact of nitric oxide in *Pseudomonas aeruginosa* biofilms. *J. Bacteriol.* 198:55–65, 2016.

45. Dalton, H. J., P. Garcia-Filion, R. Holubkov, F. W. Moler, T. Shanley, S. Heidemann, K. Meert, R. Berg, J. Berger, J. Carcillo, C. Newth, R. Harrison, A. Doctor, P. T. Rycus, M. Dean, T. Jenkins, and C. Nicholson. Association of bleeding and thrombosis with outcome in Extracorporeal Life Support. *Pediatr. Crit. Care Med.* 16:167–174, 2015.

46. Daniel, J., P. Bernard, S. Skinner, P. Bhandary, A. Ruzic, M. Bacon, and H. Ballard. Hollow Fiber Oxygenator Composition Has a Significant Impact on Failure Rates in Neonates on Extracorporeal Membrane Oxygenation: A Retrospective Analysis. *J. Pediatr. Intensive Care* 07:007–013, 2018.

47. Darouiche, R. O. Device-Associated Infections: A Macroproblem that Starts with Microadherence. *Clin. Infect. Dis.* 33:1567–1572, 2001.

48. Day, R. C., I. A. Feuerstein, and J. L. Brash. Flow patterns in a platelet adhesion test cell - Implications for adhesion measurement. , 1976.

49. Dede, S., Y. Deger, and S. Deger. Serum Copper, Zinc, and Calcium Concentrations in Lice-Infested Sheep. *Biol. Trace Elem. Res.* 88:87–90, 2002.

50. Demarest, C. T. Prolonging the Useful Lifetime of Artificial Lungs. , 2017.

51. Dornia, C., A. Philipp, S. Bauer, M. Lubnow, T. Muller, K. Lehle, C. Schmid, R. M. Muller-Wille, P. Wiggermann, C. Stroszczynski, and A. G. Schreyer. Analysis of thrombotic deposits in extracorporeal membrane oxygenators by multidetector computed tomography. *ASAIO J.* 60:652–656, 2014.

52. Dornia, C., A. Philipp, S. Bauer, C. Stroszczynski, A. G. Schreyer, T. Müller, G. E. Koehl, and K. Lehle. D-dimers Are a Predictor of Clot Volume Inside Membrane Oxygenators During Extracorporeal Membrane Oxygenation. *Artif. Organs* 39:782–787, 2015.

53. Douglass, B. H., A. L. Keenan, and D. M. Purohit. Bacterial and fungal infection in neonates undergoing venoarterial extracorporeal membrane oxygenation: An analysis of the registry data of the extracorporeal life support organization. *Artif. Organs* 20:202–208, 1996.

54. Edmond, M. B., S. E. Wallace, D. K. Mcclish, M. A. Pfaller, R. N. Jones, R. P. Wenzel, S. Clinical, I. Diseases, N. Aug, M. B. Edmond, S. E. Wallace, D. K. Mcclish, M. A. Pfaller, and R. N. Jones. Nosocomial Bloodstream Infections in

United States Hospitals : A Three-Year Analysis. *Clin. Infect. Dis.* 29:239–244, 1999.

55. ELSO. General Guidelines for all ECLS Cases. *Extracorpor. Life Support Organ.* 1–26, 2017.at <https://www.elso.org/Resources/Guidelines.aspx>

56. Ertan Taskin, M., K. H. Fraser, T. Zhang, B. P. Griffith, and Z. J. Wu. Micro-scale modeling of flow and oxygen transfer in hollow fiber membrane bundle. *J. Memb. Sci.* 362:172–183, 2010.

57. Esteban, A., A. Anzueto, F. Frutos, I. Alía, L. Brochard, T. E. Stewart, S. Benito, S. K. Epstein, C. Apezteguía, P. Nightingale, A. C. Arroliga, and M. J. Tobin. Characteristics and outcomes in adult patients receiving mechanical ventilation: A 28-day international study. *J. Am. Med. Assoc.* 287:345–355, 2002.

58. Etulain, J., M. J. Lapponi, S. J. Patrucchi, M. A. Romaniuk, R. Benzadón, G. L. Klement, S. Negrotto, and M. Schattner. Hyperthermia inhibits platelet hemostatic functions and selectively regulates the release of alpha-granule proteins. *J. Thromb. Haemost.* 9:1562–1571, 2011.

59. Evans, C. F., T. Li, V. Mishra, D. L. Pratt, I. S. K. Mohammed, Z. N. Kon, and B. P. Griffith. Externally visible thrombus partially predicts internal thrombus deposition in extracorporeal membrane oxygenators. *Perfus. (United Kingdom)* 32:301–305, 2017.

60. Evans, W., S. C. Capelle, and D. I. Edelstone. Lack of a critical cardiac output and critical systemic oxygen delivery during low cardiac output in the third trimester in the pregnant sheep. *Am. J. Obstet. Gynecol.* 175:222–228, 1996.

61. Eynden, F. Vanden, M. Carrier, S. Ouellet, P. Demers, J. Forcillo, L. P. Perrault, M. Pellerin, and D. Bouchard. Avecor trillium oxygenator versus noncoated monolyth oxygenator: A prospective randomized controlled study. *J. Card. Surg.* 23:288–293, 2008.

62. La Fayette, N. G., R. E. Schewe, J. P. Montoya, and K. E. CooK. Performance of a medarray silicone hollow fiber oxygenator. *ASAIO J.* 55:382–387, 2009.

63. FDA. Vaping Illness Update: FDA Warns Public to Stop Using Tetrahydrocannabinol (THC) - Containing Vaping Products and Any Vaping Products Obtained Off the Street. , 2019.at <https://www.cdc.gov/tobacco/basic_information/e-cigarettes/severe-lung-disease.html>

64. Fischer, S., A. R. Simon, T. Welte, M. M. Hoeper, A. Meyer, R. Tessmann, B. Gohrbandt, J. Gottlieb, A. Haverich, and M. Strueber. Bridge to lung transplantation with the novel pumpless interventional lung assist device NovaLung. *J. Thorac. Cardiovasc. Surg.* 131:719–723, 2006.

65. Fleser, P. S., V. K. Nuthakki, L. E. Malinzak, R. E. Callahan, M. L. Seymour, M. M. Reynolds, S. I. Merz, M. E. Meyerhoff, P. J. Bendick, G. B. Zelenock, and C. J. Shanley. Nitric oxide-releasing biopolymers inhibit thrombus formation in a sheep

model of arteriovenous bridge grafts. *J. Vasc. Surg.* 40:803–811, 2004.

66. Fomby, P., and A. J. Cherlin. Darcy Permeability of Hollow Fiber Bundles Used in Blood Oxygenation Devices. *J. Memb. Sci.* 72:181–204, 2011.

67. Ford, E. S., J. B. Croft, D. M. Mannino, A. G. Wheaton, X. Zhang, and W. H. Giles. COPD surveillance - United States, 1999-2011. *Chest* 144:284–305, 2013.

68. Ford, E. S., D. M. Mannino, A. G. Wheaton, W. H. Giles, L. Presley-Cantrell, and J. B. Croft. Trends in the Prevalence of Obstructive and Restrictive Lung Function Among Adults in the United States. *Chest* 143:1395–1406, 2013.

69. Francolini, I., and G. Donelli. Prevention and control of biofilm-based medical-device-related infections. *FEMS Immunol. Med. Microbiol.* 59:227–238, 2010.

70. Franke, S., G. Grass, C. Rensing, and D. H. Nies. Molecular analysis of the copper-transporting efflux system CusCFBA of Escherichia coli. *J. Bacteriol.* 185:3804–3812, 2003.

71. Frost, M. C., M. M. Reynolds, and M. E. Meyerhoff. Polymers incorporating nitric oxide releasing/generating substances for improved biocompatibility of blood-contacting medical devices. *Biomaterials* 26:1685–1693, 2005.

72. Frostell, C., and M.-D. Fratacci. Inhaled Nitric Oxide : A selective pulmonary vasodilator reversing hypoxic pulmonary vasoconstriction. *Circulation* 83:163–163, 1991.

73. Gaffney, A. M., M. J. Santos-Martinez, A. Satti, T. C. Major, K. J. Wynne, Y. K. Gun'ko, G. M. Annich, G. Elia, and M. W. Radomski. Blood biocompatibility of surface-bound multi-walled carbon nanotubes. *Nanomedicine Nanotechnology, Biol. Med.* 11:39–46, 2015.

74. Germann, P., A. Braschi, G. Della Rocca, A. T. Dinh-Xuan, K. Falke, C. Frostell, L. E. Gustafsson, P. Hervé, P. Jolliet, U. Kaisers, H. Litvan, D. J. Macrae, M. Maggiorini, N. Marczin, B. Mueller, D. Payen, M. Ranucci, D. Schranz, R. Zimmermann, and R. Ullrich. Inhaled nitric oxide therapy in adults: European expert recommendations. *Intensive Care Med.* 31:1029–1041, 2005.

75. Gkaliagkousi, E., J. Ritter, and A. Ferro. Platelet-derived nitric oxide signaling and regulation. *Circ. Res.* 101:654–662, 2007.

76. Glater-Welt, L. B., J. B. Schneider, M. M. Zinger, L. Rosen, and T. M. Sweberg. Nosocomial Bloodstream Infections in Patients Receiving Extracorporeal Life Support: Variability in Prevention Practices: A Survey of the Extracorporeal Life Support Organization Members. *J. Intensive Care Med.* 31:654–659, 2016.

77. González-Guerrero, M., D. Raimunda, X. Cheng, and J. M. Argüello. Distinct functional roles of homologous Cu+ efflux ATPases in Pseudomonas aeruginosa. *Mol. Microbiol.* 78:1246–1258, 2010.

78. Gorren, A. C. F., A. Schrammel, K. Schmidt, and B. Mayer. Decomposition of S -Nitrosoglutathione in the Presence of Copper Ions and Glutathione. *Arch.*

Biochem. Biophys. 330:219–228, 1996.

79. Grass, G., and C. Rensing. CueO is a multi-copper oxidase that confers copper tolerance in Escherichia coli. *Biochem. Biophys. Res. Commun.* 286:902–908, 2001.

80. Grass, G., and C. Rensing. Genes Involved in Copper Homeostasis in Escherichia coli. *J. Bacteriol.* 183:2145–2147, 2001.

81. Grass, G., C. Rensing, and M. Solioz. Metallic Copper as an Antimicrobial Surface. *Appl. Environ. Microbiol.* 77:1541–1547, 2011.

82. Gries, A., C. Bode, K. Peter, A. Herr, H. Bo, J. Motsch, and E. Martin. Inhaled Nitric Oxide Inhibits Human Platelet Aggregation, P-Selectin Expression , and Fibrinogen Binding In Vitro and In Vivo. *Circulation* 97:1481–1487, 1998.

83. De Groote, M. A., and F. C. Fang. NO Inhibitions : Antimicrobial Properties of Nitric Oxide. *Clin. Infect. Dis.* 21:, 1995.

84. Gupta, S., K. A. Amoako, A. Suhaib, and K. E. Cook. Multi-Modal, Surface-Focused Anticoagulation Using Poly-2-methoxyethylacrylate Polymer Grafts and Surface Nitric Oxide Release. *Adv. Mater. Interfaces* 1:, 2014.

85. Gusarov, I., K. Shatalin, M. Starodubtseva, and E. Nudler. Endogenous Nitric Oxide Protects Bacteria Against Wide Spectrum of Antibiotics. *Science (80-.).* 325:1380–1385, 2009.

86. Hakim, A. H., U. Ahmad, K. R. McCurry, D. R. Johnston, G. B. Pettersson, M. Budev, S. Murthy, E. H. Blackstone, and M. Z. Tong. Contemporary Outcomes of Extracorporeal Membrane Oxygenation Used as Bridge to Lung Transplantation. *Ann. Thorac. Surg.* 106:192–198, 2018.

87. Handa, H., T. C. Major, E. J. Brisbois, K. A. Amoako, M. E. Meyerhoff, and R. H. Bartlett. Hemocompatibility comparison of biomedical grade polymers using rabbit thrombogenicity model for preparing nonthrombogenic nitric oxide releasing surfaces. *J. Mater. Chem. B* 2:1059–1067, 2014.

88. Haneke, F., T. A. Schildhauer, A. D. Schlebes, J. T. Strauch, and J. Swol. Infections and Extracorporeal Membrane Oxygenation: Incidence , Therapy , and Outcome. *ASAIO J.* , 2016.doi:10.1097/MAT.0000000000000308

89. Haneya, A., A. Philipp, T. Mueller, M. Lubnow, M. Pfeifer, W. Zink, M. Hilker, C. Schmid, and S. Hirt. Extracorporeal circulatory systems as a bridge to lung transplantation at remote transplant centers. *Ann. Thorac. Surg.* 91:250–255, 2011.

90. Hanna, H., R. Benjamin, I. Chatzinikolaou, B. Alakech, D. Richardson, P. Mansfield, T. Dvorak, M. F. Munsell, R. Darouiche, H. Kantarjian, and I. Raad. Long-term silicone central venous catheters impregnated with minocycline and rifampin decrease rates of catheter-related bloodstream infection in cancer patients: A prospective randomized clinical trial. *J. Clin. Oncol.* 22:3163–3171,

2004.

91. Hidron, A. I., J. R. Edwards, J. Patel, T. C. Horan, D. M. Sievert, D. A. Pollock, and S. K. Fridkin. Antimicrobial-Resistant Pathogens Associated With Healthcare-Associated Infections: Annual Summary of Data Reported to the National Healthcare Safety Network at the Centers for Disease Control and Prevention, 2006–2007. *Infect. Control Hosp. Epidemiol.* 29:996–1011, 2008.

92. Hirsh, J., and R. Raschke. Heparin : Mechanism of Action , Heparin. *Fourth ACCP Conf. Antithrombotic Ther.* , 1995.

93. Hochgräfe, F., C. Wolf, S. Fuchs, M. Liebeke, M. Lalk, S. Engelmann, and M. Hecker. Nitric oxide stress induces different responses but mediates comparable protein thiol protection in Bacillus subtilis and Staphylococcus aureus. *J. Bacteriol.* 190:4997–5008, 2008.

94. Hochgräfe, F., C. Wolf, S. Fuchs, M. Liebeke, M. Lalk, S. Engelmann, and M. Hecker. Nitric oxide stress induces different responses but mediates comparable protein thiol protection in Bacillus subtilis and Staphylococcus aureus. *J. Bacteriol.* 190:4997–5008, 2008.

95. Hoehn, T., J. Huebner, E. Paboura, M. Krause, and J. U. Leititis. Effect of therapeutic concentrations of nitric oxide on bacterial growth in vitro. *Crit. Care Med.* 26:1857–1862, 1998.

96. Incze, K., J. Farkas, V. Mihalyi, and E. Zukal. Antibacterial effect of cysteine nitrosothiol and possible percursors thereof. *Appl. Microbiol.* 27:202–205, 1974.

97. Jackson, S. P. The growing complexity of platelet aggregation. *Blood* 109:5087–5095, 2007.

98. Jamiolkowski, M. A., D. D. Pedersen, W. T. Wu, J. F. Antaki, and W. R. Wagner. Visualization and analysis of biomaterial-centered thrombus formation within a defined crevice under flow. *Biomaterials* 96:72–83, 2016.

99. Jardeleza, C., A. Foreman, L. Baker, S. Paramasivan, J. Field, L. W. Tan, and P. J. Wormald. The effects of nitric oxide on Staphylococcus aureus biofilm growth and its implications in chronic rhinosinusitis. *Int. Forum Allergy Rhinol.* 1:438–444, 2011.

100. John, T., A. Rajpurkar, G. Smith, M. Fairfax, and J. Triest. Antibiotic pretreatment of hydrogel ureteral stent. *J. Endourol.* 21:1211–1215, 2007.

101. Kalchiem-Dekel, O., J. Galvin, A. Burke, S. Atamas, and N. Todd. Interstitial Lung Disease and Pulmonary Fibrosis: A Practical Approach for General Medicine Physicians with Focus on the Medical History. *J. Clin. Med.* 7:476, 2018.

102. Kao, L. S., G. M. Fleming, R. J. Escamilla, D. F. Lew, and K. P. Lally. Antimicrobial prophylaxis and infection surveillance in extracorporeal membrane oxygenation patients: A multi-institutional survey of practice patterns. *ASAIO J.* 57:231–238, 2011.

103. Kayser, F. H., and J. Wüst. Interpretive criteria for disk diffusion susceptibility testing of sparfloxacin. *Eur. J. Clin. Microbiol. Infect. Dis.* 10:163–166, 1991.

104. Keh, D., M. Gerlach, I. Kürer, S. Spielmann, T. Kerner, T. Busch, R. Hansen, K. Falke, and H. Gerlach. Nitric oxide diffusion across membrane lungs protects platelets during simulated extracorporeal circulation. *Eur. J. Clin. Invest.* 29:344–350, 1999.

105. Kelm, M. Nitric Oxide Metabolism and Breakdown.pdf. *Biochim. Biophys. Acta* 1411:273–289, 1998.

106. Kim, J., G. Saravanakumar, H. W. Choi, D. Park, and W. J. Kim. A platform for nitric oxide delivery. *J. Mater. Chem. B* 2:341, 2014.

107. Kochanek, K. D., S. L. Murphy, J. Xu, and B. Tejada-Vera. National Vital Statistics Reports Deaths : Final Data for 2014. *Centers Dis. Control Prev.* 65:, 2016.

108. Konishi, R., R. Shimzu, L. Firestone, F. R. Walters, W. R. Wagner, W. J. Federspiel, H. Konishi, and B. G. Hattler. Nitric Oxide Prevents Human Platelet Adhesion to Fiber Membranes in Whole Blood. *ASAIO J. (American Soc. Artif. Intern. Organs)* 42:M850–M853, 1996.

109. Kuehn, C., P. Orszag, K. Burgwitz, G. Marsch, N. Stumpp, M. Steisch, and A. Haverich. Microbial Adhesion on Membrane Oxygenators in Patients Requiring Extracorporeal Life Support Detected by a Universal rDNA PCR Test. *ASAIO J.* , 2013.doi:10.1097/MAT.0b013e318299fd07

110. Kutay, V., T. Noyan, S. Ozcan, Y. Melek, H. Ekim, and C. Yakut. Biocompatibility of heparin-coated cardiopulmonary bypass circuits in coronary patients with left ventricular dysfunction is superior to PMEA-coated circuits. *J. Card. Surg.* 21:572–577, 2006.

111. Kwak, J., M. B. Majewski, and W. S. Jellish. Extracorporeal Membrane Oxygenation: The New Jack of All Trades? *J. Cardiothorac. Vasc. Anesth.* 000:, 2019.

112. Lai, A., C. T. Demarest, C. C. Do-Nguyen, R. Ukita, D. J. Skoog, N. M. Carleton, K. A. Amoako, P. J. Montoya, and K. E. Cook. 72-Hour in vivo evaluation of nitric oxide generating artificial lung gas exchange fibers in sheep. *Acta Biomater.* 90:122–131, 2019.

113. Lantvit, S. M., B. J. Barrett, and M. M. Reynolds. Nitric oxide releasing material adsorbs more fibrinogen. *J. Biomed. Mater. Res. - Part A* 101:3201–3210, 2013.

114. Lazarinis, S., J. Krrholm, and N. P. Hailer. Effects of hydroxyapatite coating on survival of an uncemented femoral stem. *Acta Orthop.* 82:399–404, 2011.

115. Lecuyer, S., R. Rusconi, Y. Shen, A. Forsyth, H. Vlamakis, R. Kolter, and H. A. Stone. Shear stress increases the residence time of adhesion of Pseudomonas aeruginosa. *Biophys. J.* 100:341–350, 2011.

116. Lehle, K., A. Philipp, O. Gleich, A. Holzamer, T. Müller, T. Bein, and C. Schmid.

Efficiency in extracorporeal membrane oxygenation-cellular deposits on polymethypentene membranes increase resistance to blood flow and reduce gas exchange capacity. *ASAIO J.* 54:612–617, 2008.

117. León, C., S. Ruiz-Santana, J. Rello, M. V. De La Torre, J. Vallés, F. Álvarez-Lerma, R. Sierra, P. Saavedra, and F. Álvarez-Salgado. Benefits of minocycline and rifampin-impregnated central venous catheters: A prospective, randomized, double-blind, controlled, multicenter trial. *Intensive Care Med.* 30:1891–1899, 2004.

118. Linder, M. C., and M. Hazegh-Azam. Copper biochemistry and molecular biology. *Am. J. Clin. Nutr.* 63:797–811, 1996.

119. Lipton, S. A., Y. B. Choi, Z. H. Pan, S. Z. Lei, H. S. V. Chen, N. J. Sucher, J. Loscalzo, D. J. Singel, and J. S. Stamler. A redox-based mechanism for the neuroprotective and neurodestructive effects of nitric oxide and related nitroso-compounds. *Nature* 364:626–632, 1993.

120. Loskove, J. A., and W. H. Frishman. Nitric oxide donors in the treatment of cardiovascular and pulmonary diseases. *Am. Heart J.* 129:604–613, 1995.

121. Lundberg, J. O., E. Weitzberg, and M. T. Gladwin. The nitrate-nitrite-nitric oxide pathway in physiology and therapeutics. *Nat. Rev. Drug Discov.* 7:156–167, 2008.

122. Macomber, L., and J. A. Imlay. The iron-sulfur clusters of dehydratases are primary intracellular targets of copper toxicity. *Proc. Natl. Acad. Sci.* 106:8344–8349, 2009.

123. Major, T. C., D. O. Brant, C. P. Burney, K. a. Amoako, G. M. Annich, M. E. Meyerhoff, H. Handa, and R. H. Bartlett. The hemocompatibility of a nitric oxide generating polymer that catalyzes S-nitrosothiol decomposition in an extracorporeal circulation model. *Biomaterials* 32:5957–5969, 2011.

124. Major, T. C., D. O. Brant, M. M. Reynolds, R. H. Bartlett, M. E. Meyerhoff, H. Handa, and G. M. Annich. The attenuation of platelet and monocyte activation in a rabbit model of extracorporeal circulation by a nitric oxide releasing polymer. *Biomaterials* 31:2736–2745, 2010.

125. Mansouri, A., and A. A. Lurie. Concise review: Methemoglobinemia. *Am. J. Hematol.* 42:7–12, 1993.

126. Marcoux, J., N. Sohn, E. Mcnair, M. Rosin, G. Smith, H. Lim, T. Mycyk, and Q. Meng. Outcomes comparison of 5 coated cardiopulmonary bypass circuits versus an uncoated control group of patients undergoing cardiac surgery. *Perfusion* 24:307–315, 2009.

127. Maul, T. M., P. M. Massicotte, and P. D. Wearden. ECMO Biocompatibility: Surface coatings, anticoagulation, and coagulation monitoring. In: Extracorporeal Membrane Oxygenation - Advances in Therapy. 2016, pp. 27–56.

128. Maurer-Spurej, E., G. Pfeiler, N. Maurer, H. Lindner, O. Glatter, and D. V. Devine.

Room temperature activates human blood platelets. *Lab. Investig.* 81:581–592, 2001.

129. Mazaheri, A. R., and G. Ahmadi. Uniformity of the Fluid Flow Velocities Within Hollow Fiber Membranes of Blood Oxygenation Devices. *Artif Organs* 30:10–15, 2006.

130. Mazzeffi, M., J. Greenwood, K. Tanaka, J. Menaker, R. Rector, D. Herr, Z. Kon, J. Lee, B. Griffith, K. Rajagopal, and S. Pham. Bleeding, Transfusion, and Mortality on Extracorporeal Life Support: ECLS Working Group on Thrombosis and Hemostasis. *Ann. Thorac. Surg.* 101:682–689, 2016.

131. Menzies, P. I., H. Boermans, B. Hoff, T. Durzi, and L. Langs. Survey of the status of copper, interacting minerals, and vitamin E levels in the livers of sheep in Ontario. *Can. Vet. J.* 44:898–906, 2003.

132. Meyer, D. M., M. E. Jessen, and R. C. Eberhart. Neonatal extracorporeal membrane oxygenation complicated by sepsis. *Ann. Thorac. Surg.* 59:975–980, 1995.

133. Miller, C., B. Mcmullin, A. Ghaffari, A. Stenzler, N. Pick, D. Roscoe, A. Ghahary, J. Road, and Y. Av-gay. Gaseous nitric oxide bactericidal activity retained during intermittent high-dose short duration exposure. *Nitric Oxide* 20:16–23, 2009.

134. Mockros, L., and R. Leonard. Compact Cross-Flow Tubular Oxygenators. *Trans. - Am. Soc. Artif. Intern. Organs* 31:628–633, 1985.

135. Mohammed, A., M. Campbell, and F. G. Youssef. Serum copper and haematological values of sheep of different physiological stages in the dry and wet seasons of central trinidad. *Vet. Med. Int.* 2014:, 2014.

136. Müller, T., M. Lubnow, A. Philipp, W. Schneider-Brachert, D. Camboni, C. Schmid, and K. Lehle. Risk of Circuit Infection in Septic Patients on Extracorporeal Membrane Oxygenation: A Preliminary Study. *Artif. Organs* 35:84–90, 2011.

137. Mulvihill, J. N., A. Faradji, F. Oberling, and J. -P Cazenave. Surface passivation by human albumin of plasmaperesis circuits reduces platelet accumulation and thrombus formation. Experimental and clinical studies. *J. Biomed. Mater. Res.* 24:155–163, 1990.

138. N, L. M., R. Gary, L. Seth, and K. Clive. Hemorrhagic Complications of Anticoagulant Treatment. , 2001.doi:10.1378/chest.119.1

139. Nablo, B. J., and M. H. Schoenfisch. Poly(vinyl chloride)-coated sol-gels for studying the effects of nitric oxide release on bacterial adhesion. *Biomacromolecules* 5:2034–2041, 2004.

140. Neeves, K. B., D. A. R. Illing, and S. L. Diamond. Thrombin flux and wall shear rate regulate fibrin fiber deposition state during polymerization under flow. *Biophys. J.* 98:1344–1352, 2010.

141. Neufeld, B. H., and M. M. Reynolds. Critical nitric oxide concentration for

Pseudomonas aeruginosa biofilm reduction on polyurethane substrates. *Biointerphases* 11:, 2016.

142. Nguyen, T., D. Brunson, C. L. Crespi, B. W. Penman, J. S. Wishnok, and S. R. Tannenbaum. DNA damage and mutation in human cells exposed to nitric oxide in vitro. *Proc. Natl. Acad. Sci. U. S. A.* 89:3030–3034, 1992.

143. O'Brien, P. A., R. Kulier, F. M. Helmerhorst, M. Usher-Patel, and C. d'Arcangues. Copper-containing, framed intrauterine devices for contraception: a systematic review of randomized controlled trials. *Contraception* 77:318–327, 2008.

144. O'Neill, J., G. Schutze, M. Heulitt, P. Simpson, and B. Taylor. Nosocomial infections during extracorporeal membrane oxygenation. *Intensive Care Med.* 27:1247–1253, 2001.

145. Owen, D. R., C. M. Chen, J. A. Oschner, and R. M. Zone. Interactions of plasma proteins with selective artificial surfaces. *ASAIO J.* XXXI:240–243, 1985.

146. Paden, M. L., S. a Conrad, P. T. Rycus, R. R. Thiagarajan, and ELSO Registry. Extracorporeal Life Support Organization Registry Report 2012. *ASAIO J.* 59:202–10, 2013.

147. Pant, J., M. J. Goudie, S. P. Hopkins, E. J. Brisbois, and H. Handa. Tunable Nitric Oxide Release from S-Nitroso-N-acetylpenicillamine via Catalytic Copper Nanoparticles for Biomedical Applications. *ACS Appl. Mater. Interfaces* 9:15254–15264, 2017.

148. Pinhu, L., T. Whitehead, T. Evans, and M. Griffiths. Ventilator-associated lung injury. *Lancet* 361:332–341, 2003.

149. Plate, L., and M. A. Marletta. Nitric Oxide Modulates Bacterial Biofilm Formation through a Multicomponent Cyclic-di-GMP Signaling Network. *Mol. Cell* 46:449–460, 2012.

150. Van Poucke, S., K. Stevens, A. E. Marcus, and M. Lancé. Hypothermia: Effects on platelet function and hemostasis. *Thromb. J.* 12:1–5, 2014.

151. Ratner, B. D. The catastrophe revisited: Blood compatibility in the 21st Century. *Biomaterials* 28:5144–5147, 2007.

152. Rauch, E. D., A. H. Stammers, B. L. Mejak, S. N. Vang, and T. W. Viessman. The effects of nitric oxide on coagulation during simulated extracorporeal membrane oxygenation. *J. Extra. Corpor. Technol.* 32:214–219, 2000.

153. Ren, H., A. Colletta, D. Koley, J. Wu, C. Xi, T. C. Major, R. H. Bartlett, and M. E. Meyerhoff. Thromboresistant/anti-biofilm catheters via electrochemically modulated nitric oxide release. *Bioelectrochemistry* 104:10–16, 2015.

154. Rensing, C., and G. Grass. Escherichia coli mechanisms of copper homeostasis in a changing environment. *FEMS Microbiol. Rev.* 27:197–213, 2003.

155. Reser, D., B. Seifert, M. Klein, T. Dreizler, P. Hasenclever, V. Falk, and C. Starck.

Retrospective analysis of outcome data with regards to the use of Phisio®-, Bioline®- or Softline®-coated cardiopulmonary bypass circuits in cardiac surgery. *Perfus. (United Kingdom)* 27:530–534, 2012.

156. Riccio, D. a., K. P. Dobmeier, E. M. Hetrick, B. J. Privett, H. S. Paul, and M. H. Schoenfisch. Nitric oxide-releasing S-nitrosothiol-modified xerogels. *Biomaterials* 30:4494–4502, 2009.

157. Richards, M. J., J. R. Edwards, D. H. Culver, and R. P. Gaynes. Nosocomial infections in medical intensive care units in the United States. *Crit. Care Med.* 27:887–892, 1999.

158. Richardson, A. R., S. J. Libby, and F. C. Fang. A Nitric Oxide – Inducible Lactate Dehydrogenase Enables Staphylococcus Aureus to Resist Innate Immunity. *Science (80-.).* 319:1672–1676, 2008.

159. Santo, C. E., E. W. Lam, C. G. Elowsky, D. Quaranta, D. W. Domaille, C. J. Chang, and G. Grass. Bacterial Killing by Dry Metallic Copper Surfaces □. 77:794–802, 2011.

160. Sato, H., G. W. Griffith, C. M. Hall, J. M. Toomasian, R. B. Hirschl, R. H. Bartlett, and K. E. Cook. Seven-Day Artificial Lung Testing in an In-Parallel Configuration. *Ann. Thorac. Surg.* 84:988–994, 2007.

161. Sato, H., C. M. Hall, N. G. Lafayette, J. R. Pohlmann, N. Padiyar, J. M. Toomasian, J. W. Haft, and K. E. Cook. Thirty-Day In-Parallel Artificial Lung Testing in Sheep. *Ann. Thorac. Surg.* 84:1136–1143, 2007.

162. Savage, B., E. Saldívar, and Z. M. Ruggeri. Initiation of platelet adhesion by arrest onto fibrinogen or translocation on von Willebrand factor. *Cell* 84:289–297, 1996.

163. Schewe, R. E., K. M. Khanafer, A. Arab, J. Mitchell, D. Skoog, and K. E. Cook. Design and In Vitro Assessment of an Improved, Low-Resistance, Compliant Thoracic Artificial Lung. *ASAIO J.* 58:583–589, 2012.

164. Schewe, R. E., K. M. Khanafer, R. A. Orizondo, and K. E. Cook. Thoracic artificial lung impedance studies using computational fluid dynamics and in vitro models. *Ann. Biomed. Eng.* 40:628–636, 2012.

165. Schlanstein, P. C., F. Hesselmann, S. V. Jansen, J. Gemsa, T. A. Kaufmann, M. Klaas, D. Roggenkamp, W. Schröder, T. Schmitz-Rode, U. Steinseifer, and J. Arens. Particle Image Velocimetry Used to Qualitatively Validate Computational Fluid Dynamic Simulations in an Oxygenator: A Proof of Concept. *Cardiovasc. Eng. Technol.* 6:340–351, 2015.

166. Schmidt, M., C. Stewart, M. Bailey, A. Nieszkowska, J. Kelly, L. Murphy, D. Pilcher, K. Cooper, C. Scheinkestel, V. Pellegrino, P. Forrest, A. Combes, and C. Hodgson. Mechanical Ventilation Management During Extracoporeal Membrane Oxygenation for Acute Respiratory Distress Syndrome: A Retrospective International Multicenter Study. *Intensive Care Med.* 40:S10, 2014.

167. Schraufnagel, D. E. Interstitial lung disease. In: Breathing in America: Diseases, Progress, and Hope. 2010.doi:10.1016/0011-5029(91)90022-4

168. Schwan, W. R., P. Warrener, E. Keunz, C. Kendall Stover, and K. R. Folger. Mutations in the cueA gene encoding a copper homeostasis P-type ATPase reduce the pathogenicity of Pseudomonas aeruginosa in mice. *Int. J. Med. Microbiol.* 295:237–242, 2005.

169. Scipione, C. N., R. E. Schewe, K. L. Koch, A. W. Shaffer, A. Iyengar, and K. E. Cook. Use of a low-resistance compliant thoracic artificial lung in the pulmonary artery to pulmonary artery configuration. *J. Thorac. Cardiovasc. Surg.* 145:, 2013.

170. Sehgal, S., and B. Storrie. Evidence that differential packaging of the major platelet granule proteins von Willebrand factor and fibrinogen can support their differential release. *J. Thromb. Haemost.* 5:2009–2016, 2007.

171. Serikov, V. B., and E. H. Jerome. Noninvasive measurements of cardiac output in sheep: An improved thermometry method. *Med. Eng. Phys.* 19:618–629, 1997.

172. Shin, E. K., H. Park, J. Y. Noh, K. M. Lim, and J. H. Chung. Platelet shape changes and cytoskeleton dynamics as novel therapeutic targets for anti-thrombotic drugs. *Biomol. Ther.* 25:223–230, 2017.

173. Siller-Matula, J. M., R. Plasenzotti, A. Spiel, P. Quehenberger, and B. Jilma. Interspecies differences in coagulation profile. *Thromb. Haemost.* 100:397–404, 2008.

174. Singha, P., J. Pant, M. J. Goudie, C. D. Workman, and H. Handa. Enhanced antibacterial efficacy of nitric oxide releasing thermoplastic polyurethanes with antifouling hydrophilic topcoats. *Biomater. Sci.* 5:1246–1255, 2017.

175. Skoog, D. J., J. R. Pohlmann, D. S. Demos, C. N. Scipione, A. Iyengar, R. E. Schewe, A. B. Suhaib, K. L. Koch, and K. E. Cook. Fourteen Day in Vivo Testing of a Compliant Thoracic Artificial Lung. *ASAIO J.* 63:644–649, 2017.

176. Slutsky, A. S. Lung injury caused by mechanical ventilation. *Chest* 116:, 1999.

177. Sohn, N., J. Marcoux, T. Mycyk, J. Krahn, and Q. Meng. The impact of different biocompatible coated cardiopulmonary bypass circuits on inflammatory response and oxidative stress. *Perfusion* 24:231–237, 2009.

178. Solioz, M., H. K. Abicht, M. Mermod, and S. Mancini. Response of Gram-positive bacteria to copper stress. *J. Biol. Inorg. Chem.* 15:3–14, 2010.

179. Strueber, M., M. M. Hoeper, S. Fischer, M. Cypel, G. Warnecke, J. Gottlieb, A. Pierre, T. Welte, A. Haverich, A. R. Simon, and S. Keshavjee. Bridge to thoracic organ transplantation in patients with pulmonary arterial hypertension using a pumpless lung assist device. *Am. J. Transplant.* 9:853–857, 2009.

180. Sudha, V. B. P., S. Ganesan, G. P. Pazhani, T. Ramamurthy, G. B. Nair, and P. Venkatasubramanian. Storing Drinking-water in Copper pots Kills Contaminating Diarrhoeagenic Bacteria. *J. Heal. Popul. Nutr.* 30:17–21, 2012.

181. Sulemankhil, I., J. G. Ganopolsky, C. A. Dieni, A. F. Dan, M. L. Jones, and S. Prakash. Prevention and treatment of virulent bacterial biofilms with an enzymatic nitric oxide-releasing dressing. *Antimicrob. Agents Chemother.* 56:6095–6103, 2012.

182. Sun, H.-Y. Infections occuring during extracorporeal oxygenation use in adult patients. *J. Thorac. Cardiovasc. Surg.* 140:1125–1132, 2010.

183. Tanaka, M., T. Motomura, M. Kawada, T. Anzai, Yuu Kasori, T. Shiroya, K. Shimura, M. Onishi, and Akira Mochizuki. Blood compatible aspects of poly(2-methoxyethylacrylate) (PMEA)-relationship between protein adsorption and platelet adhesion on PMEA surface. *Biomaterials* 21:1471–1481, 2000.

184. Taylor, M. B., K. Christian, and K. B. Churchwell. Methemoglobinemia: Toxicity of Inhaled Nitric Oxide (NO) Therapy. *Am. Acad. Pediatr.* 682, 1999.

185. Theil, E. C., and K. T. Calvert. The effect of copper excess on iron metabolism in sheep. *J. Biochem.* 170:137–43, 1978.

186. Thiara, A. S., V. Y. Andersen, V. Videm, T. E. Mollnes, K. Svennevig, T. N. Hoel, and A. E. Fiane. Comparable biocompatibility of Phisio- and Bioline-coated cardiopulmonary bypass circuits indicated by the inflammatory response. *Perfusion* 25:9–16, 2010.

187. Toomasian, J. M., R. J. Schreiner, D. E. Meyer, M. E. Schmidt, S. E. Hagan, G. W. Griffith, R. H. Bartlett, and K. E. Cook. A polymethylpentene fiber gas exchanger for long-term extracorporeal life support. *ASAIO J.* 51:390–397, 2005.

188. Toomasian, J. M., R. J. Schreiner, D. E. Meyer, M. E. Schmidt, S. E. Hagan, G. W. Griffith, R. H. Bartlett, and K. E. Cook. A polymethylpentene fiber gas exchanger for long-term extracorporeal life support. *ASAIO J.* 51:390–397, 2005.

189. Tsuno, K., P. Prato, and T. Kolobow. Acute lung injury from mechanical ventilation at moderately high airway pressures. *J. Appl. Physiol.* 69:956–961, 1990.

190. Ueyama, K., K. Nishimura, T. Nishina, T. Nakamura, T. Ikeda, and M. Komeda. PMEA coating of pump circuit and oxygenator may attenuate the early systemic inflammatory response in cardiopulmonary bypass surgery. *ASAIO J.* 50:369–372, 2004.

191. Ukita, R., K. Wu, X. Lin, N. M. Carleton, C. C. Do-Nguyen, A. Lai, C. T. Demarest, N. Naito, S. Jiang, and K. E. Cook. In vivo sheep and rabbit models for evaluating low-fouling zwitterionic polymer coatings in artificial lungs

192. Vaughn, M. W., L. Kuo, and J. C. Liao. Estimation of nitric oxide production and reaction rates in tissue by use of mathematical model. *Am. J. Pphysiology* 43:H2163, 1998.

193. Weaver, L., J. O. Noyce, H. T. Michels, and C. W. Keevil. Potential action of copper surfaces on meticillin-resistant Staphylococcus aureus. 2200–2205, 2010.doi:10.1111/j.1365-2672.2010.04852.x

194. Williams, D. L. H. Nitric oxide release from S-nitrosothiols (RSNO) - the role of copper ions. *Transit. Met. Chem.* 21:189–191, 1996.

195. Wink, D. A., K. S. Kasprzak, C. M. Maragos, R. K. Elespuru, M. Misra, T. M. Dunams, T. A. Cebula, W. H. Koch, A. W. Andrews, S. Allen, L. K. Keefer, D. A. Wink, K. S. Kasprzak, C. M. Maragos, R. K. Elespuru, M. Misra, T. M. Dunams, T. A. Cebula, W. H. Koch, A. W. Andrews, J. S. Allen, and L. K. Keefer. DNA Deaminating Ability and Genotoxicity of Nitric Oxide and Its Progenitors. *Science (80-.).* 254:1001–1003, 1991.

196. Wright, R. O., W. J. Lewander, and A. D. Woolf. Methemoglobinemia: Etiology, pharmacology, and clinical management. *Ann. Emerg. Med.* 34:646–656, 1999.

197. Wu, W.-T., N. Aubry, W. R. Wagner, J. Antaki, and M. Massoudi. Multi-Constituent Simulation of Thrombus Deposition. *ResearchGate* , 2016.

198. Wu, W., M. A. Jamiolkowski, W. R. Wagner, N. Aubry, M. Massoudi, and J. F. Antaki. Multi-Constituent Simulation of Thrombus Deposition. *Nat. Sci. Reports* 1–16, 2017.doi:10.1038/srep42720

199. Wu, W., F. Yang, J. Wu, N. Aubry, M. Massoudi, and J. F. Antaki. High fidelity computational simulation of thrombus formation in Thoratec HeartMate II continuous flow ventricular assist device. *Nat. Sci. Reports* 1–11, 2016.doi:10.1038/srep38025

200. Xu, H., M. M. Reynolds, K. E. Cook, A. S. Evans, and J. P. Toscano. 2-Hydroxy-5-nitrobenzyl as a diazeniumdiolate protecting group: Application in no-releasing polymers with enhanced biocompatibility. *Org. Lett.* 10:4593–4596, 2008.

201. Xu, L. C., Y. Wo, M. E. Meyerhoff, and C. A. Siedlecki. Inhibition of bacterial adhesion and biofilm formation by dual functional textured and nitric oxide releasing surfaces. *Acta Biomater.* 51:53–65, 2017.

202. Yoshida, Y., S. Furuta, and E. Niki. Effects of metal chelating agents on the oxidation of lipids induced by copper and iron. *Biochim. Biophys. Acta (BBA)/Lipids Lipid Metab.* 1210:81–88, 1993.

203. Yusen, R. D., L. B. Edwards, A. I. Dipchand, S. B. Goldfarb, A. Y. Kucheryavaya, B. J. Levvey, L. H. Lund, B. Meiser, and J. W. Rossano. The Registry of the International Society for Heart and Lung Transplantation : Thirty-third Adult Lung and Heart – Lung Transplant Report — 2016 ; Focus Theme : Primary Diagnostic Indications for Transplant. *J. Hear. Lung Transplant.* 35:1170–1184, 2016.

204. Yusen, R. D., L. B. Edwards, A. Y. Kucheryavaya, C. Benden, A. I. Dipchand, F. Dobbels, S. B. Goldfarb, B. J. Levvey, L. H. Lund, B. Meiser, and J. Stehlik. The Registry of the International Society for Heart and Lung Transplantation: Thirty-first Adult Lung and Heart–Lung Transplant Report—2014; Focus Theme: Retransplantation. *J. Hear. Lung Transplant.* 33:1009–1024, 2014.

205. Zaborowska, M., K. Welch, R. Branemark, P. Khalilpour, H. Engqvist, P. Thomsen, and M. Trobos. Bacteria-material surface interactions: Methodological

development for the assessment of implant surface induced antibacterial effects. *J. Biomed. Mater. Res. - Part B Appl. Biomater.* 103:179–187, 2015.

206. Zhang, J., X. Chen, J. Ding, K. H. Fraser, M. Ertan Taskin, B. P. Griffith, and Z. J. Wu. Computational Study of the Blood Flow in Three Types of 3D Hollow Fiber Membrane Bundles. *J. Biomech. Eng.* 135:121009, 2013.

207. Zhang, J., T. D. C. Nolan, T. Zhang, B. P. Griffith, and Z. J. Wu. Characterization of membrane blood oxygenation devices using computational fluid dynamics. *J. Memb. Sci.* 288:268–279, 2007.

208. Zhang, X. X., and P. B. Rainey. Regulation of copper homeostasis in Pseudomonas fluorescens SBW25. *Environ. Microbiol.* 10:3284–3294, 2008.

209. Zitka, O., D. Huska, S. Krizkova, V. Adam, G. J. Chavis, L. Trnkova, A. Horna, J. Hubalek, and R. Kizek. An Investigation of Glutathione-Platinum(II) Interactions by Means of the Flow Injection Analysis Using Glassy Carbon Electrode. *Sensors* 7:1256–1270, 2007.

7 Appendix

7.1 Shear Stress and Reynolds Numbers for each Flow Chamber

Packing Density	Void Fraction	Path Length (m)	Root Mean Square Shear Stress (Pascal)	Reynolds Number
0.6	0.4	0.02	5.62	64.92
0.5	0.5	0.02	4.88	77.91
0.4	0.6	0.02	5.89	97.39
0.5	0.5	0.04	4.56	77.91
0.5	0.5	0.02	4.16	64.89
0.5	0.5	0.02	5.98	98.51

7.2 FIJI Macro for Clot Analysis

```
//Open image stack you are interested in that is in binary. Make
sure it is saved as a Tiff stack
//that has already been cropped and aligned using the 3DSlicer
software
//
//This macro runs through the slices of an already opened TIFF
stack to collect the histogram
//value for each bin, 0-255, a grayscale 8-bit image

run("Clear Results");
setOption("ShowRowNumbers", false);
for (slice=1; slice<=nSlices; slice++) {
setSlice(slice); //sets the slice as the current slice
getRawStatistics(n, mean, min, max, std, hist);
for (i=0; i<hist.length; i++) {
setResult("Value", i, i);
setResult("Count"+slice, i, hist[i]);
}
}
```

7.3 Thrombin and FXa Activity from Select Flow Chamber Experiments

	n = 6		*n = 2*	
	2 cm	**4 cm**	**4.38 mL/min**	**5.64 mL/min**
Thrombin	0.06 ± 0.02	-0.01 ± 0.02	0.15 ± 0.04	0.02 ± 0.00
FXa	-0.02 ± 0.01	-0.06 ± 0.05	0.41 ± 0.14	0.40 ± 0.12